Technische Universiteit Delft

# A Novel Fitts' Law:

## Evaluating touch-based flight deck interfaces in atmospheric turbulence

Robert F. Jacobson

TU Delft

# A Novel Fitts' Law:

## Evaluating touch-based flight deck interfaces in atmospheric turbulence

by

Robert F. Jacobson

Student number: 4288289
Project duration: March 1, 2020 – January 26, 2021
Thesis committee:
Prof. Dr. Ir. M. Mulder, TU Delft, supervisor
Dr. Ir. M. M. Van Paassen, TU Delft, supervisor
Dr. Ir. C. Borst, TU Delft, supervisor
Dr. Ir. D. M. Pool, TU Delft, supervisor
Dr. O. A. Sharpans'kykh, TU Delft, external supervisor

An electronic version of this thesis is available at http://repository.tudelft.nl/.

TU Delft

# Acknowledgements

The research described in this MSc thesis is the culmination of seven and a half extraordinary years at university. During my BSc, the faculty offered me a great opportunity to broaden my view through a variety of extracurriculars. The faculty offered me a position in the Board of Studies for which I am very grateful. As well as facilitating me to join board positions in committees in both my student association and the VSV. I am convinced these opportunities have taught me a lot and offered experiences I would not otherwise have had the chance to have had.

From my first day in the $C\&S$ department, Clark, we have been in touch on how to organise the MSc programme in such a way that it was possible for me to do both my internship and an exchange abroad, without unnecessary delays. Thanks a lot for your flexibility and help in organising this, as well as helping me find this MSc thesis topic, while I was still on my exchange in Toulouse, France. You helped me a lot, not only during my thesis but throughout my whole MSc programme you were a great mentor.

Daan, I think I have practically spent more time with you than with anyone in the past year. I would like to thank you for your incredible dedication and relentless patience in helping me through my thesis, from the the countless hours of programming in DUECA to the final reviewing of my paper during the Christmas holiday. You always greeted me with a smile, helped me, and most remarkably, always managed to send me on my way again with a smile too!

Max, you enthused me to pursue my master in the $C\&S$ department through your enthusiasm in your BSc courses, and this was only confirmed during the MSc courses you gave. I would like to thank you for all our insightful and most of all, fun meetings.

René, I would like to thank you for help and willingness to join the project after your unexpected return from the United States due to Covid. Thanks for all your feedback during the meetings and your help in DUECA. Furthermore, I would like to specifically thank Olaf and Olaf, for your help in running and operating the Simona Research Simulator.

Furthermore, I would like to specifically thank my friends Casper Dek, Thomas Kuperus, Anthonie Abbenhuis, and others, who have helped me a lot during the entire thesis process, by offering helping hands as well as an extra pair of eyes to proofread all the documents.

Finally, I would like to thank my parents and my brothers. You have helped to keep me going and always answered the phone when I needed a peptalk to counter some of the Corona loneliness.

Thank you all, I couldn't have done it without you!

Kind regards,

*Bart (RF) Jacobson*
*Delft, January 2021*

# Contents

# List of Figures

# List of Tables

# Nomenclature

| | |
|---|---|
| $\beta$ | Temperature decrease rate of air (adiabatic ascent) $[\frac{^\circ}{m}]$ |
| $\Delta$ | Difference [-] |
| $\lambda$ | Geometric lapse rate of air temperature $[\frac{^\circ}{m}]]$ |
| $\tau$ | Scalar time separation |
| $\underline{\xi}$ | Three-dimensional time separation vector |
| $\vec{u}_g$ | Longitudinal turbulence gust velocity vector, positive backwards as seen from the aircraft $[\frac{m}{s}]$ |
| $\vec{v}_g$ | Side turbulence gust velocity vector, positive to the left as seen from the aircraft $[\frac{m}{s}]$ |
| $\vec{w}_g$ | Vertical gust velocity vector, positive upwards as seen from the aircraft $[\frac{m}{s}]$ |
| $A$ | Target distance Fitts' law |
| $a$ | Y-intercept coefficient in Fitts' law |
| $B$ | Stability of air in turbulence |
| $b$ | Y-intercept coefficient in Fitts' law |
| $c$ | Y-intercept coefficient Fitts' law |
| $D$ | Rate at which turbulent energy is transformed into heat |
| $H$ | Horizontal windshear $[\frac{m}{s}]$ |
| $h$ | Altitude [m] |
| $S$ | Vertical windshear $[\frac{m}{s}]$ |
| $T$ | Air temperature [K] |
| $V$ | RMS value of atmospheric turbulence magnitude $[\frac{m}{s^2}]$ |
| $W$ | Target width Fitts' law |
| $W_e$ | Effective target width Fitts' law |
| K | Kurtosis value |
| P | Patchiness parameter |

# Acronyms

**BDFT** Biodynamic Feedthrough. 3, 4, 28, 29, 38

**CCD** Cursor Control Device. 1

**CDU** Control Display Unit. 39, 48

**DASMAT** Delft University Aircraft Simulation Model and Analysis Tool. 28, 29

**DUT** Delft University of Technology. 3, 28, 53, 56

**ETW** Effective Target Width. 39

**ID** Index of Difficulty. 31, 33, 47, 49, 50

**LRU** Line Replacable Unit. 1

**MCP** Mode Control Panel. 48

**MFD** Multi-Function Display. 2

**MT** Movement Time. 31, 47, 49, 50, 53, 55, 56

**PFD** Primary Flight Display. 2

**QNL** quantitative non-linearity. 77

**RMS** Root-mean-square. 35, 47, 56

**SRS** SIMONA Research Simulator. 4, 28, 29, 53, 56

# 1 Introduction

This is the introduction of the preliminary thesis report on the development of a predictive model describing the usability of touch-based interfaces in atmospheric turbulence. First a general introduction of this preliminary thesis will be shared in section 1.1, containing a background on the proposed research. Next, an overview of the current state of the industry will be shared in section 1.2. Once this is clear, a specific problem statement will be given in section 1.3, including the specific motivation of the research, the objectives of the research, and also the scope and research questions of the research. Finally the different sections of the preliminary thesis will be outlined in detail, in section 1.4.

## 1.1. Introduction

Aviation has experienced a huge leap in technology since the Wright Brothers first took flight in 1903. From the first propeller powered wood and canvas aircraft to the modern day aluminium and carbon fibre reinforced plastics jet aircraft [33], aviation has evolved. Next to the evolution of materials and aircraft going from propeller to high bypass ratio turbofan engines, the flight deck of aircraft has seen an incredible advance in technology. It has gone from countless gauges displaying all kinds of information to the pilots towards a digital flight deck, displaying information on screens. The latest step has been the introduction of touchscreens, allowing pilots to interact with the displayed information directly [2]. The novel use of touch-based interfaces allows for a lot of benefits like the direct interaction with information as mentioned, however, there are several drawbacks when using a touch-based interface. A main one is the difficulty of interaction with a touch-based interface when in a turbulent motion environment [6]. Research has been done before on the usability of touch-based interfaces when in an atmospheric turbulence environment, such as by Cockburn et al. in 2017 [6], but this work focuses on mitigating the effects of the atmospheric turbulence. On the other hand, research has been done on constructing a predictive model for the usability of a touchscreen, as performed by Bi et al. in [3], but this was in a stationary environment. In this research thesis a predictive model will be constructed that incorporates the effects of atmospheric turbulence into Fitts' Law, [11], and Finger Fitts' Law specifically, [3], in order to predict the usability of touch-based interfaces under various levels of atmospheric turbulence.

## 1.2. Current touchscreen use and design

As has been discussed in section 1.1, the technology on the flight deck of aircraft has come a very long way. The demand for operating more and more systems accessible from the seat of the two pilots means that more information has to be shown from the same available flight deck area. To ensure that all required information is visible to the pilots, screens are used that offer the possibility of going through various levels or menus [46]. Conventional glass cockpits use a Cursor Control Device (CCD) or physical buttons to operate their Line Replacable Unit (LRU). Glass cockpits have been successfully used since the 80's, but they have their issues as well. Conventional screens and their operating systems can, however, take quite some time to operate via the CCD, or the limit of available LRU's is reached to be able to accommodate all functions [46].
To accommodate for these limitations of current cockpit screens, touchscreens have been introduced on the conventional flight deck displays. The use of touchscreens on flight decks has been widespread

for several years, but their use has been limited to personal devices, such as IPad's, and they have not seen large scale introduction to flight critical equipment such as the Multi-Function Display (MFD) or Primary Flight Display (PFD) until recent years [46]. Gulfstream was an early adopter of touchscreen technology on the Symmetry flight deck of their G500 and G600 aircraft [46]. By using as many as 10 touchscreens on their flight deck, as can be seen in fig. 1.1a, however excluding the PFD and MFD, they claim to minimise crew workload and crew error. Garmin has taken the implementation a step further by adding touchscreen functionality to their PFD and MFD displays on their Garmin 3000 and Garmin 5000 suite as seen in fig. 1.1b, [12].


(a) Gulfstream Symmetry Flight Deck, [46]

(b) Garmin G5000 and G3000 Flight Decks, [12]

Figure 1.1: Evolution of Touch Based Interfaces

As can be seen in fig. 1.1, touch-based interfaces have well and truly been introduced on the flight deck, but as was mentioned in section 1.1, they still have their challenges. This thesis describes research aimed at solving those challenges, specifically in predicting the usability of touchscreens under turbulence, as will be explained next.

## 1.3. Problem statement

Throughout the evolution of touch based interfaces and their introduction on the flight deck, quite some research has been done on mitigating the adverse effect atmospheric turbulence has on their use. For instance Dodd et al. [9], has performed research on the effects of target size, spacing and type of touchscreen on the usability of touchscreens during turbulence. Cockburn et al. [6], [5], performed extensive research on braced touch designs to mitigate the influence of turbulence on the use of touchscreens. Also, a study by Avsar et al. [2], focused on designing a novel touch based interface, showing its potential benefits but also highlights the effect turbulence might have on the proposed design. As shown, most research focuses on designing aids to counter the effects of turbulence and thus improving the usability and data throughput rate of touch based interfaces, however, hardly any research is done specifically on predicting exactly how well a touch based flight deck interface can be used when using it under atmospheric turbulence conditions. A well known way of predicting the usability and data throughput of any interface, be it a touch based interface, a keyboard, or a mouse or other interfaces, is by means of Fitts' law, [11]. The full explanation of Fitts' law and its derivatives is shared in chapter 3, but it is relevant as there does not yet exist a version of Fitts' law specifically tailored towards use of a touch based flight deck interface under turbulent motion conditions.

### 1.3.1. Motivation

Previous research at Delft University of Technology (DUT), performed by Van Zon et al. [40], [41], has shown the functionality of Finger Fitts' law when applied to touch based interfaces on the flight deck. Finger Fitts' law, [3], is the modification of the original Fitts' law that specifically shows the relationship between the interface of a touchscreen and the throughput of data that can be achieved through that interface. The research performed by Van Zon et al. [40], [41], is of specific importance to this thesis, as the original Finger Fitts' law, as constructed by Bi et al. [3], was only applicable to handheld devices. Demonstrating the functionality of the Finger Fitts' law on flight deck touch based interfaces, thus offers a clear starting point for expanding Fitts' law further to incorporate the influence of atmospheric turbulence. As Van Zon et al. demonstrated the usability of Finger Fitts' law specifically for the touch based navigation display, performing a waypoint dragging task, [40], that will be the task performed in this research as well, to be able to verify the functionality of the novel extension as well as possible. On the other hand, research performed by Khoshnewiszadeh, [20], and Mobertz et al. [28], showed the influence of atmospheric turbulence on the performance of the pilots operating a flight deck interface, specifically focusing on the Biodynamic Feedthrough (BDFT), and in the case of Khoshnewiszadeh, [20], mitigating its influence. The research performed by both Khoshnewiszadeh, [20], and Mobertz et al. [28], is valuable to this research as they both accurately showed the effects a motion environment can have on the performance of an operator, however, they did not use realistic atmospheric turbulence, instead, they used a sum of sines input as disturbance input. Therefore combining both the Fitts' law research by Van Zon et al. [41] and the turbulence and BDFT research as conducted by Mobertz et al. [28] and Khoshnewiszadeh, [20], offers a defined starting point to this thesis' research.

### 1.3.2. Thesis objective

The objective of this thesis is therefore to develop a novel predictive model, accurately indicating the achievable data throughput a touch based navigation display flight deck interface can achieve under specific levels of turbulence. The new Fitts' law extension will offer designers of touch based flight deck interfaces a valuable starting point in their designing process, as they will be able to evaluate the usability and data throughput of their interface designs for adjustable levels of turbulence without requiring a test flight or motion simulator test for each new iteration. Offering an extra means of verifying the usability of touchscreens under turbulent environments, will further improve the safety of aviation, as interface designers will be able to know beforehand whether or not the required data throughput for specific tasks can be met by pilots operating the system.

### 1.3.3. Scope

The scope of this project includes the two main aspects of the extension of Finger Fitts' law. Firstly, the focus will lie on accurately describing and researching Finger Fitts' law and extending it to include the influence of atmospheric turbulence. Secondly, the focus of this thesis will lie on modelling atmospheric turbulence as accurately as possible. This is specifically relevant as previous literature on the performance of pilots on using flight deck interfaces in turbulent environment very scarcely involve accurate and realistic atmospheric turbulence. The scope of this thesis therefore does not include other human factors, such as the perceived workload of operating a touch based interface, as done by Avsar et al. [2] or Kaminani, [19]. The research will also not focus on further detailing BDFT models, control systems or braces mitigating the adverse effects of atmospheric turbulence as performed by Khoshnewiszadeh, [20] and Cockburn et al. [6], [5].

### 1.3.4. Research question

The research question of this thesis can be assembled from the problem statement, motivation, thesis objective and scope. As has been stated before, a lot of research regarding the use of touch based flight deck interfaces under turbulent conditions has focused on mitigating the effects. Therefore the research question of this thesis will focus on predicting the usability of a touch based interface under certain levels of atmospheric turbulence. Therefore the research question of this thesis is as follows.

> How can Finger Fitts' Law be extended to reliably predict a turbulence threshold for the safe use of a touch-based navigation display flight deck interface in atmospheric turbulence conditions?

This research question can be further split up into several sub-questions, further detailing the specific parts of the research and collectively answering the main research question.

1. How can Finger Fitts' law be expanded to evaluate touch screen use in a turbulent cockpit environment?
2. What is the required level of throughput [bits/sec] to safely use a touch based navigation display under realistic atmospheric turbulence and how does a change in level of atmospheric turbulence affect the throughput achieved by pilots operating a touch based display?
3. What are the levels of atmospheric turbulence encountered by pilots when using a touch based navigation display at cruise level?

The first sub-question can be answered by means of an extensive literature review, detailing the functionality of Fitts' law and the way it can be expanded. It can later be validated by performing an experiment in a motion simulator like the SIMONA Research Simulator (SRS). Proving the influence the atmospheric turbulence has on the movement time of the operator of the touch based interface is according to the extended Finger Fitts' law. The second research question can be answered by measuring the amount of touches required to successfully reroute an aircraft around bad weather using a touch based navigation display. The impact of the change in atmospheric turbulence on the throughput achieved by the pilots as measured in the validation experiment can answer the second part of question two and in turn answer whether or not the touch based interface is safe to use under specific levels of turbulence. The third sub-question can be answered by performing a literature study on available data on atmospheric turbulence encountered at cruise level for a Cessna Citation 2 aircraft like the PH-LAB.

## 1.4. Thesis outline

The outline of this thesis is as follows. First, in part I a scientific paper is presented, detailing the performed Fitts' law experiment as well as the determination of the novel Fitts' law. Later, in part II in chapter 2, the literature review of the thesis will start out with research into atmospheric turbulence. It will be reviewed what types of atmospheric turbulence exist and what their specific characteristics are. The modelling of atmospheric turbulence and aircraft behaviour will also be discussed. Next, in chapter 3, the literature review will focus on Fitts' law. The origin of catching speed-accuracy tradeoff into Fitts' law will be shown as well as Fitts' law's ability to be extended and customised to many different specific scenarios. Finally, in chapter 4, the use of touchscreens in turbulent environments will be reviewed. The effects of Biodynamic Feedthrough will be discussed, as well as current ways of mitigating the adverse effects of turbulence. Specifically, what these methods offer in lessons for use of touchscreens in turbulent environments, thus offering insights into how the effects can be accurately incorporated into the Finger Fitts' law extension. Extending Finger Fitts' law will be explained in part III, in chapter 5. It will be shown how turbulence and Finger Fitts' law are combined into one equation. A preliminary sensitivity analysis will show the feasibility of the extension. Finally, in part IV, in chapter 6, the future research is further elaborated. The proposed validation experiment setup is discussed, along with the hypotheses and verification and validation strategy.

# I

# Paper

# A novel Fitts' law: Evaluating touch-based flight deck interfaces in atmospheric turbulence

R. F. Jacobson
*Delft University of Technology*
*Aerospace Engineering, Control & Simulation*
Delft, The Netherlands

***Abstract*—A novel Fitts' law is proposed, evaluating the performance on touch-based flight deck interfaces under high altitude atmospheric turbulence disturbances. An experiment has been performed, where subjects dragged a simulated waypoint under four levels of patchy Dryden modelled atmospheric turbulence. Along with the experiment, a novel Fitts' law model is proposed, incorporating the magnitude of the atmospheric turbulence into the Fitts' law coefficients through a single term $V$. The proposed model is evaluated against the experiment data and yields an average $R^2$ fit of $R^2 = 0.95$. Through continuous touch data tracking the finger trajectories across the screen, the quantitative non-linearity is shown to increase $19\%$ for severe turbulence. This yields an expansion of Fitts' law that incorporates the effect of atmospheric turbulence on the performance of pilots operating a touch-based navigation display. Thereby offering a predictive model on the usability, expressed in movement time per waypoint dragging task, of touch-based cockpit interfaces for four levels of atmospheric turbulence, that can be used by interface designers to evaluate new designs.**

***Index Terms*—Atmospheric Turbulence, Cockpit displays, Fitts' law, Finger Fitts' law, Touchscreen**

## I. Introduction

The advance in technology in the aviation industry has been very visible on the flight deck of aircraft, where countless gauges have been replaced by a digital environment with screens displaying vast amounts of information to the pilots. The latest step has been the introduction of touch-based interfaces, allowing pilots to interact with the displayed information directly and intuitively [1]. Next to the direct interaction with the displayed information, touch-based interfaces offer high information densities per screen as toggling through various menus is easy and fast, requiring lower cognitive effort as well as increasing operational awareness [2], [3], [4].

Despite the advantages touch-based interfaces offer, disadvantages in their usability as flight deck interfaces remain [2], [3]. Key aspects, such as the lack of tactile feedback when selecting an object, the loss of muscle memory as a consequence of scrolling through menus before accessing information, or glare, which can make a screen difficult to read, all make touchscreens widely contested on flight decks [2], [3]. However, the main issue of touch-based interfaces as controller of flight management computers on the flight deck is the impact physical vehicle accelerations and vibrations, e.g., as a consequence of turbulence, have on the usability of touchscreens [5], [6].

So far, previous literature has focused on mitigating the adverse effects of turbulence on the use of touchscreens. For instance, Dodd et al. [7], performed research on the effect of increasing target size and spacing on the usability of touchscreens during atmospheric turbulence. Cockburn et al. [5], [6] performed research on braced touch designs, enabling pilots to steady their grip when using a touchscreen during atmospheric turbulence, mitigating its effects. Avsar et al. [1], focused on designing a new interface, that is more suitable during atmospheric turbulence. Furthermore, Van den Berg et al. [8], Mobertz et al. [9], and Khoshnewiszadeh et al. [10], focused on modelling movement thresholds in the touchscreen, and on explicitly modelling pilot Biodynamic Feedthrough (BDFT) in order to cancel the adverse effects of atmospheric turbulence through model based cancellation of false inputs. BDFT is the involuntary movement of body and limbs due to specific forces caused by accelerations on the human body [11].

Little research has been done on predicting the usability of touch-based interfaces under specific magnitudes of atmospheric turbulence. Quantifying the usability of interfaces can be done by using Fitts' law [12]. Fitts' law has proven to be very suitable to being tailored towards specific interfaces, such as has been done for touchscreens in a relation called Finger Fitts' law, developed by Bi et al. [13]. Van Zon et al. [14], demonstrated the usability of Finger Fitts' law on flight deck interfaces as opposed to hand-held devices in the original Finger Fitts' law. Coutts et al. [15] expanded a regular version Fitts' law to explicitly incorporate the influence of atmospheric turbulence.

The goal of this paper is to expand Finger Fitts' law to include the effects of turbulence. It investigates the effects of four levels of atmospheric turbulence on the usability of touch-based flight deck interfaces. This is done to develop both a predictive model that can be used as safety reference when developing novel touch-based interfaces and the procedures for their use. A proposed extension of Fitts' law is used to evaluate experiment data generated by 16 participants performing a dragging task on a touch-based interface in a full motion simulator, demonstrating its accuracy under four levels of atmospheric turbulence, ranging from no turbulence to severe turbulence.

The highest level of atmospheric turbulence, severe turbu-

lence with an average magnitude of $0.78$ $[\frac{m}{s^2}]$, has not yet been evaluated in previous literature [15]. Special emphasis will be placed on ensuring the turbulence disturbance is as realistic as possible, therefore Dryden-modelled patchy atmospheric turbulence will be used [16].

The extension of Fitts' law will be performed in two steps, first the Fitts' law coefficients will be determined for a stationary environment, then the influence of the turbulence disturbance will be added through two extra Fitts' law coefficients and an extra term for the turbulence magnitude, thereby constructing a Fitts' law that is applicable for both stationary and turbulent environments. Furthermore, using a continuous data logger, the trajectory of the input finger across the screen will be logged at $100$ [Hz]. This trajectory will be used to determine the average path length increase as a consequence of increasing levels of atmospheric turbulence. Also the quantitative non-linearity of the trajectory will be determined as a measure of the deviation from the shortest path from object to target [17].

The process of extending Fitts' law is described in Section II. The design of the experiment demonstrating the proposed extension of Finger Fitts' law is detailed in Section III. Next, the results of the experiment and the consequent validation of the expansion of Finger Fitts' law will be shared in Section IV. Along with the results, their sensitivities and applicability will be discussed in Section V, before concluding the research in Section VI.

## II. Extending Fitts' law

In this section, the speed-accuracy trade-off will be explained in Section II-A. The widely used equation quantifying the speed-accuracy trade-off, Fitts' law, will then be shown in various forms in Section II-B, before being extended to tailor it towards the use case of adding the influence of atmospheric turbulence in Section II-C. The proposed determination method of Fitts' law coefficients will be discussed in Section II-D. Finally, a note on the continuous finger input data will be given in Section II-E.

### A. Fitts' law

The first to capture the speed-accuracy trade-off experienced when selecting a target was Fitts in 1954 [12]. Fitts' law is a widely used human performance model that relates the time it takes to reach a certain target, the movement time (MT), to the associated difficulty of selecting the target, i.e., the index of difficulty (ID). Thus relating the time it takes to select a target to the size and distance of the target. The larger and closer the target is, the easier and thus faster it is to select that target. Conversely, the further away and smaller a target is, the more difficult and thus slower users will be in selecting that target, thereby creating a trade-off between speed and accuracy when selecting a target. Fitts' law can be seen expressed as:

$$\text{MT} = a + b \cdot \text{ID} = a + b \cdot \log_2 \left( \frac{2A}{W} \right). \tag{1}$$

Here, the least-squares linear regression coefficients, y-intercept $a$ and slope $b$, are found empirically to fit the measured MT in [s] to the calculated ID in [bit] [18]. Furthermore, $W$ represents the input tolerance range, or target size and $A$ the average amplitude of the particular class of movements, or the distance from the target. In determining the $a$ and $b$ coefficients, the aim is for the Fitts' law to match the data with a coefficient of correlation, $R^2$, above $0.900$ [18], [19]. In later research the ID has been changed to ensure only positive values are provided [20], as can be seen in (2):

$$\text{ID} = \log_2 \left( \frac{A}{W} + 1 \right). \tag{2}$$

The original Fitts' law, as shown in (1) and (2), was developed for selection tasks in one dimension. However, Fitts' law has been proven to be suitable to extensions tailoring it towards specific scenarios as for instance later research has shown its applicability in two dimensional input tasks as well [21].

### B. Finger Fitts' law

A specific extension of Fitts' law has been tailored for touch-based interfaces and is called Finger Fitts' law [13]. Finger Fitts' law is based on the "dual-distribution hypothesis", stating that the distribution of end points as found when using a touch-based interface is the sum of two independent normal distributions. The first one characterises the speed-accuracy trade-off as performed by the human motor system while the second accounts for the absolute precision of the input finger not taking the speed-accuracy trade-off into account, effectively showing the error in accuracy a finger has when used as selection device. Finger Fitts' law can be expressed as:

$$\text{MT} = a + b \cdot \log_2 \left( \frac{A}{\sqrt{2\pi e(\sigma^2 - \sigma_a^2)}} + 1 \right) \tag{3}$$

In (3), $\sigma^2$ and $\sigma_a^2$ indicate the variance of the touch location of the operator on the touchscreen and the variance of the error from the target, respectively. Therefore, (3) essentially dissects the touch locations actually selected by participants from the location participants intended to select. The variance of the distribution of the error induced by the inaccuracy of using a finger as an input selection device, $\sigma_a^2$, is typically found by performing a separate experiment, in which there is no speed-accuracy trade-off. Participants, therefore, have ample time to select targets, yielding the accuracy of finger inputs.

By adjusting the index of difficulty for the finger accuracy using a normalised effective width $W_e$ [19], the ID values are scaled towards the mean ID value when compared to Fitts' laws that use the original target width $W$, such as in (2). As high IDs mean targets that are difficult to select, and thus finger inputs will often miss the target, the selected area will become larger, thus increasing the effective width, $W_e$, and decreasing the ID. The opposite occurs when the ID is low, and the target size is large, finger inputs will then be in a smaller area than the target size, reducing the effective target

width, $W_e$ and thus relatively increasing the ID. This scaling of the effective width towards a mean value means the Fitts' law coefficients $a$ and $b$ will have a different value than in the original Fitts' law as in (1), where $a$ typically has a lower value and $b$ a higher value. The effective width scaled ID used in Finger Fitts' law will be called $\text{ID}_e$ in this paper.

### C. Extending Finger Fitts' law

The functionality of Finger Fitts' law when applied to flight deck interfaces as opposed to hand-held touch-based devices has been demonstrated by Van Zon et al. [14]. Furthermore, Coutts et al. [15] has demonstrated a promising extension of the original Fitts' law as shown in (1), incorporating the effect of atmospheric turbulence on the MT. Their proposed extension can be expressed as:

$$\text{MT} = (-0.56 - 2.5 \cdot V) + (0.29 + 0.88 \cdot V) \cdot \log_2 \left( \frac{2A}{W} \right) \quad (4)$$

As can be seen, (4) uses the original ID as proposed by Fitts [12]. Furthermore, in (4), $V$ represents the root-mean-square (rms) weighted magnitude of the atmospheric turbulence accelerations. The Fitts' law coefficients were then found empirically to derive values for $a$ and $b$ against $V$, using interaction data from multiple touchscreens [15]. Finger Fitts' law as derived by Bi et al. [13], and verified for flight deck use by Van Zon et al. [14], as well as the extension incorporating the effect of atmospheric turbulence on the MT in a basic version of Fitts' law as found by Coutts et al. [15], offer a clear starting point for developing an extension of Fitts' law governing the speed-accuracy trade-off for touch-based interface use in atmospheric turbulence. A novel version of Finger Fitts' law is therefore proposed in this paper, expressed as:

$$\text{MT} = (a + b \cdot V) + (c + d \cdot V) \cdot \log_2 \left( \frac{A}{\sqrt{2\pi e(\sigma^2 - \sigma_a^2)}} + 1 \right) \quad (5)$$

As shown in (5), both extensions by [13] and [15] governing the use of touch-based interfaces and atmospheric turbulence have been combined into a single expression. (5) thus tailors Fitts' law further such that it can be used as a tool predicting data throughput for certain magnitudes of atmospheric turbulence and interface designs.

### D. Estimating Fitts' law coefficients

When determining the Fitts' law coefficients $a$, $b$, $c$ and $d$, as shown in symbolically in (5) and numerically in (4), in their extension of Fitts' law incorporating the influence of turbulence, Coutts et al. [15] indicate the values of $a$, $b$, $c$ and $d$ are found empirically using data from multiple experiments on multiple screens in both stationary and turbulent environments. Incorporating the influence turbulence has on Fitts' law coefficients that could also be used in stationary environments would seem to misrepresent the stationary situation and might therefore not be accurate. Special emphasis has therefore been placed, in this paper, on determining the model coefficients for the proposed Fitts' law extension. A solution starting from the coefficients from the Fitts' law describing a stationary environment will be analysed, before separately adding the influence of atmospheric turbulence. Therefore, the $a$ and $b$ coefficients as found in (3) will be used as values for $a$ and $c$ in (5). Next, the influence of turbulence will be added through coefficients $b$ and $d$ in the same equation, (5). This approach will be called the "return-to-zero" method in this paper as it returns to the exact Fitts' law found for zero turbulence, in case the turbulence disturbance $V = 0$.

### E. Continuous input trajectory data

The continuous input trajectories as performed by the finger on the touch-based interface will be logged at 100 [Hz]. This will be done to further understand the process of operating a touchscreen under turbulent motion environments and will therefore help in verifying the proposed Fitts' law extension. Recording the trajectory across the screen offers the possibility of determining the overshoot of the target and following increased path length as compared to the nominal distance from object to target. Furthermore the quantitative non-linearity will be determined [17] as a measure of "wobbliness" of the input signal. The quantitative non-linearity of the signal is defined as the root-mean-square (rms) of the deviation of a function from an ideal straight line. In this case the function is the trajectory as performed by the finger across the screen and the ideal straight line is the shortest path from object to target.

## III. Experiment Design

In order to expand Finger Fitts' law to accurately predict the movement time for certain levels of atmospheric turbulence, an experiment was conducted in a moving-base flight simulator. The objective of the experiment was to measure the movement time of participants whilst performing a dragging task on a touch-based display under various levels of turbulence. This was done in order to determine how the coefficients of Finger Fitts' law vary with turbulence intensity and thus verify the proposed extension. The overall design of the experiment is discussed in this section, along with the tasks and procedures of the participants. Finally, the hypotheses are formulated.

### A. Task

The tasks performed by the participants were twofold and similar to the tasks performed in the experiment by Van Zon et al. [14]. First, a calibration of the participants' accuracy in using their finger as selection tool was found. To determine the variance of accuracy of the finger input locations, $\sigma_a^2$, the speed-accuracy trade-off was eliminated, as explained in Section II. Participants were asked to select circular targets with a diameter of 1 cm. The calibration task was only performed in stationary conditions to ensure any inaccuracies caused by the atmospheric turbulence disturbances would not be taken as inaccuracies of the operator and therefore in the calibration, but would be seen by higher MT. For the Fitts' law task, participants were asked to drag a white circular

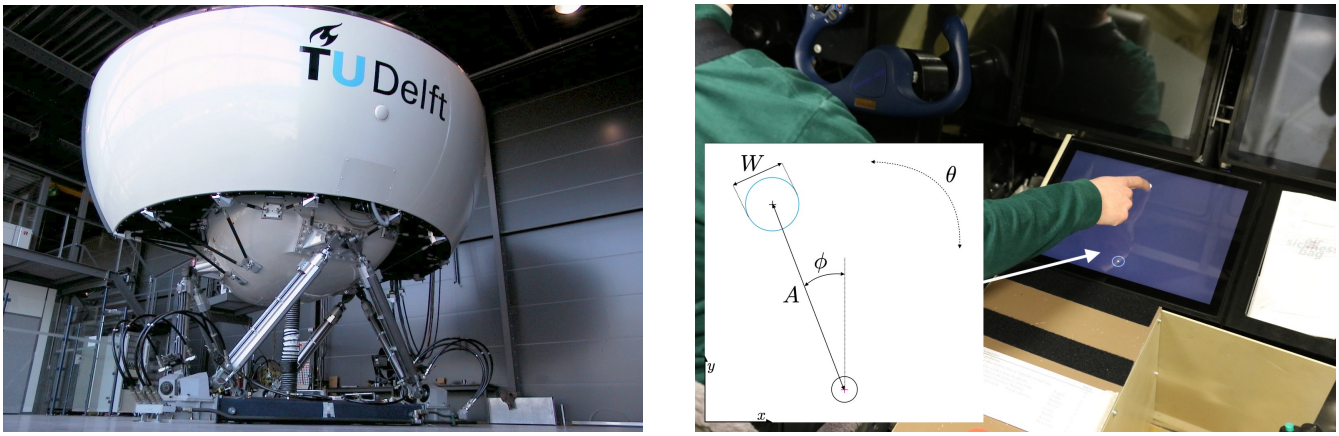


(a) SIMONA research simulator (SRS)

(b) Cabin overview

Figure 1. Experiment apparatus set-up

object with a magenta crosshair towards a cyan target circle with a black crosshair, see Fig. 1b. As soon as the magenta crosshair was within the target circle the target was met and both symbols would turn green. Both the target width $W$ and the distance or amplitude $A$ were varied. As indicated by Van Zon et al. [14] and Soukoreff and Mackenzie [18], the direction of the swiping task can also be a confounding influence, despite not changing the ID. Therefore two other variables were introduced, a directional heading variable $\phi$ and display rotation variable $\theta$. Where $\phi$ indicates the direction the target is located relative to the origin and $\theta$ rotates the entire reference frame of the display [14]. Measurements of the MT started as soon as the participant commenced the dragging task and ended as soon as the participant successfully selected the target and stopped moving the object for a full second, after which the stationary second was deducted again to find the MT [14].

### B. Conditions

The swiping task varied in difficulty through a changing target width, $W$ and changing target amplitude, $A$, to ensure movement times can be measured for various indexes of difficulty, thus allowing for a least squares regression and determination of the Fitts' law coefficients [14]. A direction heading variable $\phi$ and display rotation variable $\theta$ were also introduced, but they did not change the ID, as further explained in Section III-A. The control variables in the task were therefore $W$, $A$, $\phi$ and $\theta$. The overview of variations in task variables can be seen below [14].

- $A$ = [45, 80, 115, 150] [mm]
- $W$ = [5, 15, 25, 35] [mm]
- $\phi$ = [-25, 0, 25] [deg]
- $\theta$ = [0, 90, 180, 270] [deg]

The 16 ($= 4 \cdot 4$) combinations of $A$ and $W$ offered an ID range of [1.19-4.95], when using the Fitts' law ID formulation as shown in (2). Adding the variation in directional heading variable $\phi$ and display rotation variable $\theta$ offered $4 \cdot 4 \cdot 3 \cdot 4 =$ 192 different conditions, and thus 192 tasks were performed by the participants per turbulence condition.

The atmospheric turbulence is varied between four levels of atmospheric turbulence intensity, ranging from no turbulence to severe turbulence. Thus ensuring the change in movement times as a result of varying magnitudes of atmospheric turbulence can be determined, thereby quantifying the relationship between the magnitude of atmospheric turbulence and the time it takes to successfully perform a task [15].

### C. Design

The experiment had been set up as a within participants design in which 16 participants performed the experiment in a balanced randomised order over four levels of atmospheric turbulence. The specifics of the task are explained in Section III-A. Other research, e.g., [5], [6], [15], regarding the usability of touch-based flight deck interfaces under atmospheric turbulence conditions has not specifically reported the characteristics of the turbulence disturbance input. Either a stochastic input signal without any shared properties was used or a sum of sinusoids input signal is used as disturbance for the experiment. To ensure the research in this article is relevant, special attention has therefore been focused on constructing an accurate disturbance signal.

Four levels of atmospheric turbulence were chosen to represent high altitude atmospheric turbulence as experienced on the flight deck of a Cessna Citation II as closely as possible. The aircraft was simulated to fly through the high-altitude clear-air Dryden patchy turbulence signal at cruise altitude and speed in order to find the aircraft (angular) accelerations on and around its centre of gravity. This was done as the task performed by participants resembles a waypoint dragging task on a navigation display as would be performed by pilots in the cruise phase of a flight [14].

The Cessna Citation II was chosen as it is the test aircraft of DUT and the SRS operated an accurate model, called the DASMAT model [22], of the aircraft dynamics. This model was used to model the disturbances of the atmospheric

Table I
TURBULENCE VALUES AS USED IN FITTS' LAW EXTENSION VALIDATION EXPERIMENT

| Turbulence level | Filter [Hz] | $\ddot{x}$ $[\frac{m}{s^2}]$ | $\ddot{y}$ $[\frac{m}{s^2}]$ | $\ddot{z}$ $[\frac{m}{s^2}]$ | $\dot{q}$ $[\frac{rad}{s^2}]$ | $\dot{p}$ $[\frac{rad}{s^2}]$ | $\dot{r}$ $[\frac{rad}{s^2}]$ | Total, $V$ $[\frac{m}{s^2}]$ |
|---|---|---|---|---|---|---|---|---|
| T0: No movement | - | 0 | 0 | 0 | 0 | 0 | 0 | 0 |
| T1: Low turbulence | 2-10 | 0.038 | 0.082 | 0.243 | 0.050 | 0.021 | 0.010 | 0.26 |
| T2: Medium turbulence | 2-10 | 0.076 | 0.164 | 0.486 | 0.100 | 0.043 | 0.021 | 0.52 |
| T3: Severe turbulence | 2-10 | 0.113 | 0.246 | 0.729 | 0.150 | 0.064 | 0.031 | 0.78 |

turbulence through to the cockpit accelerations as would be experienced by the pilots.

To accurately model the atmospheric turbulence, Dryden functions were used [23]. Dryden functions offer a rational spectral density function while maintaining an accurate representation of the actual turbulence [24] [25]. Real-life atmospheric turbulence is not always constant over time and space, as areas containing high levels of atmospheric turbulence may be followed by areas containing less intense atmospheric turbulence, in a phenomenon called $patchiness$ or $intermittency$ [16]. To obtain a turbulence profile that approaches reality, patchiness was added to the turbulence input signal. In adding patchiness, caution was taken to ensure the patchiness parameter, and thus the patch size, was such that participants experienced turbulence disturbances in the duration of every performed task, while still experiencing the surprise effect achieved by adding patchiness to the turbulence simulation. As it was expected that a dragging task would last three seconds, the patchiness was arranged as such.

It is very difficult as well as impractical to try to have every participant perform every task under the exact same disturbance, as even when the starting times of all dragging tasks would be linked to specific moments in the turbulence disturbance signal, participants would still react with different speeds and would thus experience different turbulence disturbances. Therefore an rms weighted turbulence magnitude was chosen per intensity, with the patchiness ensuring the realistic surprise effect of the disturbance would still be present. The signal was then filtered to a range of [2-10] Hz ensure it would be in the operating range of the simulator while still being in the range of affecting BDFT [9].

Next, the motion space of the simulator was optimised for the accelerations present, after which the magnitudes of the accelerations were scaled to fit with the two non-zero turbulence magnitudes as used by Coutts et al. [15], of $0.26\frac{m}{s^2}$ and $0.52\frac{m}{s^2}$, to ensure the experiment as performed by Coutts et al. [15] could be properly verified. A higher level of atmospheric turbulence magnitude, $0.78\frac{m}{s^2}$, was added to demonstrate the linearity of the Fitts' law extension.

Details of the turbulence (angular) accelerations as experienced in the simulator used in the experiment can be found in Table I. As stated in Section II-C, $V$ represents the rms weighted magnitude of the atmospheric turbulence accelerations. To determine the value of $V$, only the $\ddot{x}$, $\ddot{y}$ and $\ddot{z}$ accelerations were used, in similar fashion to [15]. The rms weighted magnitude of angular accelerations, in pitch $\dot{q}$, roll $\dot{p}$ and yaw $\dot{r}$, that were present in the cockpit as a consequence of the translated accelerations around the aircraft centre of gravity are also shown in Table I. The patchiness parameter and power spectral density analysis of the patchy turbulence disturbance input signal can be found in [26].

Table II
PARTICIPANT PROFILES

| | |
|---|---|
| Profile | 16 MSc and Phd students from DUT |
| Gender | 4 female, 12 male |
| Age | Ranging from 21 to 31, average 25.1 years |
| Handedness | 3 left handed, 13 right handed |

### D. Participants

The participants of the experiment represented a homogeneous group of students of Delft University of Technology (DUT). No previous simulator or piloting experience was required to successfully complete the simplified waypoint dragging tasks. Even though pilots have more experience in moving a waypoint, few have experience doing so on a touch-based interface. Also, the task had been simplified compared to accurately placing waypoints, such that basic hand-held touchscreen experience was deemed sufficient to generate representative and homogeneous data. An overview of the participants' characteristics can be found in Table II. The age of the group was deliberately narrow, in order to rule out the effect of age on reaction time. Also, as left-handed captains would also operate the touch-based interface with their right hand, three left-handed participants were included in the experiment to ensure a realistic use case [27].

### E. Apparatus

In order to conduct an experiment in which the participants experience realistic atmospheric turbulence, the SIMONA Research Simulator (SRS) of DUT was used, shown in Fig. 1a. This is a 6 degree-of-freedom full motion research simulator and is thus capable of offering a realistic environment in which atmospheric turbulence can be replicated at various levels. The cockpit of the SRS was configured in a basic aircraft lay-out, with a control column installed at the left-hand seat. The filter details of the SRS can be found in [26].

A touch-based interface was installed at the typical Control Display Unit (CDU) location, in the mid console off the right-hand knee of the captain. An overview of the cockpit can be


Figure 2. Experiment session planning

seen in Fig. 1b. The touchscreen used in the experiment is an Iiyama ProLite TF1534MC. The software used to control both the SRS and the touchscreen is called DUECA or Delft University Environment for Communication and Activation [28]. Through DUECA and the Iiyama screen it was possible to register both the Fitts' law MT as well as the continuous trajectory data of the finger across the screen for each individual task performed. The continuous trajectory data were logged at 100 [Hz], thus facilitating the determination of the quantitative non-linearity and increased path lengths of the touch input trajectories.

### F. Procedure

Before participants were invited to perform the experiment, the experiment set-up and procedures were approved by the Human Research Ethics Committee of DUT, under application number 1155. Prior to performing the experiment, participants received a written briefing document that was also discussed in the face-to-face briefing. The briefing document detailed the background of the research, the type of task the participant would be performing and explained to participants that they were free to withdraw from the experiment at any time, should they feel uncomfortable in any way. The planning of the experiment session was also discussed, as shown in Fig. 2, demonstrating the four sessions containing 192 tasks each. Next, participants received a briefing on the safety procedures of the SRS in case of an emergency situation. After signing a consent form the participant would commence the experiment.

Special emphasis was placed on the participants aiming for maximum speed and accuracy in order to meet the goal of $96\%$ success rate in the dragging task, as also emphasised by [14] and [18] in their Fitts' law experiments. Feedback on the performance of participants was given via a two-way radio connection between the SRS control room and participant, ensuring the participant met the $96\%$ accuracy requirement.

### G. Hypotheses

The following hypotheses were formulated based on a conducted literature review.

*1) The T0 experiment condition yields an $R^2$ fit on the data higher than 0.9:* Hypothesis 1 provides validations of the current experiments' outcomes ensuring the Fitts' law experiment is set-up properly [19], [18]. Finger Fitts' law is part of the proposed extension of Fitts' law incorporating the effect of atmospheric turbulence, shown in (5). Therefore it is important the experiment is performed properly before adding the influence of turbulence disturbances. The results will be checked against those found by Van Zon et al. [14]. Special emphasis will be placed on comparing the Fitts' law coefficients $a$ and $b$ governing the experiment data.

*2) The movement time increases along with the turbulence level $V$:* Hypothesis 2 governs the second part, indicating the influence of atmospheric turbulence $V$ on the MT of the proposed extension of Fitts' law as shown in (5). The same methodology is to be used as in [15], as the novel return-to-zero approach in determining the Fitts' law coefficients is governed by hypothesis 3. The relation between MT and $V$ is also expected to hold for the severe turbulence magnitude T3, shown in Table I, even though it has not been demonstrated before by [15].

*3) The return-to-zero method of finding the Fitts' law coefficients has a higher $R^2$ value on the experiment data than previous methods:* The return-to-zero method starts with the coefficients $a$ and $b$ of Fitts' law (1) as found in a stationary condition and uses these values for $a$ and $c$, respectively, in the proposed extension (5) before separately adding the influence of atmospheric turbulence through coefficients $b$ and $d$. Hypothesis 3 states that this yields a closer fit to the experiment data than the method as used by Coutts et al. [15]. As the experiment results from the stationary and turbulent environments are separately modelled instead of combined.

*4) The Finger Fitts' law offers a closer fit than the conventional Fitts' law on the experiment data:* The Finger Fitts' law $\mathrm{ID}_e$ is proposed in the extension of Fitts' law in (5) to accurately describe the touchscreen input data. Hypothesis 4 states that Finger Fitts' law more closely predicts the experiment data than the conventional Fitts' law. This closer fit can be determined by demonstrating a higher value of $R^2$ and implies that the Finger Fitts' law more accurately predicts the usability of the touchscreen. Therefore, $\mathrm{ID}_e$ is more suitable to be used in the proposed extension as opposed to the conventional Fitts' law ID.

*5) The travelled finger path length and quantitative non-linearity during the dragging task across the screen increases along with larger atmospheric turbulence magnitudes:* Hypothesis 5 governs the finger trajectories of participants operating the touch-based interface. It is expected that the average track path length from object to target will increase along with a higher disturbance from atmospheric turbulence. Therefore the MT required to complete a task will also increase. A performance difference, where a longer path length is a worse performance, is expected between push and pull tasks, with the push task expected to perform worse. The participants' hands may block the target when pushing the object to the target. Also the accuracy phase of actually selecting the target is expected to be more difficult with the arm extended, causing the push tasks to possibly take longer. Furthermore, the quantitative non-linearity is expected to increase for larger turbulence magnitudes.

## IV. Results

In this section the experiment results are presented, facilitating the analysis of the hypotheses. The first two hypotheses can be evaluated using the results shared in Section IV-A, detailing the results from the Fitts' law experiment. Further attention will be given to the proposed extension of Fitts' law,

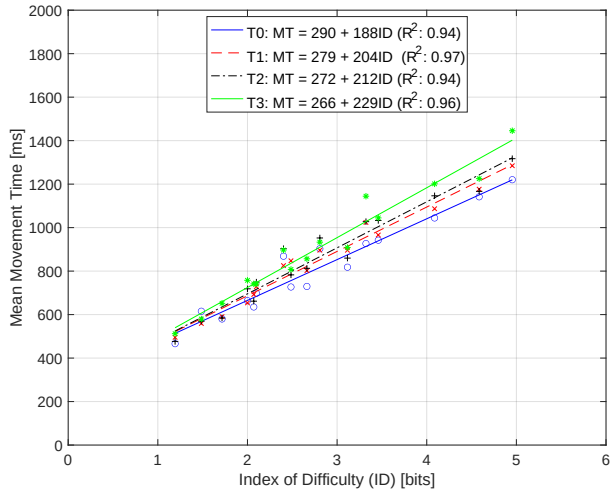


(a) Conventional Fitts' law models for all four atmospheric turbulence magnitudes, plotted in a single graph for comparison.

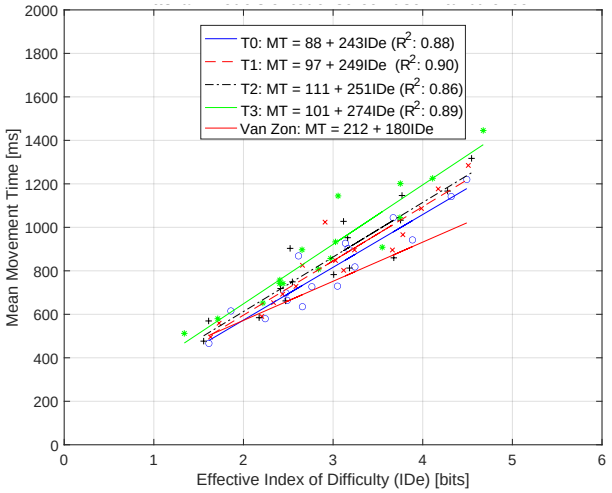


(b) Finger Fitts' law models for all four atmospheric turbulence magnitudes, as well as the Fitts' law as found in [14] plotted in a single graph for comparison.

Figure 3. Experiment results, conventional and finger Fitts' law fits over data

Table III
COEFFICIENT VALUES FOR CONVENTIONAL ID

| ID | Experiment data | | | Prediction | | | | | |
|---|---|---|---|---|---|---|---|---|---|
| | | | | Method by Coutts et al. [15] | | | Return-to-zero method | | |
| | a | b | $R^2$ | a | b | $R^2$ | a | b | $R^2$ |
| T0 | 290 | 188 | 0.94 | 288 | 188 | 0.94 | 290 | 188 | 0.94 |
| T1 | 279 | 204 | 0.97 | 281 | 202 | 0.97 | 280 | 202 | 0.97 |
| T2 | 272 | 212 | 0.94 | 273 | 215 | 0.94 | 271 | 216 | 0.94 |
| T3 | 266 | 229 | 0.96 | 265 | 228 | 0.96 | 262 | 230 | 0.96 |

Table IV
COEFFICIENT VALUES FOR EFFECTIVE IDE

| IDe | Experiment data | | | Prediction | | | | | |
|---|---|---|---|---|---|---|---|---|---|
| | | | | Method by Coutts et al. [15] | | | Return-to-zero method | | |
| | a | b | $R^2$ | a | b | $R^2$ | a | b | $R^2$ |
| T0 | 88 | 243 | 0.88 | 91 | 240 | 0.88 | 88 | 243 | 0.88 |
| T1 | 97 | 249 | 0.90 | 97 | 249 | 0.90 | 96 | 250 | 0.90 |
| T2 | 111 | 251 | 0.86 | 102 | 259 | 0.85 | 105 | 257 | 0.86 |
| T3 | 101 | 274 | 0.89 | 107 | 268 | 0.89 | 113 | 264 | 0.89 |

shown in (5), in Section IV-B, again sharing Hypotheses 1 and 2, as well as showing the different values for the Fitts' law coefficients found through the two methods as stated in Hypothesis 3. Hypothesis 4 will also be evaluated at the hand of these data, as the predicted Fitts' law will be compared to the data from the experiment, facilitating the comparison between Finger Fitts' law and the conventional Fitts' law. The final hypothesis governing the path length and quantitative non-linearity of the trajectory over the screen will be presented along with the data shown in Section IV-C.

### A. *Fitts' law experiment results*

The results of the Fitts' law experiment as described in Section III can be seen in Fig. 3a and Fig. 3b, each showing the four Fitts' law fits found for four different levels of atmospheric turbulence. First, Fig. 3a shows the results for the conventional ID as used in (2). These results are shown as a benchmark against which the Finger Fitts' law results can be compared. The results for the effective width correction for touch screen use as found by Bi et al. [13] can be seen in Fig. 3b. As can be seen in both Fig. 3a and 3b, the Fitts' laws plotted become progressively steeper, 22% and 13%,

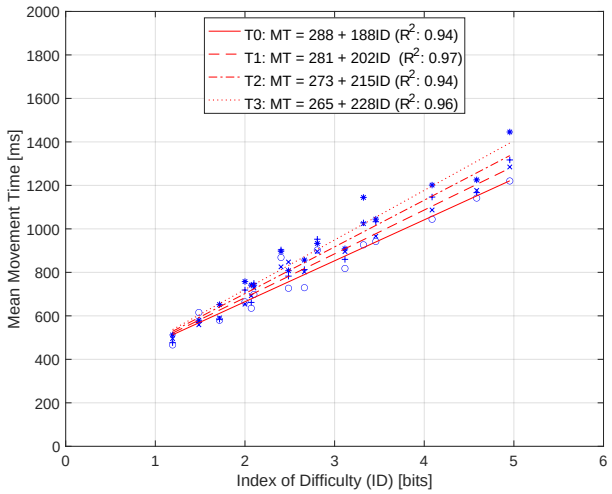


(a) Fitts' law extension, using basic ID, method by Coutts et al. [15], as shown in (6).

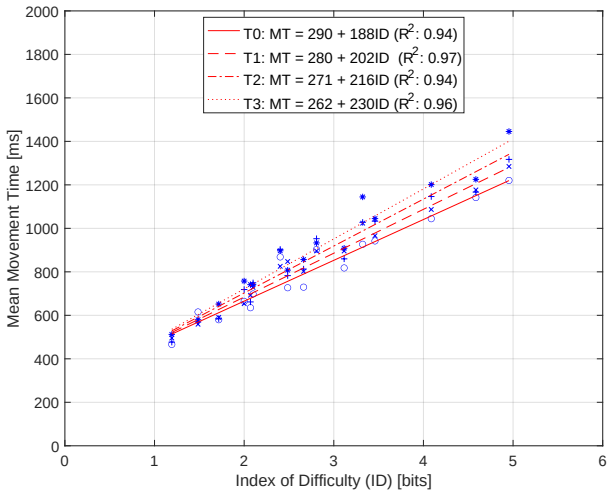


(b) Fitts' law extension, using basic ID, using return-to-zero method as shown in (7).

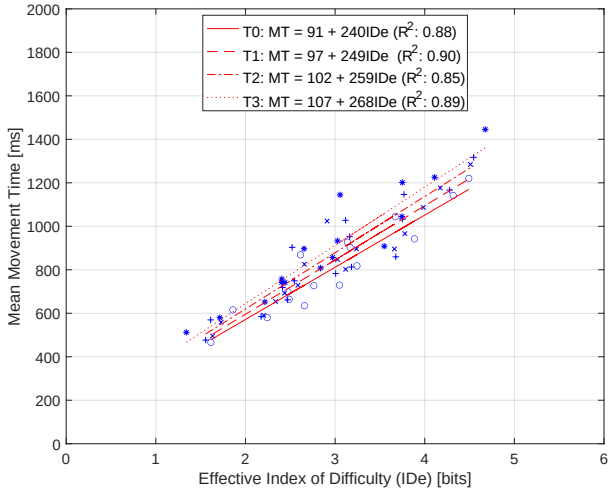


(c) Fitts' law extension, using Finger Fitts' law $ID_e$, using method by Coutts et al. [15] as shown in (8).

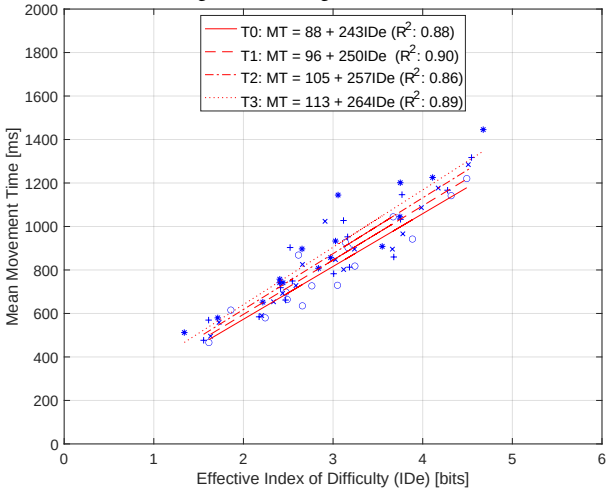


(d) Fitts' law extension, using Finger Fitts' law $ID_e$, and return-to-zero method as shown in (9).

Figure 4. Fitts' law extensions plotted over experiment data

respectively, when comparing the no turbulence to the severe turbulence cases, indicated in the plots by $T0$ for no atmospheric turbulence through to $T3$ for the highest magnitude of atmospheric turbulence. The steeper line indicates a higher MT for a similar ID, demonstrating that a task of similar difficulty takes longer to complete when performed in an environment with stronger atmospheric turbulence. The increase in MT as a consequence of increased turbulence magnitude is relevant as it demonstrates and quantifies the influence atmospheric turbulence has on the usability of touch-based interfaces, as will be further discussed in Section V. In Fig. 3a, the high $R^2$ value of $0.94$ for T0, indicates the conventional Fitts' law accurately governs the speed-accuracy trade-off as performed by the participants in the experiment. In Fig. 3b, the ID scaling performed by the effective width correction can be seen when looking at the extreme values of ID that are closer towards the mean ID value compared to those in Fig. 3a. As explained in Section II, the effective width scaling also affects the value of the coefficients $a$ and $b$, therefore causing a steeper Fitts' law, explaining the smaller percentage increase as a result of the increase in atmospheric turbulence. Furthermore, the effective width scaling has decreased the $R^2$ values, to $0.88$ for T0, for the Finger Fitts' law shown in Fig. 3b compared to those shown in Fig. 3a. Even though the value for $R^2 = 0.88$ for both the experiment performed by [14], and this experiment, the results are not consistent with [14] as the values of the Fitts' law coefficients are significantly different, with $a = 212$ and $b = 180$ in [14] and T0 Fitts' law indicating $a = 88$ and $b = 243$. This will be further discussed in Section V.

### B. Extension of Finger Fitts' law

Based on the results of the experiment as shown in Section IV-A, the proposed extension of Fitts' law could be further determined, as the coefficients for this set-up could be found. These are shown in Table III for the basic index of difficulty and in Table IV for the effective width corrected index of

difficulty. The tables show the coefficients found directly from the experiment data in the first column. The second column shows the coefficients found using the method by Coutts' et al. [15], and the third column shows the coefficients found using the return-to-zero method. The method by Coutts' et al. [15] uses the four pairs of $a$ and $b$ found from the experiment data, shown in the first column of Table III and IV, and uses the four values of $V$, to find the coefficients shown in (6) and (8) for ID and $\text{ID}_e$, respectively. Least-squares linear regression is used to determine the values of the coefficients. The return-to-zero method starts off by using the values of the $a$ and $b$ T0 coefficients found from the experiment data in the first column of Table III and IV, for the first and third coefficient of the proposed extension, (5). This ensures that if $V = 0$ the proposed extension incorporating turbulence returns to the exact Fitts' law as found for stationary conditions. Next the values for T1, T2 and T3 as found in the first column of Table III and IV are used to determine the second and fourth coefficient of the proposed extension (5), through a least-squares linear regression, thus combining the magnitude of atmospheric turbulence, $V$, with the measured change in Fitts' law coefficients. Therefore ensuring the coefficients are scaled by the magnitude of the atmospheric turbulence and through them the MT is scaled according to the atmospheric turbulence magnitude. The resulting coefficients are shown in (7) and (9).

Four equations are shown, (6)-(9), using both the conventional ID, in (6) and (7), as introduced earlier in (2), as well as the effective width correction of $\text{ID}_e$ used in Finger Fitts' law, in (8) and (9), as introduced previously in (3).

$$\text{MT} = (288.4 - 30.1 \cdot V) + (188.3 + 51.0 \cdot V) \cdot \text{ID} \quad (6)$$

$$\text{MT} = (289.9 - 36.2 \cdot V) + (187.7 + 54.1 \cdot V) \cdot \text{ID} \quad (7)$$

$$\text{MT} = (91.2 + 20.8 \cdot V) + (240.1 + 36.0 \cdot V) \cdot \text{ID}_e \quad (8)$$

$$\text{MT} = (87.7 + 32.8 \cdot V) + (242.8 + 26.8 \cdot V) \cdot \text{ID}_e \quad (9)$$

The results of both methods of determining the Fitts' law coefficients are also shown along with the experiment data in Fig. 4a to 4d. The return-to-zero method prediction shown in (7) and (9) has been combined with the experiment data in Fig. 4b and 4d, respectively. The method used by Coutts et al. [15] shown in (6) and (8) are combined with the experiment data in Fig. 4a and 4c, respectively. The resulting coefficients can be seen in the figures, as well as in Table III and IV.

The $R^2$ value, showing the accuracy of the prediction over the actual data show that both the prediction methods have the same $R^2$ values as the actual experiment data for the conventional ID, shown in Table III. The values of $R^2 = 0.94$, $R^2 = 0.97$, $R^2 = 0.94$ and $R^2 = 0.96$ indicate the Fitts' law is very accurate in describing the data across all four turbulence levels, both for the predictions as for the experiment data when using the conventional ID. The $R^2$ values for $\text{ID}_e$, shown in Table IV are almost all the same for the experiment data as well as the predictions. Only in the T2 case, the method by Coutts' et al. [15] is less accurate with $R^2 = 0.85$ as opposed to $R^2 = 0.86$ for both the experiment data Fitts' law and the predicted Fitts' law using the return-to-zero method.

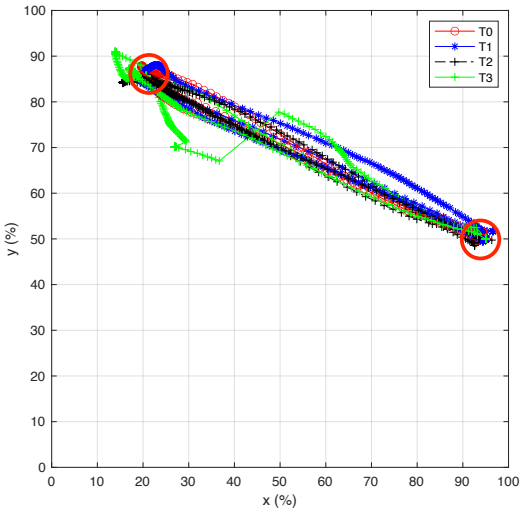


Figure 5. Example of participants' dragging path affected by turbulence.

### C. Finger trajectories

During the Fitts' law experiment the continuous touch data were logged at 100 [Hz], in order to see the trajectory of the finger across the screen during the dragging task.

*1) Total path length:* An isolated case is presented as plotting all tasks at once does not offer a clear view of the actual touch inputs. Shown in Fig. 5 is an example of 3 participants performing the same condition, index 79, where the object is dragged from right to left, and the target distance, $A$, is at the maximum value of 150 [mm] and target size, $W$, at the minimum value of 5 [mm]. Two participants are shown as an example of dragging tasks that are performed accurately, however, one participant experienced significant difficulty as a consequence of the high atmospheric turbulence, increasing the path length by $18\%$ compared to the nominal distance from object to target. Even though not all dragging tasks are so clearly influenced by the presence of atmospheric turbulence, the average path lengths' percentage increase during the experiment, as shown in Table V, indicate a higher atmospheric turbulence increases the path length of the finger dragging across the screen. As can be seen in Table V, the difference in increased finger trajectories across the screen between push and pull tasks is large. Especially for medium turbulence and severe turbulence intensities, the increased trajectories are $46\%$ and $42\%$ higher for a push task as opposed to a pull task for the case of maximum distance, A, and minimum target size, W. The average path lengths' increase for all participants and conditions is also shown in Table V. It is shown that the

Table V
AVERAGE DRAGGING PATH LENGTH, PERCENTAGE INCREASE

| | Zero turbulence | Low turbulence | Medium turbulence | Severe turbulence |
|---|---|---|---|---|
| Push, max A, min W | 6.5% | 6.8% | 8.6% | 9.8% |
| Pull, max A, min W | 5.3% | 6.2% | 5.9% | 6.9% |
| Overall, max A, min W | 5.9% | 6.5% | 7.3% | 8.3% |
| Overall, all conditions | 7.8% | 8.6% | 10.2% | 11.8% |

Table VI
AVERAGE QUANTITATIVE NON-LINEARITY VALUES

| | Zero turbulence | Low turbulence | Medium turbulence | Severe turbulence |
|---|---|---|---|---|
| Push, max A, min W [mm] | 2.9 | 2.8 | 2.4 | 2.9 |
| Pull, max A, min W [mm] | 2.7 | 3.0 | 2.7 | 3.2 |
| Overall, max A, min W [mm] | 2.8 | 2.9 | 2.6 | 3.1 |
| Overall, all conditions [mm] | 2.1 | 2.2 | 2.3 | 2.5 |

increase in path lengths travelled across the screen increased by $51\%$, when comparing the severe turbulence disturbance to the zero turbulence case.

*2) Quantitative non-linearity:* Using the continuous touch data also offers the possibility of determining the quantitative non-linearity of the dragging trajectory. The average values of non-linearity per turbulence condition for the maximum distance, A, and minimum target size, W, can be seen in Table VI. It can be seen that for the low and severe turbulence, the deviation from the ideal path increases, by $5.1\%$ and $11.2\%$, respectively, however, for the medium atmospheric turbulence disturbance the quantitative non-linearity decreases by $7.6\%$ to a deviation of $2.6$ [mm]. When looking at the average values for all conditions, the quantitative non-linearity is seen to increase along with the turbulence magnitudes. The quantitative non-linearity increases $19\%$, when comparing the zero turbulence case to the severe turbulence case, indicating the turbulence affects the dragging path across the screen. The overview of all continuous touch data results is shared in [26].

## V. GENERAL DISCUSSION

In this paper an extension of Fitts' law is presented for accurately predicting the usability of touch-based interfaces under specific levels of atmospheric turbulence. An accurate model predicting the influence of atmospheric turbulence on the MT required to perform a dragging operation on a touchscreen is proposed as research has not previously offered such a predictive model and has mainly focused on mitigating the effects [5], [15]. In this section the implications and sensitivities found in the performed experiment will be discussed.

### A. Hypotheses

The Fitts' laws found governing the T0 experiment data offer different fits depending on the type of ID used. The conventional ID offers a close fit on the T0 experiment data of $R^2 = 0.94$, indicating the Fitts' law found is accurate enough to base a prediction upon [18]. When using the $\text{ID}_e$, however, the data do not fit quite as well, with $R^2 = 0.88$ for the T0 experiment. As the $R^2$ value is below the threshold of $R^2 = 0.90$ the Finger Fitts' law found is not deemed accurate enough to use as a predictive model in this experiment [18]. Hypothesis $1$ is therefore rejected.

The $R^2$ value of $R^2 = 0.88$ of the Finger Fitts' law is similar to the one found by Van Zon et al. [14], however, it was expected the $R^2$ value would increase with a higher accuracy score by the participants. As a consequence, the participants in this experiment were instructed to lean more towards accuracy instead of speed when performing the speed-accuracy trade-off. The y-intercept $a$-coefficient in this experiment is lower than the one reported in [14], for similar experiment conditions, thus using $\text{ID}_e$ and without a turbulence disturbance. This experiment found $a = 88$, as opposed to $a = 212$ reported in [14]. The difference can be explained by the effective index of difficulty range. Van Zon et al. [14] found a wider range of $\text{ID}_e$ as a result of a lower accuracy achieved by the participants. The accuracy achieved by participants in their experiment was $95\%$, whereas the accuracy achieved in this experiment was $99.7\%$. This also indicates participants took more time to complete the task in the experiment described in this paper as opposed to Ref. [14], which can be seen by the higher $b$-coefficient. As a result of the lower accuracy, the smaller targets are registered as even more difficult by the effective width scaling, thus increasing the ID and scaling the $\text{ID}_e$ further apart. This creates a more horizontal line, thereby increasing the $a$-coefficient and decreasing the $b$-coefficient, when compared to this experiment.

Another factor attributing to the difference in $a$ and $b$ coefficients is the fact that both experiments used a different touchscreen. As indicated by Vrouwenvelder [29], the Iiyama ProLite TF1534MC touchscreen used in this experiment is much faster than the Dell P2314T touchscreen used by Van Zon et al. [14], causing the y-intercept coefficient to be smaller

in this experiment as the measured reaction time is much lower as a consequence of the faster touchscreen.

The $R^2$ value of the basic ID Fitts' laws shows a surprisingly good fit of $R^2 = 0.94$ on the experiment data, as it was expected the basic ID would not govern the data found in a touch-based interface as closely as the $ID_e$ method, which is specifically tailored towards touchscreen interaction [13]. Furthermore, the expected difference in magnitude of the Fitts' law coefficients is present between the ID and $ID_e$ methods. For the T0, ID experiment case $a = 290$ and $b = 188$ as opposed to $a = 88$ and $b = 243$ for T0, $ID_e$ experiment case, as explained in Section II, and stated in Hypothesis 1.

### *B. Fitts' law extension*

This second part of the discussion will be on the effectiveness and accuracy of the proposed Fitts' law extension, first proposed in (5) and with coefficients determined in multiple ways in (6), (7), (8) and (9). As Coutts et al. [15] did not report any $R^2$ values on the accuracy of their Fitts' law extension, it is not possible to compare the accuracy of the extension found in this research to their extension. However, the method as proposed in Ref. [15], where a single term $V$ is used, therefore including the atmospheric turbulence magnitude in both the $a$ and $b$ coefficients of Fitts' law, does show a good fit on the data, when comparing the $R^2$ value of the prediction to the $R^2$ fit found on the Fitts' law fits taken directly from the experiment data. With an average value of $R^2 = 0.95$ for the conventional ID predictions and $R^2 = 0.88$ as average value for the $ID_e$ predictions, these $R^2$ values are similar to the values found directly from the experiment data and thus demonstrate the incorporation of atmospheric turbulence into Fitts' law can be accurately done by adding the term $V$. Hypothesis 2 can therefore be accepted.

Next, as can be seen, the differences in the Fitts' law coefficients between (6) and (7) for basic ID and (8) and (9) for $ID_e$, are very small. However, to ensure the most accurate fit over the Fitts' law experiment data, the method of determining the Fitts' law coefficients is relevant. Especially when expanding for even higher levels of turbulence than $V = 0.78[\frac{m}{s^2}]$, accurate modelling is important and therefore the method of determination of coefficients is relevant. Both methods of extending Fitts' law hold well when combined with the experiment data, as indicated by the average $R^2$ values of the extension, $R^2 = 0.95$ and $R^2 = 0.88$ for ID and $ID_e$ methods, respectively, being the same as the $R^2$ value as found over the experiment data.

When comparing the two methods, the return-to-zero method has a very slight advantage in $R^2$ values, $R^2 = 0.86$ as opposed to $R^2 = 0.85$ found using the method by Coutts et al. [15], against the experiment fit of $R^2 = 0.86$. Even though the difference is barely significant, it can also be argued that the method starting from a Fitts' law without motion present is more accurate than the method by Coutts et al. [15] as it splits the two phenomena of stationary and turbulent environments, depending on what situation is encountered, thus accurately incorporating either environment by itself instead of taking an average value. By doing so, the method offers the possibility of using a single Fitts' law expression for use in both stationary and turbulent environments, where the Fitts' law for use in a stationary environment can be changed by adding the turbulence magnitude through the term $V$, which is generally predominantly driven by the magnitude of vertical turbulence which is about three times larger than lateral turbulence and six times larger than frontal turbulence disturbances. Therefore offering predictions on use of a single touch-based interface for various stationary or turbulent environments. Hypothesis 3 can thus be accepted.

Evaluating the suitability of Finger Fitts' law $ID_e$ versus the conventional Fitts' law ID for use in the proposed extension of Fitts' law can be done by comparing the $R^2$ values the extensions have over the experiment data. The $R^2$ values of the basic ID are higher than those found when using $ID_e$, $R^2 = 0.95$ versus $R^2 = 0.88$ on average, respectively. Therefore the combination of using the conventional ID and coefficients as found through the return-to-zero method is deemed the most suitable expansion of Fitts' law. It was expected the $ID_e$ method as found in Finger Fitts' law would offer a more accurate fit [13] as the calibration task that was performed was expected to cancel out the inaccuracy of using a finger as selection tool. However, even though Van Zon et al. [14] demonstrated the usability of Finger Fitts' law on flight deck interfaces, a possible explanation for the low $R^2$ value of $R^2 = 0.88$ is that the calibration task was performed by asking participants to select individual targets as opposed to performing a dragging task as performed during the experiment, thus causing the calibration to be inaccurate in filtering out finger input errors for a dragging task. Also, the $R^2 = 0.88$ value as found by Van Zon et al. [14] was expected to increase when decreasing the error rate. Even though the success rate in this experiment was $99.7\%$ as opposed to $95\%$ as found by Van Zon et al. [14], the $R^2$ values for $ID_e$ were similar at $R^2 = 0.88$, indicating the task accuracy does not improve the $R^2$ value and thus Fitts' law fit over the data. The conventional ID method is therefore chosen for the proposed extension of Fitts' law and Hypothesis 4 is rejected. An additional advantage in using the ID over $ID_e$ is that it is easier for interface designers to apply this version of Fitts' law, as no scaling for finger accuracy is required and the design of the screen interface can thus be evaluated directly.

### *C. Continuous touch data*

Evaluating the path length the finger has travelled across the screen gives an insight into the influence of atmospheric turbulence disruptions on touchscreen inputs. However, to determine the consequences, more than the average extension of path lengths is required, as the increased MT is an important characteristic to combine with the path lengths when determining the usability of a touch-based interface. In the case of the example shown in Fig. 5, the recorded MT was $2.4$ [s], well above the average value for the highest ID. The recorded overall turbulence disturbance during the task had a magnitude of $0.38$ $[\frac{m}{s^2}]$, which is in between the average medium and

low turbulence magnitudes shown in Table I. However, the turbulence disturbance contained a high acceleration in x-direction of $0.26$ $[\frac{m}{s^2}]$, which is about twice as high as the average acceleration in x-direction for the severe turbulence profile, as can be seen in Table I.

In Fig. 5, an example is shown of the influence a patchy atmospheric turbulence disturbance can have on operating a touch-based interface, even though it might not be as visible in the averaged data shown in the Fitts' law figures or the total average increase in path lengths. Individual cases can occur containing disturbances that severely impact the use of a touch-based interface. The data in Table V on itself do not offer a concluding answer on the usability of a touchscreen, it does show clearly that the path from object to target increases along with the atmospheric turbulence intensities. Hypothesis 5 can therefore be accepted.

The data shown in Table V also reveal a difference in additional path lengths for push tasks, which is the case when the object is moved away from the operator towards the target, when compared to pull tasks, when moving the object towards the operator. The significant difference of a percentage point for zero and low turbulence and almost 3 percentage points for medium and severe turbulence can be explained by the fact that the operator can see the target when pulling as opposed to pushing, where the target is easily overshot. Also, participants indicated that pushing a target on a touchscreen was more difficult than pulling a target, as more force was applied to the finger on the screen, making it more difficult to accurately operate the screen. The general increase in path lengths along with the increase in turbulence disturbance can also be seen, as the increase starts at $7.8\%$ for zero turbulence disturbance, and ends up at $11.8\%$ path length increase. Further to the extended path length, the quantitative non-linearity of the paths taken across the screen can be analysed [17], offering an insight into the BDFT experienced by the operator.

Logging the continuous touch input trajectories offers an opportunity at quantifying the disturbance from the atmospheric turbulence on the screen input. In order to do so, the quantitative non-linearity is used [17]. By taking the rms value of the distance between the finger input trajectory and the shortest path between the object and the target, the influence of the four turbulence levels on the wobbliness of the finger input can be determined. The quantitative non-linearity of the finger input is shared both for varying turbulence levels as for separate push and pull tasks. It can be seen that the average quantitative non-linearity, for all conditions, for the severe turbulence case is $19\%$ higher than that in the stationary environment. This indicates the severe level of turbulence negatively influences the performance on the dragging task and increases the wobbliness of the input signal.

The quantitative non-linearity, for maximum target distance A and minimum target size W, for medium turbulence level indicates a decrease in non-linearity of $7.6\%$, when compared to the stationary scenario. This could be caused by the fact that participants stiffen up for increasing levels of turbulence, steadying their hand, up to a certain level, as for the severe level of turbulence this can no longer be held up, indicated by the high increase of quantitative non-linearity of $11.2\%$, when compared to the no motion case. Furthermore it is interesting to analyse the difference between the push and pull values of quantitative non-linearity. The average value for a pull task is $5.1\%$ higher than that of a push task. This indicates the pull tasks have a larger deviation from the ideal line when compared to push tasks. Comparing this with the average path length increase data confirms that push tasks accurately follow the ideal line towards the target, but overshoot it, whereas pull tasks are more accurate in selecting the target but do so with a larger deviation from the ideal line, i.e., with a larger curvature.

### *D. Recommendations*

Overall, despite recording the continuous touch data of the input on the touchscreen, this research has not focused on combining the Fitts' law data with the BDFT cancellation work as performed by [9] and [10]. Combining the data could yield a more accurate predictive tool as it is better understood what the influence of turbulence is on the actual inputs on the touch-based interface, potentially creating a predictive cancellation of false inputs.

Also the research could be conducted with an increased realism of both the task and the turbulence profile. Increasing the level of realism in the task by using an actual navigation display interface would demonstrate task generalisability as the proposed Fitts' law model could be used to predict for weather avoidance tasks such as performed by Van Zon [30].

The atmospheric turbulence could be varied in a follow-up experiment to demonstrate the turbulence generalisability of the proposed Fitts' law extension. The turbulence could be varied by comparing both a patchy to a non-patchy atmospheric turbulence profile. Furthermore the turbulence could be varied within a single run, as opposed to having a run per turbulence magnitude, further adding to the unpredictability of the turbulence disturbance.

Further increasing the realism of the experiment also offers the possibility of looking into the human factors further. Having a broader set of participants could demonstrate the generalisability of the Fitts' law further and could tailor the Fitts' law coefficients to individuals specifically. Having personalised Fitts' law coefficients would facilitate research into pilot behaviour and performance for instance in circumstances where they are warned about the atmospheric turbulence versus when it comes as a total surprise. The effects of fatigue could then be analysed as well, both for a short patch of turbulence at the end of a long flight, or finding out the change in pilot performance when under a continued turbulence disturbance.

## VI. Conclusion

To fill the gap in existing literature this paper has described the development of a predictive model describing the usability of touch-based interfaces under four levels of atmospheric turbulence. To do so, Fitts' law has been extended, based on earlier work by Coutts' et al. [15]. Two Fitts' law models have

been compared, Finger Fitts' law [13] and the conventional Fitts' law in Shannon form [20].

An extension of Fitts' law is proposed that incorporates the influence of atmospheric turbulence in the Fitts' law coefficients and that has an effective index of difficulty $\mathrm{ID}_e$ in the dual distribution hypothesis form as found in Finger Fitts' law [13]. The $\mathrm{ID}_e$ is evaluated in an experiment against the Shannon form ID for comparison. The conventional $a$ and $b$ coefficients of Fitts' law are split up into four new coefficients, $a$, $b$, $c$ and $d$, where the new $a$ and $b$ coefficients resemble the conventional Y-intercept $a$ coefficient and the new $c$ and $d$ coefficients represent the conventional slope $b$. This method of determining the values of the coefficients starts with the conventional coefficients $a$ and $b$ of Fitts' law as found in a stationary condition and uses these values for $a$ and $c$, respectively, in the proposed extension before separately adding the influence of atmospheric turbulence through multiplying coefficients $b$ and $d$ with the turbulence magnitude $V$. $V$ resembles the root mean square (rms) value of the magnitude of atmospheric turbulence accelerations in x, y and z direction of the body frame of reference of the aircraft as measured in the cockpit.

The novel model has been evaluated in an experiment in a motion based simulator where participants were asked to perform 192 dragging tasks on a touch-based interface under four levels of atmospheric turbulence, ranging from no to severe atmospheric turbulence, ranging in magnitude from $V = 0$ $[\frac{m}{s^2}]$ to $V = 0.26$ $[\frac{m}{s^2}]$, $V = 0.52$ $[\frac{m}{s^2}]$ and $V = 0.78$ $[\frac{m}{s^2}]$ and with tasks ranging over an ID range of [1.19-4.95].

It is found that the Shannon form of ID offers an average $R^2$ value of $R^2 = 0.95$ across the four levels of turbulence, whereas the proposed Fitts' law $\mathrm{ID}_e$ offers an $R^2$ value of $R^2 = 0.88$ across the four levels of turbulence. The conventional Shannon formulation is therefore selected as ID on the Fitts' law extension as it offers an $8\%$ closer fit on the experiment data.

Using continuous touch input data the trajectories of the participants' fingers across the touchscreen have been recorded. Comparing these trajectories has shown that the overall increase in path lengths has increased by $51\%$ from $7.8\%$ to $11.8\%$ path length increase when compared to the nominal object-target distance when comparing the no turbulence to the severe turbulence case. The quantitative non-linearity, defined as the root-mean-square of the distance from the finger trajectory to the shortest path from object to target, has increased by $19\%$ when comparing the zero turbulence case to the severe turbulence case. It also demonstrates that push tasks are prone to overshooting the target as opposed to more accurate pull dragging tasks. The continuous touch data further quantify the negative influence of atmospheric turbulence on the usability of touch based interfaces.

With the proposed Fitts' law model, interface designers can verify their designs to be usable under the four magnitudes of atmospheric turbulence. The predicted movement time can be found for a target size, ranging from $5$ [mm] to $35$ [mm] and distance, ranging from $45$ [mm] to $150$ [mm]. Combining the found MT with the required data throughput of the task offers an insight into the safety of the interface.

## REFERENCES


[1] H. Avsar, J. E. Fischer, and T. Rodden, "Designing touch screen user interfaces for future flight deck operations," in *2016 IEEE/AIAA 35th Digital Avionics Systems Conference (DASC)*, vol. 2016-Decem. IEEE, 9 2016, pp. 1–9. [Online]. Available: http://ieeexplore.ieee.org/document/7777976/

[2] A. Degani, E. A. Palmer, and K. G. Bauersfeld, ""SOFT" CONTROLS FOR HARD DISPLAYS: STILL A CHALLENGE," Tech. Rep., 1992.

[3] S. Kaminani, "Human computer interaction issues with touch screen interfaces in the flight deck," in *AIAA/IEEE Digital Avionics Systems Conference - Proceedings*, 2011.

[4] C. B. Watkins, C. Nilson, S. Taylor, K. B. Medin, I. Kuljanin, and H. B. Nguyen, "Development of touchscreen displays for the gulfstream G500 and G600 Symmetry™ flight deck," in *AIAA/IEEE Digital Avionics Systems Conference - Proceedings*, vol. 2018-Septe. Institute of Electrical and Electronics Engineers Inc., 12 2018.

[5] A. Cockburn, C. Gutwin, P. Palanque, Y. Deleris, C. Trask, A. Coveney, M. Yung, and K. MacLean, "Turbulent touch: Touchscreen input for cockpit displays," in *Conference on Human Factors in Computing Systems - Proceedings*, vol. 2017-May. New York, New York, USA: Association for Computing Machinery, 5 2017, pp. 6742–6753. [Online]. Available: http://dl.acm.org/citation.cfm?doid=3025453.3025584

[6] A. Cockburn, D. Masson, C. Gutwin, P. Palanque, A. Goguey, M. Yung, C. Gris, and C. Trask, "Design and evaluation of braced touch for touchscreen input stabilisation," *International Journal of Human Computer Studies*, vol. 122, pp. 21–37, 2 2019.

[7] S. Dodd, J. Lancaster, A. Miranda, S. Grothe, B. De Mers, and B. Rogers, "Touch screens on the flight deck: The impact of touch target size, spacing, touch technology and turbulence on pilot performance," in *Proceedings of the Human Factors and Ergonomics Society*, vol. 2014-Janua. Human Factors an Ergonomics Society Inc., 2014, pp. 6–10.

[8] R. Van Den Berg, "Investigating the Effects of Turbulence and Spatial Gesture Thresholds on Multi-Touch Interaction," *MSc Thesis*, 2014.

[9] X. R. Mobertz, D. M. Pool, M. M. Van Paassen, and M. Mulder, "A cybernetic analysis of biodynamic effects in touchscreen operation in turbulence." American Institute of Aeronautics and Astronautics Inc, AIAA, 2018.

[10] A. Khoshnewiszadeh, "Model-Based Mitigation of Biodynamic Feed through for Touchscreen Dragging Tasks in Turbulence," *MSc Thesis*, 2020.

[11] R. W. McLeod and M. J. Griffin, "Review of the effects of translational whole-body vibration on continuous manual control performance," *Journal of Sound and Vibration*, vol. 133, no. 1, pp. 55–115, 8 1989.

[12] P. M. Fitts', "THE INFORMATION CAPACITY OF THE HUMAN MOTOR SYSTEM IN CONTROLLING THE AMPLITUDE OF MOVEMENT 1," Tech. Rep. 6, 1954.

[13] X. Bi, Y. Li, and S. Zhai, *FFitts Law: Modeling Finger Touch with Fitts' Law*. CHI 2013: Changing Perspectives, Paris, France, 2013.

[14] N. C. van Zon, C. Borst, D. M. Pool, and M. M. van Paassen, "Touchscreens for Aircraft Navigation Tasks: Comparing Accuracy and Throughput of Three Flight Deck Interfaces Using Fitts' Law," *Human Factors*, vol. 62, no. 6, pp. 897–908, 9 2020.

[15] L. V. Coutts, K. L. Plant, M. Smith, L. Bolton, K. J. Parnell, J. Arnold, and N. A. Stanton, "Future technology on the flight deck: assessing the use of touchscreens in vibration environments," vol. Ergonomics, no. 62:2, pp. 286–304, 2018. [Online]. Available: https://doi.org/10.1080/00140139.2018.1552013

[16] G. A. J. Van de Moesdijk, "The description of patchy atmospheric turbulence, based on a non-gaussian simulation technique," Tech. Rep., 1975.

[17] K. Emancipator and M. H. Kroll, "A quantitative measure of nonlinearity," *Clinical Chemistry*, vol. 39, no. 5, pp. 766–772, 1993.

[18] R. W. Soukoreff and I. S. Mackenzie, "Towards a standard for pointing device evaluation, perspectives on 27 years of Fitts' law research in HCI," *Int. J. Human-Computer Studies*, vol. 61, pp. 751–789, 2004. [Online]. Available: www.elsevier.com/locate/ijhcs

[19] I. S. MacKenzie, "Fitts' Law as a Research and Design Tool in Human-Computer Interaction," *Human–Computer Interaction*, vol. 7, no. 1, pp. 91–139, 1992.

[20] I. S. Mackenzie, "A note on the information-theoretic basis for fitts' law," *Journal of Motor Behavior*, vol. 21, no. 3, pp. 323–330, 1989.
[21] I. S. MacKenzie and W. Buxton, "Extending Fitts' law to two-dimensional tasks," in *Conference on Human Factors in Computing Systems - Proceedings*. New York, New York, USA: Publ by ACM, 1992, pp. 219–226. [Online]. Available: http://portal.acm.org/citation.cfm?doid=142750.142794
[22] C. A. A. M. Van Der Linden, "DASMAT-Delft University Aircraft Simulation Model and Analysis Tool, A Matlab/Simulink Environment for Flight Dynamics and Control Analysis," Tech. Rep., 1998. [Online]. Available: https://repository.tudelft.nl/islandora/object/uuid%3A25767235-c751-437e-8f57-0433be609cc1
[23] H. L. Dryden, "A Review of the statistical theory of turbulence," Tech. Rep., 1942.
[24] J. C. Houbolt, *Dynamic response of airplanes to atmospheric turbulence including flight data on input and response.* National Aeronautics and Space Administration - Technical report, 1964.
[25] J. A. Mulder, J. C. van der Vaart, and M. Mulder, "Aircraft Responses to Atmospheric Turbulence," *Lecture Notes*, no. November, p. 447, 2016.
[26] R. Jacobson, "A novel Fitts' law: Evaluating touch-based flight deck interfaces in atmospheric turbulence," *MSc Thesis*, 2021.
[27] D. Nakamura, "Report of the PARC/CAST Flight Deck Automation WG," Tech. Rep., 2013.
[28] M. M. van Paassen, O. Stroosma, and J. Delatour, "DUECA - Data-driven activation in distributed real-time computation," in *Modeling and Simulation Technologies Conference*. American Institute of Aeronautics and Astronautics Inc., 2000.
[29] S. Vrouwenvelder, F. M. Postema, and D. M. Pool, "Measuring the Drag Latency of Touchscreen Displays for Human-in-the-Loop Simulator Experiments." AIAA Modeling and Simulation Technologies conference, 2021, pp. 1–10.
[30] N. C. M. van Zon, "Evaluation of a touch-based navigation display for lateral weather avoidance," *MSc Thesis*, 2017.

# II

# Literature Review

Note: This part has already been evaluated under the course: AE4020 - 'Literature Study'

# 2

# Atmospheric turbulence

In this first chapter of the literature review, atmospheric turbulence will be discussed. First in section 2.1 several turbulence profiles will be explained and their differences highlighted. It will be shown how altitude affects the type of turbulence aircraft can encounter and what type of turbulence is dominant at what altitude. Next, in section 2.2, the modelling of turbulence will be explained. Along with aircraft models it is shown how distinct turbulence scenarios can be simulated in a research simulator.

## 2.1. Description of atmospheric turbulence

In this section the concept of atmospheric turbulence is explained. First, in section 2.1.1, the separate velocity vectors will be shown that are used to break down perceived turbulence. These gust velocity vectors make it possible to analyse turbulence gusts and their impact on the aircraft dynamics. Next, the main driving phenomenon of turbulence, vertical stability, will be explained in section 2.1.2. Vertical stability refers to the root causes of an unstable layer of air, causing turbulence. It is caused by differences in the geometric and process temperature lapse rates of air as will be elaborated in section 2.1.2. Finally, section 2.1.3 explains what the impact of altitude is on the type of turbulence that can be encountered. It is shown how various altitudes have different types of atmospheric turbulence and thus also have different consequences for pilots.

### 2.1.1. Turbulence velocity vectors

To understand the behaviour of aircraft in turbulent air and subsequently the consequences turbulence may have on touchscreen use, first the turbulence itself must be analysed. As shown in fig. 2.1, [30], atmospheric turbulence creates a velocity field, which, once coupled with the dynamics of the aircraft, yields certain aircraft motions. These can then be studied to see the influence of atmospheric turbulence on, for example, the use of touchscreen interfaces in the cockpit. However, before the aircraft dynamics can be incorporated, the velocity field of the atmospheric turbulence should be understood. To analyse an aircraft flying through atmospheric turbulence, the velocity components of that turbulence are often split into three separate perpendicular vectors, as is stated by Mulder et al. in [30]. These vectors represent a vertical gust velocity vector $\vec{w}_g$, positive upwards, a side gust velocity vector $\vec{v}_g$, positive to the left, and a longitudinal velocity vector $\vec{u}_g$, positive backwards, as seen from the pilot seat. Of these three vectors, two are of specific interest, the perpendicular vectors $\vec{w}_g$ and $\vec{v}_g$, as these gusts are normal to the flight path [30]. The vertical gust velocity vector $\vec{w}_g$ induces large normal aerodynamic forces on the aircraft as well as inducing pitching moments. The side gust velocity vector $\vec{v}_g$ causes forces on the vertical tail and the fuselage of the aircraft, these cause yawing and rolling motions. The longitudinal velocity vector has less of an effect on perceived motion of the aircraft, but is important in low level turbulence as these gusts influence the airspeed of the aircraft, so they should be taken into account when flying at low speeds [30].

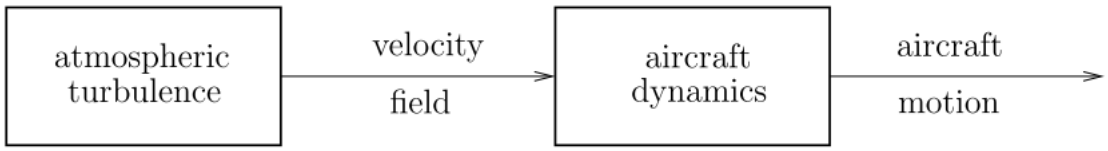


Figure 2.1: Breakdown of the flight in atmospheric turbulence problem [30]

### 2.1.2. Vertical stability

At different altitudes, different types of turbulence can be observed. To understand why there are such differences in turbulence, first the meteorological phenomenon that drives atmospheric turbulence will be explained shortly. The driving factor behind turbulence is vertical stability, which is for a large part driven by the geometric temperature lapse rate $\lambda$, shown in eq. (2.1) as is explained in [30].

$$\lambda = \frac{\Delta T}{\Delta h} \tag{2.1}$$

Where $\Delta T$ is the change in temperature in $[K]$ and $\Delta h$ the change in altitude in $[m]$. However, this is the geometric temperature lapse rate. When looking at a parcel of dry air in adiabatic ascent, the change of temperature rate is $\beta_{dry} = -0.0098^{\circ}/m$. For saturated air there is even a bigger difference, depending on the pressure and temperature, but the change of temperature rate can get as low as $\beta_{sat} = -0.0030^{\circ}/m$. Because there is this difference between the actual temperature lapse rate $\lambda$ and the geometric process lapse rate $\beta$, which is the change in temperature due to height differences when a parcel of air rises or descends, it is possible that pockets of air become unstable. This happens when $|\lambda| > |\beta|$, here the temperature lapse rate is higher than the geometric process lapse rate, meaning that an ascending parcel of air will cool down slower than the air around it. This means that the parcel of air will have a higher temperature than the surrounding air after a similar rise in altitude. As there is no pressure difference between the surrounding air and the parcel of air, the density of the parcel of warmer air will be lower, causing the pocket of air to float on the surrounding air, thus creating an upward movement and an unstable situation. The temperature difference is shown in eq. (2.2).

$$T' = T_0 + \beta \cdot \Delta h > T_0 + \lambda \cdot \Delta h \tag{2.2}$$

If $|\lambda| < |\beta|$, the inverse happens and the buoyancy of air is negative so the parcel would want to return to its original position, making it a stable situation. These conditions for vertical stability can be summarised according to fig. 2.2. It shows that if $\lambda$, the geometric lapse rate, which is the relationship between the change in altitude and the change in temperature as depicted in fig. 2.2, lies to the right of $\beta_{sat}$, the atmosphere is absolutely stable. If it lies in between of $\beta_{dry}$ and $\beta_{sat}$ it is conditionally stable, and if it lies to the left of $\beta_{dry}$ it is absolutely unstable. If the air is conditionally stable, the air is stable if it is not saturated and unstable if it is saturated.

### 2.1.3. Atmospheric turbulence at various altitudes

Different altitudes generally contain different types of turbulence, as they are caused by different reasons [30]. Near the ground the effect of windshear is dominant. Windshear is caused by the mechanical friction between layers of air and is indicated by the rate of change in the velocity vectors of turbulence as shown in section 2.1.1. Higher up, in clouds, the process explained in section 2.1.2 takes place. Inside cumulus clouds the air is saturated and thus unstable. Turbulence in clouds is made worse if the cloud produces precipitation. These downdrafts of water cause friction which adds to the turbulence in the cloud. Generally above the clouds at altitudes of around $10,000$ to $12,000$ $[m]$ there is clear air. If this clear air contains turbulence, this is called clear air turbulence. Clear air turbulence is used to describe the form of turbulence that can be found at high altitudes, away from the ground, out of clouds and in free atmosphere. At this altitude strong winds cause turbulence due to the mechanical friction between the layers of air, also the air is adiabatic and thus the air is not stable enough to offset the turbulence caused by the mechanical friction of wind. Therefore, both windshear turbulence as well as vertical stability induced turbulence occur for different reasons and mainly at different altitudes, but they can also be present simultaneously. The interaction of both kinds of turbulence can be shown

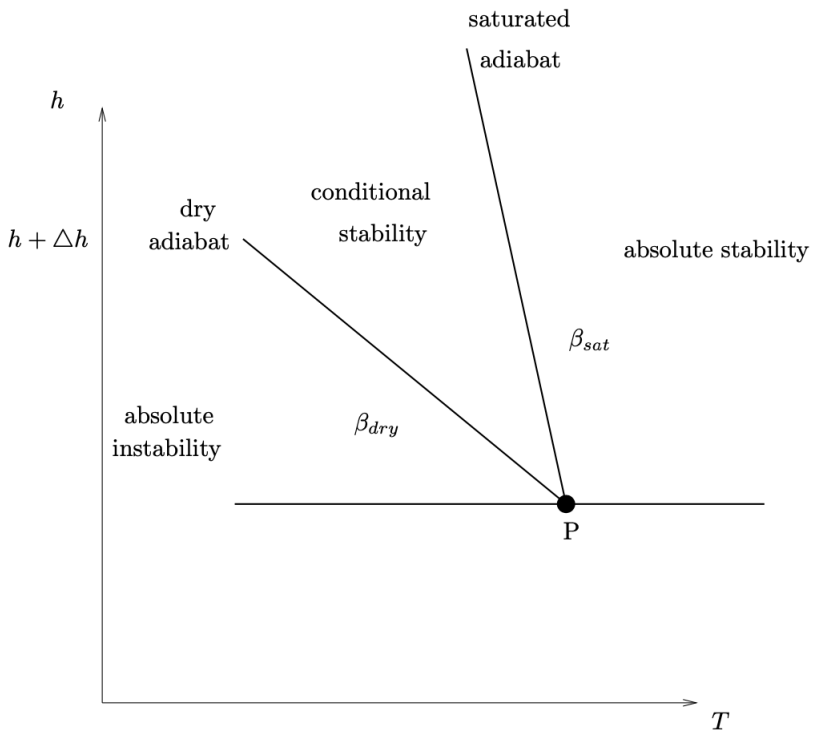


Figure 2.2: Vertical stability criteria, as shown in [30]

through eq. (2.3), which shows the Eddy energy equation, detailing the contributing factors to the total turbulent kinetic energy.

$$\frac{\delta E}{\delta t} = S + H + B - D \tag{2.3}$$

In eq. (2.3), $E$ is the turbulent kinetic energy, $S$ is the positive term related to vertical windshear, $H$ is the positive term related to horizontal windshear, $B$ is a term related to the stability of the air and $D$ is a term related to the rate at which turbulent energy is transformed to heat. $B$ has a positive value for unstable air and a negative value for stable air. $D$ is always positive and is dependent on the amount of turbulent kinetic energy.

## 2.2. Turbulence and aircraft models

In this section the steps taken towards modelling the actual turbulence and its impact on aircraft will be shown. First in section 2.2.1, the governing covariance matrix will be shown in eq. (2.5). Next, the assumptions made to simplify the model are shown. The trade-off between the Dryden and Von Karman functions will be shown next, explaining why the Dryden functions will be used to model the atmospheric turbulence. Finally in section 2.2.4 a short description will be provided on the aircraft model that will be used for the experiment.

### 2.2.1. Modelling atmospheric turbulence

Atmospheric turbulence is a random process that describes the chaotic motion of the air [39]. Before a random process like turbulence can be modelled, several assumptions are made. These assumptions break down the complexity of the problem and lead to significant simplifications in modelling turbulence [30], [39].

Firstly though, a general statistical description of turbulence should be given. when analysing turbulence, the total velocity field of the atmosphere is taken into account. Specifically for turbulence, the variations to the mean velocity matter, therefore the mean value is taken out of consideration by taking an atmospheric frame of reference $F_a$, relative to which the mean motion is zero [30]. This leaves the

velocity vector that is variable in both space and time. At location $\underline{r} = (x_1, x_2, x_3)^T$ and time $t$, the velocity vector is found in eq. (2.4).

$$\underline{\overline{u}}(\underline{r}, t) = (\overline{u}_1, \overline{u}_2, \overline{u}_3)^T \tag{2.4}$$

The vector $\underline{\overline{u}}(\underline{r}, t)$ is a random function in both space and time, composed of three elements, each with four variables, $(x_1, x_2, x_3, t)$. When dealing with such a function, the both the scalar time separation $\tau$ and the three-dimensional separation vector $\underline{\xi} = (\xi_1, \xi_2, \xi_3)^T$ are taken into account. The covariance matrix shown in eq. (2.5), shows that both the scalar time separation $\tau$ as well as the three-dimensional separation vector $\xi$ are present in the modelled turbulence, before assumptions, making the modelling of atmospheric turbulence a multivariable multidimensional problem [30].

$$\begin{aligned} &C_{\underline{\bar{u}}\underline{\bar{u}}}(\underline{r}, t; \underline{r} + \underline{\xi}, t + \tau) = E\{\underline{\overline{u}}(\underline{r}, t) \cdot \underline{\bar{u}}(\underline{r} + \underline{\xi}, t + \tau)\} = \\ &= \begin{bmatrix} E\left\{\bar{u}_1(\underline{r}, t) \cdot \bar{u}_1(\underline{r} + \underline{\xi}, t + \tau)\right\} & E\left\{\bar{u}_1(\underline{r}, t) \cdot \bar{u}_2(\underline{r} + \underline{\xi}, t + \tau)\right\} & E\left\{\bar{u}_1(\underline{r}, t) \cdot \bar{u}_3(\underline{r} + \underline{\xi}, t + \tau)\right\} \\ E\left\{\bar{u}_2(\underline{r}, t) \cdot \bar{u}_1(\underline{r} + \underline{\xi}, t + \tau)\right\} & E\left\{\bar{u}_2(\underline{r}, t) \cdot \bar{u}_2(\underline{r} + \underline{\xi}, t + \tau)\right\} & E\left\{\bar{u}_2(\underline{r}, t) \cdot \bar{u}_3(\underline{r} + \underline{\xi}, t + \tau)\right\} \\ E\left\{\bar{u}_3(\underline{r}, t) \cdot \bar{u}_1(\underline{r} + \underline{\xi}, t + \tau)\right\} & E\left\{\bar{u}_3(\underline{r}, t) \cdot \bar{u}_2(\underline{r} + \underline{\xi}, t + \tau)\right\} & E\left\{\bar{u}_3(\underline{r}, t) \cdot \bar{u}_3(\underline{r} + \underline{\xi}, t + \tau)\right\} \end{bmatrix} \end{aligned} \tag{2.5}$$

To simplify the covariance matrix as shown in eq. (2.5), the following assumptions are made, that lead to calculation simplifications as the problem will no longer be multivariable and multidimensional.

1. **Atmospheric Turbulence is a random process with a Gaussian distribution.**
   Even though in reality atmospheric turbulence has been found to not necessarily be Gaussian distributed, research has shown it to be a viable assumption [39]. Even though this assumption does not affect the way the turbulence is represented by the covariance and PSD functions, it does make a large difference as by assuming a Gaussian distribution the covariance matrix of atmospheric turbulence alone is enough to represent a full statistical description of atmospheric turbulence.

2. **Atmospheric Turbulence is a stationary process**
   This assumption is based on the magnitude difference between the turbulence velocity vectors as shown in section 2.1.1 and the velocity vector of the aircraft traversing the turbulence. As the aircraft is flying at a much higher velocity than the turbulence velocity vectors, the aircraft is able to traverse a large amount of turbulence in a short time, thus allowing the turbulence velocity vectors hardly any time to change which leads to the assumption that they do not change. What this means is that the input $t$ can be left out of the general matrix of covariance functions.

3. **Atmospheric Turbulence is homogeneous along the flight path**
   When flying at high altitude, the turbulence encountered occurs in various large patches which can each be assumed to be homogeneous, even though there might be differences between the patches. As a consequence of this assumption the covariance and spectral density matrices no longer depend on $\bar{r}$. When turbulence is both stationary and homogeneous it is also ergodic, which means that time averages may replace ensemble averages.

4. **Atmospheric Turbulence is an isotropic process**
   The isotropic process assumption indicates that the three mean-square (variance) atmospheric turbulence velocity vectors as indicated in section 2.1.1 are all equal. This is because at high altitudes, near the Earth's boundary layer, the statistical properties of atmospheric turbulence are independent of their axes. The variance at high altitudes typically has a value of around $\sigma^2 = 1\frac{m^2}{s^2}$ [39].

Having a simplified problem allows for modelling of the turbulence, this can be done via the Von Karman [44] and Dryden spectra [16], that look at the spectral density properties of the turbulence signal.

### 2.2.2. Dryden spectra

Using the assumptions from section 2.2.1, several analytical functions to model the turbulence spectra can be used. Both the Von Karman, [44], [45], and Dryden [10] functions yield spectra that fit the experimental and theoretical data of atmospheric turbulence quite accurately. Even though the Von Karman functions seem to fit the data slightly more accurate than the Dryden functions, specifically at higher frequencies, both in the longitudinal and lateral spectrum [30], in this research the Dryden functions are used. This is done because the Dryden functions are rational spectral density functions and the Von Karman functions are not, which means the Dryden functions greatly simplify the calculations, whilst maintaining the same low-frequency asymptote as the Von Karman spectal densities, as can be seen in fig. 2.3, [30], [16].

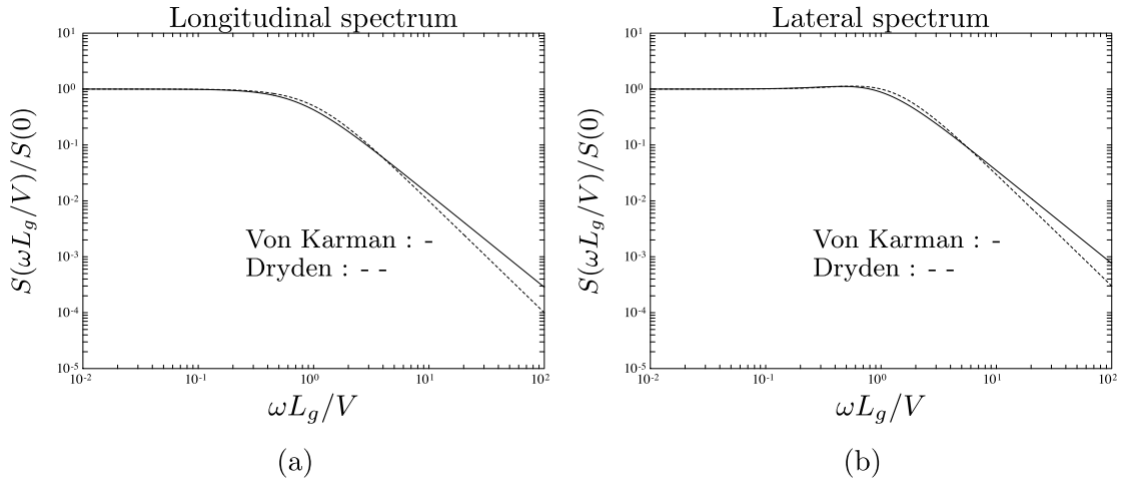


Figure 2.3: a) The longitudinal spectrum, b) The lateral spectrum [30]

The Dryden spectra can be seen below, in eq. (2.6).

$$
\begin{aligned}
S_{\tilde{u}_g\tilde{u}_g}(\omega) &= 2\sigma^2 \frac{L_g}{V} \frac{1}{1+\left(L_g\frac{\omega}{V}\right)^2} \\
S_{\tilde{v}_g\tilde{v}_g}(\omega) &= \sigma^2 \frac{L_g}{V} \frac{1+3\left(L_g\frac{\omega}{V}\right)^2}{\left[1+\left(L_g\frac{\omega}{V}\right)^2\right]^2} \\
S_{\tilde{w}_g\tilde{w}_g}(\omega) &= \sigma^2 \frac{L_g}{V} \frac{1+3\left(L_g\frac{\omega}{V}\right)^2}{\left[1+\left(L_g\frac{\omega}{V}\right)^2\right]^2}
\end{aligned}
\tag{2.6}
$$

Where $S_{\overline{xx}}$ represents the spectral density in $u, v, w$. The variance of the gust velocity is given by the term $\sigma^2$, $L_g$ is the integral scale of turbulence, $\omega$ is the circular frequency encountered at the aircraft's centre of gravity and $V$ is the aircraft velocity, [30].

### 2.2.3. Patchy atmospheric turbulence

The magnitude of atmospheric turbulence is not always constant over time and space. Areas containing significant levels of atmospheric turbulence may be followed by areas of less intense atmospheric turbulence. This phenomenon is called patchiness or intermittency [36]. Patchiness is characterised by the measured deviation from the normal (Gaussian) velocity distribution. A high deviation from the normal distribution, indicated by the fourth order central moment value or Kurtosis value, $K$, represents high patchiness in the atmospheric turbulence. Simulations of atmospheric turbulence are often modelled only on the spectral density values of the atmospheric turbulence, causing a rather stable and 'unsurprising' turbulence disturbance input. Adding patchiness to the turbulence input thus adds to

the startle effect pilots may experience when encountering atmospheric turbulence and thus adds to the accuracy in the conclusions drawn from simulator studies performed with atmospheric turbulence [36], [31]. A block diagram of the generation of a patchy atmospheric turbulence signal can be seen in fig. 2.4.

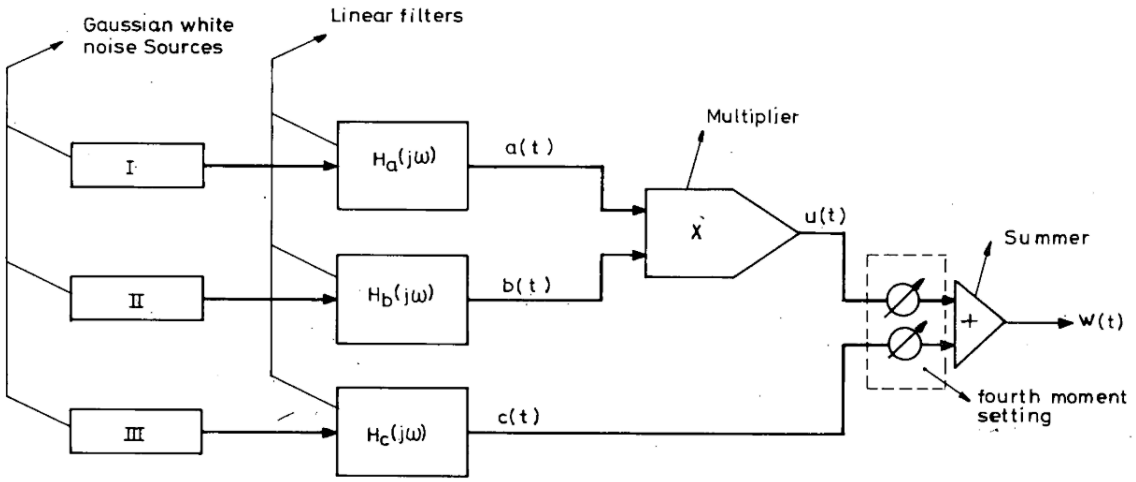


Figure 2.4: Block diagram representing the generation of a non-Gaussian patchy process having an arbitrary fourth order moment. [36]

The linear filters as indicated in fig. 2.4, are the Dryden spectra as discussed in section 2.2.2. The fourth order central moment value, or Kurtosis value, $K$, indicates the weight of the tails of the normal distribution. Values higher than 3 indicate heavy tails and thus a non-Gaussian distributed signal. The patchiness parameter $P$ indicates the amount of patchiness in the signal and is defined in eq. (2.7), [36], it increases as the Kurtosis value, $K$, increases from the value of 3.

$$P = \frac{\sigma_z^2(\tau)_{non-normal}}{\sigma_z^2(\tau)_{normal}} \tag{2.7}$$

In eq. (2.7), the time constant is indicated by $\tau$. The variance of the non-normal input signal $u(t)$, as shown in fig. 2.4, is indicated by $\sigma_z^2(\tau)_{non-normal}$ and the variance of the input signal $c(t)$, as shown in fig. 2.4, is represented by $\sigma_z^2(\tau)_{normal}$. A higher value for the patchiness parameter, $P$, therefore indicates the simulated atmospheric turbulence is less predictable to the pilot.

### 2.2.4. Aircraft model

To model how pilots are influenced in their performance on touch based interfaces due to the presence of atmospheric turbulence the modelled Dryden turbulence input should be fed through an aircraft model first, before the accelerations and rotations as experienced by the pilot in the cockpit can be reproduced [31], [38]. Van der Linden, [38], developed such an aircraft model, called the DASMAT software package. Delft University Aircraft Simulation Model and Analysis Tool (DASMAT) is designed around a nonlinear aircraft model which is available as a SIMULINK S-function, [38]. The dynamics of the DUT test aircraft, PH-LAB, a Cessna Citation 2, are simulated in DASMAT, [38]. DASMAT does not only model the aircraft dynamics but also offers the functionality of plotting the time responses of an aircraft simulation as well as fitting aerodynamic models. The DASMAT model can be used as input for the SIMONA Research Simulator (SRS), which is a full motion simulator an can in turn be used to verify the influence of turbulent environments on pilot behaviour, by both looking at BDFT, [20], and via the Fitts' law, [7]. As indicated by both Khoshnewiszadeh, [20], and Cockburn et al. [6], [5], the use of accurate turbulence models in combination with accurate aircraft models is imperative to accurately verifying the influence atmospheric turbulence has on the performance of pilots, despite it being more complex than using a sum of sines disturbance signal, [20].

## 2.3. Summary

In this chapter the phenomenon of atmospheric turbulence is explained. Understanding atmospheric turbulence is an important part of this research as it is imperative it is modelled correctly when validating and verifying the model describing the usability of touchscreens in atmospheric turbulence. As the proposed model is a first, when modelling the influence atmospheric turbulence has on the usability of touchscreens, an accurate verification and verification process is required before it can be used as a design tool for future touchscreens, for example. This is where the turbulence modelling comes in as it determines the setting in which test pilots will be evaluated using a touch based interface, which in turn will be used to verify whether or not the model is accurate. Validation of the turbulence as modelled in the simulator will be done by interviewing pilots that have extensive experience in the aircraft model the experiment will be performed in, this will be detailed further in part III. The turbulence velocity vectors as described in section 2.1.1 are important as they are used when programming the SIMONA research simulator, in which the experiments as detailed in part III will take place. Vertical stability and the explanation of turbulence at various altitudes as shown in section 2.1.2 and section 2.1.3, respectively, are important as they influence the type of turbulence experienced by the aircraft based on the initial conditions and assumptions in which the experiment is to take place. Specifically they are influenced by the altitude the aircraft will fly at during the experiment. Next, in section 2.2, the details associated with modelling turbulence are shown. Specifically the four assumptions that are made here along with the fact that Dryden modelling is used in the simulation are of significant importance. Also it is shared that the aircraft model that is used will be the model of the Cessna Citation II test aircraft of the Delft University of Technology (PH-LAB) will be used when modelling the aircraft behaviour. The patchy turbulence modelling is used in order to keep the turbulence surprising to the pilots operating the touchscreens on the flight deck. If the turbulence is not patchy enough, pilots can brace themselves, locking out BDFT for a large part and thus causing unrealistic results, [36]. As accurate turbulence models are used in the verification of the extension of Finger Fitts' law, it is equally important to use an accurate aircraft model, accurately translating the accelerations the aircraft experiences around its centre of gravity towards the accelerations and rotations the pilots experience in the cockpit of the aircraft. To model the translations of these accelerations the DASMAT model is used. The combination of accurate patchy Dryden atmospheric turbulence inputs and an accurate aircraft model driving a full motion simulator, such as the SIMONA Research Simulator yield an accurate representation of the flight deck of the Cessna Citation II in real life atmospheric turbulence.

# 3

# Fitts' law

In this chapter the concept of a speed-accuracy trade-off in input tasks will be explained. First in section 3.1, the governing equation as found by Fitts, [11], will be explained. The relevance and various extensions to Fitts' law will be shown in section 3.2 along with some of their use cases, including finger Fitts' law in section 3.2.2. Next, in section 3.2.3 the current use of Fitts' law and its extensions in motion environments will be discussed. Finally, in section 3.3 the key takeaways from the chapter will be given as well as a recap of the parts of Fitts' law that will be used in the proposed research.

## 3.1. Fitts' law

The first to capture the speed-accuracy trade-off in an equation and accurately predicting the time it would take to select a target of a certain size was Fitts, [11]. Fitts found the relationship between both target size and target distance on one hand and the time it takes to select the target on the other, and called it Fitts' law [11]. In other words Fitts' law is a human performance model that relates the time it takes to reach a certain target, the Movement Time (MT), to the associated difficulty of selecting the target, the Index of Difficulty (ID), as shown in eq. (3.1).

$$MT = a + b \cdot ID \tag{3.1}$$

Where the coefficients $a$ and $b$ are found empirically to fit the relation between the measured MT in $[s]$ and calculated ID in $bit$. They indicate the efficiency of the system and thus the ease of use when selecting a target. The following binary index of difficulty was proposed by Fitts [11], as can be seen in eq. (3.2).

$$ID = \log_2\left(\frac{2A}{W}\right) \tag{3.2}$$

Where $W$ is the tolerance range and $A$ is the average amplitude of the particular class of movements, or in other words, $W$ is the target size and $A$ is the distance from the target. The Index of difficulty is expressed in bits of information, thus allowing for a $[bit/s]$ evaluation. In later research such as in [22], [4], [3] the ID as proposed by Fitts has been used in a slightly different form, called the Shannon form. It was first proposed in [23], as shown in eq. (3.3).

$$ID = \log_2\left(\frac{A}{W} + 1\right) \tag{3.3}$$

The Shannon formulation is used mainly in modern literature as it only provides positive values of ID and it fits the information theory governing the equation better [23]. In general, it can be said that Fitts' law is a way of displaying the speed-accuracy trade-off that is faced when selecting a target. The larger the target and the closer it is, the easier and thus faster it is to select that target. The smaller and further away the target is, the longer it takes to accurately select the target, thus creating a trade-off between speed and accuracy or as expressed in Fitts' law in eq. (3.1), Movement Time and Index of Difficulty. The first Fitts' law was found when selecting tangible items in one dimension [11], but as will

be shown in section 3.2, there are many extensions to Fitts' law, making it applicable to many platforms that require a speed-accuracy trade-off.

## 3.2. Fitts' law extensions

Fitts' law has been used in many different circumstances and has been shown capable of being tailored towards many specific situations. Examples include an extension towards $2D$ pointing tasks [25] and towards the use of touchscreens in [3]. Both will be detailed in section 3.2.1 and section 3.2.2, respectively. However, the extensions of Fitts' law do not end there, as over the years there have been many more extensions to Fitts' law, incorporating use of for instance: keypads [48], rotational tasks [34], capture of moving targets [17], [14] and even shrinking targets [15], and many more. In this section, however, the focus will lie on the extension from $1D$ to $2D$ pointing tasks and the extension towards Finger Fitts' law [3], encompassing the use of touchscreens.

### 3.2.1. Fitts' law for two-dimensional tasks

Before the more detailed use case of touchscreens can be assessed, first the basic extension from Fitts' original one-dimensional task towards the more widely used two-dimensional pointing task should be known. The first to extend Fitts' law to two-dimensional tasks were MacKenzie and Buxton, [25]. In their research they propose two models to test against the "STATUS-QUO" model, in which $W$ is always the horizontal extent of a target. The first one is the "$W'$- MODEL", or "$W$-prime" model, in which they replace the $W$ as found in the original Fitts' law in Shannon form as shown in eq. (3.3), by $W'$, which represents the actual target size, when taking into account the angle $\theta_A$ the target is approached from and thus the length of the approach vector. By doing so it effectively allows a one-dimensional approximation of a two-dimensional scenario. A schematic of the new situation, displaying $W'$ is shown in fig. 3.1. This model, however, has a drawback in that it requires knowledge of $A, W, H$ and $\theta_A$ as well as a geometric calculation, before $W'$ is found.

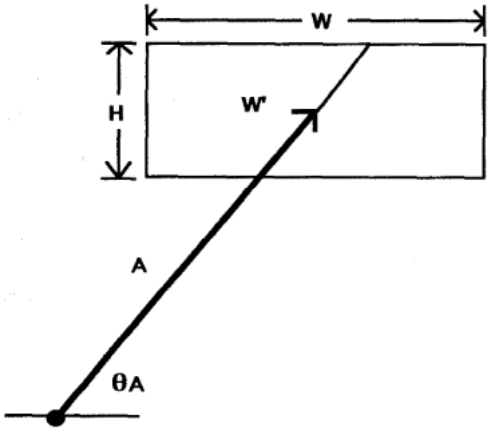


Figure 3.1: W', showing the length of the approach vector, [25]

The other model as proposed by MacKenzie and Buxton, [25], is called the "SMALLER-OF" model. It has the benefit over the $W'$-model, that it does not require any knowledge of the target angle $\theta_A$. It is more intuitive to use therefore as it just assesses what the smallest dimension of the target is, which then becomes the target axis against which the speed-accuracy trade-off is evaluated. These two proposed models have been among the first extensions of Fitts' Law to incorporate evaluation of a two-dimensional target [25], thus paving the way for future more specific extensions of Fitts' Law, such as the Finger Fitts' Law as is elaborated in the next section, section 3.2.2.

### 3.2.2. Finger Fitts' law

A specific extension of Fitts' law was published in 2013 by Bi et al. [3], in which Fitts' law was extended to model the use of touch-based displays. Here, the touch input is split up into two specific distributions, called "the dual-distribution hypothesis". The dual-distribution hypothesis states that the distribution of end points as found when using a touch-based interface is the sum of two independent normal

distributions. The first one shows the distribution of touch points based on the basic speed-accuracy trade-off as performed by the human motor system of the operator, basically the point the operator aims at and tries to select. The second one depicts the distribution of touches as the absolute precision of the input finger not taking the speed-accuracy trade-off into account, basically showing the error a finger has when trying to select a target. Further on in [3], Fitts' law is successfully expanded to include the dual-distribution hypothesis and thus to form Finger Fitts' Law, as seen in eq. (3.4).

$$MT = a + b \cdot \log_2 \left( \frac{A}{\sqrt{2\pi e(\sigma^2 - \sigma_a^2)}} + 1 \right) \tag{3.4}$$

Where $a, b$ and $A$ are the same as in the original Fitts' law, as shown in eq. (3.1) and eq. (3.3). Furthermore, $\pi$ and $e$ represent the number pi and Euler's number $e$, respectfully. Next, $\sigma^2$ and $\sigma_a^2$ indicate the variance of the location of touch of the pilot on the screen and the error from the target, respectively. Finger Fitts' law, or FFitts' law for short, as shown in eq. (3.4) shows several noticeable changes in the Index of Difficulty when compared to Fitts' law in its conventional Shannon formation, as found in eq. (3.3). The first difference is that the effective width, $W_e$, is used instead of $W$. When comparing eq. (3.4) with eq. (3.3), it can be seen that the denominator of the ID in eq. (3.3) is the target width, $W$. In eq. (3.4), the denominator in the ID is a normalised effective width, called $W_e$. The effective width has been used in previous literature, [24], [47], where it is defined as $W_e = \sqrt{2\pi e}\sigma$. As also explained in [3], the effective width allows the incorporation of the full variability in endpoints, as they are normally distributed over the target centre. In [3], the variability of the endpoints is split up into the variance of the distribution of the location that is actually touched by the pilot operating the screen, $\sigma$ and the variance of the distribution of the error induced by the inaccuracy of using a finger as a pointing device, $\sigma_a$. Where $\sigma_a$ is typically found by asking pilots to select targets on a touch-based interface without adding a time limit for the selection [41], thus eliminating the speed-accuracy trade-off and finding an accurate variance on the error that occurs when using fingers as input device. The FFitts' law was originally designed for hand-held touch-based devices, however, Van Zon et al. [40], [41], has demonstrated its functionality when applied to a touch-based navigation display on a flight deck.
Finger Fitts' law has not yet been evaluated for use in a turbulent environment, such as when used in atmospheric turbulence on the flight deck. Before FFitts' law can be evaluated in turbulent environments, first the general applicability of Fitts' law in motion environments should be researched. This is shown in the next section, section 3.2.3.

### 3.2.3. Fitts' law and motion

Adding motion to Fitts' law has been a large step in extending Fitts' law further. There has not yet been a lot of research into incorporating motion into Fitts' law. First, the Fitts' law extensions that incorporate moving targets will be discussed after which the Fitts' law extensions for operation in a moving environment will be shown. The research into Fitts' law extensions incorporating the effects of moving targets is relevant for this thesis as it was the first research that added the effects of motion into the speed-accuracy trade-off [17]. Even though selecting a moving target from a stationary environment is the inverse of selecting a stationary target from a moving environment, it offers many lessons towards incorporating motion into Fitts' law, as shown below.

#### Moving target selection

Jagacinski, [17], was the first to research the applicability of Fitts' law on moving target selection. He found that the conventional Index of Difficulty by Fitts' law offered a bad fit on the data from moving target selection. He proposed an alternative to the conventional Fitts' law, shown in eq. (3.5), including a term for the constant velocity at which the target moves, $V$. In his equation $A$ and $W$ were similar to the original Fitts' law as found in eq. (3.1), however, $A$, $W$ and $V$ are expressed in degrees of visual angle. Furthermore, $c, d$ and $e$ are regression coefficients.

$$MT = c + dA + e(V + 1)\left(\frac{1}{W} - 1\right) \tag{3.5}$$

Hoffmann, [14], continued the research into capturing moving targets in which he proposed three extensions to Fitts' law. A first and second order control-system model were proposed along with a two component model. Hoffmann, [14], also uses the constant velocity $V$ in his models and introduces a

gain constant $K$ which is to be determined empirically. For the two component model the initial distance covering phase, following coefficient $b$ and the accuracy phase, following coefficient $c$, were split up, as seen in eq. (3.6). Where $a, b$ and $c$ are regression constants to be determined empirically and $A$ and $W$ are the same as in the original Fitts' law, eq. (3.1).

$$MT = a + b \cdot log_2\left(A + \frac{V}{K}\right) - c \cdot log_2\left(\frac{W}{2} + \frac{V}{K}\right) \tag{3.6}$$

The results of Jagacinski, [17], and Hoffmann, [14], have been used by Al Hajri et al. [1], to refine the Index of Difficulty for moving target selection even further. It has been extended further to include the two-dimensional target velocity vector, by breaking up $V$ into $V_x = Vcos(\theta)$ and $V_y = Vsin(\theta)$. This resulted in the following Index of Difficulty, as seen in eq. (3.7)

$$ID = log_2\left(\sqrt{f_W(\theta)\left(\frac{D \pm \frac{V_x}{K}}{\frac{W}{2} - \frac{V_x}{K}}\right)^2 + f_H(\theta)\left(\frac{D \pm \frac{V_y}{K}}{\frac{H}{2} - \frac{V_y}{K}}\right)^2} + 1\right) \tag{3.7}$$

Where $f_W$ and $f_H$ are empirically determined weighting parameters for each component in the weighted Euclidian model, [1]. The other component that is empirically determined is $K$, which serves as the coefficient that determines the target velocity above which there is no successful selection possible [4], [1], [14]. The coefficient $D$ acts as the coefficient $A$ in the conventional Fitts' law, eq. (3.1), and quantifies the distance from the target, $W$ and $H$ represent the horizontal and vertical target size, respectively. The $\pm$ sign indicates whether the target is approaching $(-)$ or moving away $(+)$ from the indicator, as was the case during the experiment validating the extension of Fitts' law, [14].
The previous extensions of Fitts' law by Jagacinski, eq. (3.5), [17], Hoffmann, eq. (3.6), [14] and Al Hajri et al. eq. (3.7), [1], have several important aspects in common which make them both useful for this thesis' research, but also mean some are not directly implementable. Four aspects will be highlighted below.

- The first is that all of them return to the original Fitts' law when the target is stationary. This is an important, useful, aspect as it makes their respective Fitts' law extension very useful and robust, even for situations in which there is both a moving and a stationary target. This is important to include in the research of this thesis as it is the case for aircraft flying in and out of turbulence.

- The second, useful, lesson that can be drawn from the equations is the way they have evolved to increase a moving target in the Fitts' law extension more and more accurately. Jagacinski, [17], started off by just adding a single term for velocity in the index of difficulty in eq. (3.5). Next, Hoffmann, [14], added more detail by splitting up the two tasks into a distance covering phase and accurate phase, in eq. (3.6). Finally, Al Hajri et al went a step further by breaking up the target velocity into several components, more accurately describing the target velocity vector against the target size in that direction. These consequent increases in level of detail of Fitts' law extensions offer a good, and useful, indication for the approach of the research as proposed in this thesis and offer a good starting point for further research.

- The third, less useful, aspect is that the target is assumed to move at constant velocity in all three Fitts' law extensions. In this paper the research is focused on a turbulent environment, which thus implies that the velocity to be taken into account is never constant, and causes this important assumption not to hold in the scenario the research of this thesis is focused on.

- The fourth is that all three extensions include provisions to include a moving target scenario and not a moving environment scenario that includes a stationary target, which is what this research focuses on. The implication this has can be found in the fact that the three Fitts' law extensions as shown have all three only changed the Index of Difficulty and have ignored the scaling coefficients, rating how well the Index of Difficulty is accessible. Having a stationary target in a turbulent environment suggests that the Index of Difficulty of selecting the target itself does not change, however, it suggests a turbulent environment would make it more difficult to actually engage in

the speed-accuracy trade-off as portrayed by the Index of Difficulty. Therefore it is suggested a change should be made in the y-intercept coefficients $a$ and $b$, to include this increased difficulty in Fitts' law.

In the next part the specifics of the speed-accuracy trade-off in a motion environment will be further discussed, the main difference between the Fitts Law extensions regarding a moving target versus a moving environment will also be mentioned.

### Fitts' law in motion environments

Evaluating the speed-accuracy trade-off in a turbulent environment with a stationary target might seem similar to evaluating the speed-accuracy trade-off for a moving target in a stationary environment, but there are several differences, as will be shown in this section.
A recent extension to Fitts' law to include extraneous motion in an aerospace context was found by Coutts et al. in 2018, [7]. Here an additional term $V$ was added to the conventional Fitts' law y-intercept as found in eq. (3.1), representing the Root-mean-square (RMS) weighted value of the aircraft's turbulence accelerations in x, y and z-direction, respectively. Furthermore the button size and proximity were taken into account in similar fashion as done in eq. (3.2). The equation as published by Coutts et al. [7], is similar to eq. (3.1), however, the y-intercepts $a$ and $b$ were found to be as shown in eq. (3.8) and eq. (3.9), respectively. Unfortunately, Coutts et al. [7], only published the Fitts' law equation, thus leaving out an indicative graph into the influence of turbulence on the slope of the Fitts' law around the measured data.

$$a = -2.5 \cdot V - 0.56 \tag{3.8}$$

And similarly,

$$b = 0.88 \cdot V + 0.29 \tag{3.9}$$

These values were found by Coutts et al. [7], by plotting the empirically obtained values for the y-intercept coefficients $a$ and $b$, as found by performing the experiment, against the increasing levels of the RMS turbulence value $V$. To obtain the coefficients shown in eq. (3.8) and eq. (3.9), a least-squares fit was used.
Only incorporating the influence of atmospheric turbulence in the y-intercept part of Fitts' Law and not in the Index of Difficulty, as was done by Coutts et al. [7], suggests several things. Firsly, that the atmospheric turbulence only has an impact on the time it takes to perform a successful touch and that it has no influence on the difficulty of the speed-accuracy trade-off performed. Secondly, in a statement supported by Cockburn et al. [6], Coutts et al. [7], states that where turbulence increases, both the movement time and the amount of erroneous inputs increase. This would explain why the turbulence intensity term, $V$, is included in both the $a$ and $b$ coefficients, as the $a$ term describes the time before the selection action starts and $b$ indicates the share the Index of Difficulty plays in the overall movement time.

### Moving target versus moving environment

The difference between the two aspects of motion included in Fitts' Law lies in whether the target is moving or the surroundings of the person performing the speed-accuracy trade-off move. The consequence being that to include motion in Fitts' Law in the case of a moving target, the Index of Difficulty needs to be changed. Whereas in order to include a turbulent or moving environment the change to the original Fitts' Law should be in the y-intercept coefficients $a$ and $b$. The aspect both types Fitts' Law extension have in common is that they both return to the original Fitts' Law in case there is no motion. This ensures they are widely applicable as only a single formulation can be used to evaluate both moving and stationary situations.

## 3.3. Summary

In summary, it is shown that Fitts' Law offers a good model to approximate the speed-accuracy trade-off. Also, in section 3.2, it is shown that Fitts' Law offers a robust basis for extensions towards specific situations. This is important towards the research as proposed in this thesis, as it is what will be done to create a predictive model for the usability of touchscreens in atmospheric turbulence. Specifically the Finger Fitts' Law extension as shown in eq. (3.4) to the basic Fitts' Law is important in this thesis as it will form a basis for the new model for the usability of touchscreens in atmospheric turbulence. Next, in section 3.2.3 specifically the scenario of motion incorporated in Fitts' Law is explained. This comprises the other important step of the model that will be constructed to model the usability of touchscreens in atmospheric turbulence as it will be built up out of both Finger Fitts' Law and the inclusion of motion as proposed by Coutts et al. in [7], thus combining the accuracy of the Finger Fitts' Law model with respect to using a touch-based interface and the incorporation of atmospheric turbulence as done by Coutts et al. in their extension of the basic Fitts' Law. The details of the new model will be shown in the next part of this thesis, part III. It will be shown how the new model is constructed as well as showing steps towards validation and verification of the new model.

# 4

# Usability of touch based interfaces

As has been stated in the introduction, in chapter 1, the evolution of touch based interfaces on the flight deck has made a significant advance over the last couple of years. However, before touch based interfaces can be introduced in the aviation industry on a large scale and especially on primary flight displays, the major drawbacks should be analysed. One of the main concerns for the use of touch based interfaces is their usability in atmospheric turbulence [6], [28]. This chapter analyses what the pros and cons of using touch based interfaces are and focuses specifically on the influence of turbulence on involuntary body motions and further discusses the use of touchscreens on the flight deck in turbulent environments.

## 4.1. Advantages and disadvantages of touch based interfaces

Touchscreens have been around for quite some time, they were first introduced in the 60's by Johnson, [18], but saw their introduction to the general public much later with the launch of the first Iphone in 2007. With the familiarisation of the general public with touch based interfaces as means of controlling computers, the demand for further integration on the aircraft flight deck has come [46]. However, despite the many advantages introducing touch based interfaces to the flight deck may have, there are several serious drawbacks as well [19], [8]. Both will be discussed below.

### 4.1.1. Advantages touch based flight deck interfaces

The use of touchscreen interfaces has many advantages over conventional interfaces that require buttons or knobs to interact with a computer. An overview of advantages is presented below, [46], [19], [8], [29], [40], [37].

- Intuitive direct manipulation of information
- Variable interfaces allow for high information density
- Workload and operational effort are minimised
- Decluttering of interfaces allows for lower cognitive effort and higher operational awareness

The advantages presented above are some of the main arguments used in the introduction of touch based interfaces on the flight deck [35], [12], [46]. Also the general familiarisation of pilots with touch based interfaces as a result of experience in using touch based interfaces such as tablets or smart-phones offer an argument for the introduction of touch based interfaces on flight decks, [40]. Despite all the advantages, however, some significant disadvantages of touch based interaction with a computer remain.

### 4.1.2. Disadvantages touch based flight deck interfaces

Despite the advantages touchscreen interaction can offer, several drawbacks associated with the use of touchscreens should be taken into account, before they can be introduced on the flight decks of aircraft. Based on previous research, an overview of the identified drawbacks of using touch based interfaces in the cockpit of aircraft is presented below, [46], [19], [8], [29], [40], [37].

- The absence of buttons means there is no tactile feedback
- Necessity of navigation through menus before accessing information, both costing time and causing loss of muscle memory
- Glare effects, sunlight reflecting off the screen can cause the screen to become unreadable
- Environmental effects such as atmospheric turbulence can increase the accidental erroneous inputs

Of these drawbacks in the use of touch based interfaces as a flight deck interface, the main concern generally recognised is the usability of a touchscreen when flying through atmospheric turbulence [46], [8], [6]. The usability issues that arise when flying through turbulence are caused by involuntary movement of limbs by the operator of the touchscreen, which, in turn is caused by the operator being moved in his seat due to the turbulence. This involuntary movement of limbs is called biodynamic feedthrough and is discussed in the next section, thus further analysing the main drawback in the use of touch based interfaces on flight decks.

## 4.2. Biodynamic feedthrough

Biodynamic Feedthrough (BDFT) is the involuntary movement of body and limbs due to specific forces caused by accelerations on the human body [27], [20]. These specific forces can have a significant impact on the ability of a person to perform a certain control task [27]. The effects of the specific forces vary, as they can cause partial loss of eye-sight through blurring of the visual image, neuro-muscular interference can occur because the brain finds it more difficult to dissect intended and unintended motion and the central cognitive process can be overloaded, causing the control of the movement of limbs to slow down, [27], [20]. A basic schematic is shown in fig. 4.1, detailing the control process as involuntary response to acceleration when operating a touch based interface, [13], [20], [26]. Biodynamic Feedthrough can be further split up into two separate control situations, the open and closed loop control of a system. Biodynamic feedthrough occurs in a closed loop system when the person that experiences the biodynamic feedthrough also controls the system that generates the specific forces, such as through a control column or sidestick [42]. An example of biodynamic feedthrough in an open loop system is when the person that experiences the biodynamic feedthrough is performing a task that does not directly affect the specific forces causing the biodynamic feedthrough, such as when panning through a map on a touchscreen in the cockpit of an aircraft [13], [20], [42].

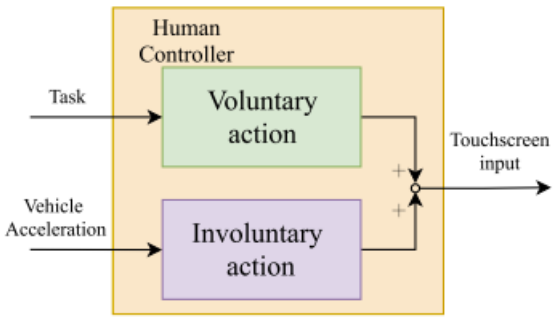


Figure 4.1: Definition of BDFT as an involuntary response to acceleration [20], [26].

## 4.3. Impact of biodynamic feedthrough on touchscreen use

As expected, the presence of atmospheric turbulence and following BDFT has a significant effect on the usability of touchscreens [28]. It is, however, not only the fact that atmospheric turbulence is present that causes an adverse effect on the usability of touchscreens, but also the location of the touch based interface used by pilots that has a large impact on the usability [2], [32]. Avsar et al, [2], showed that holding a hand-held touchscreen device is prone to much less errors when compared to fixed touch based interface devices. Rider and Martin, [32], conducted an experiment detailing the influence of the location of the touch based display on the usability of a touch based interface. Below, in fig. 4.2, it can be seen what distances Rider and Martin used between their participants and the interface, to conduct their experiment.

Figure 4.2: Touch locations used by Rider and Martin, [32], adopted from [29]

| Button Name | Description | Dist. [m] |
|---|---|---|
| Overhead | Above right shoulder | 1.2 |
| Radio | Elbow height arm at rest | 0.8 |
| Floor | On floor, 45 deg right | 0.6 |
| Glove Box | Hip height, 45 deg right | 1.0 |
| Steering Column | Fwd of elbow, arm at rest | 0.5 |
| Speedometer | Fwd of right shoulder | 1.0 |

In the figure below, in fig. 4.3, the impact of location can be seen on the usability of various locations of touch based interfaces, as performed by Rider and Martin, [32]. The figure shows an estimate of the required Effective Target Width (ETW), which is a quantification of the required target size to ensure $95\%$ of targets are to be selected successfully.

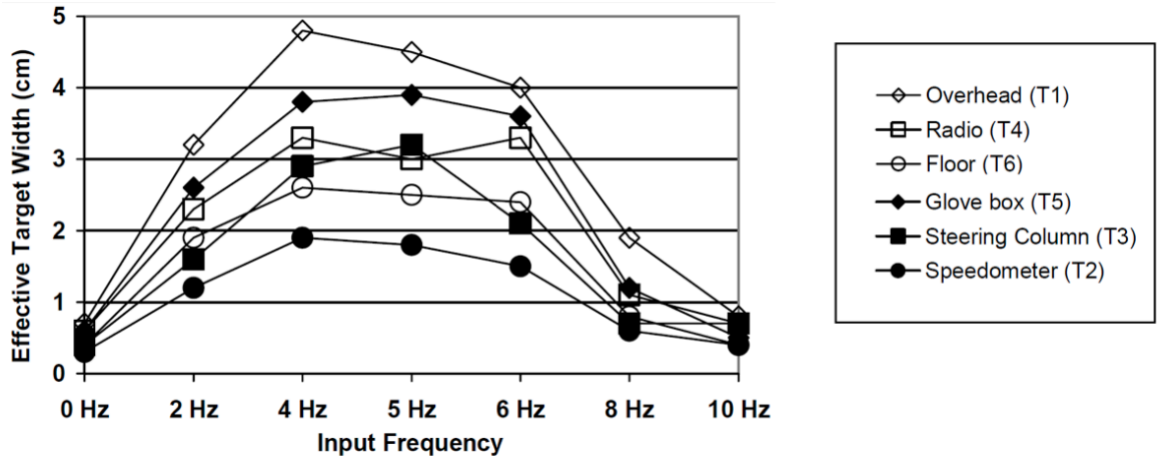


Figure 4.3: Estimate of effective target widths required should $95\%$ of touches be successful, [32], [29]

As can be seen in fig. 4.3, the experiment varied both the locations of the endpoints and the frequency of the vertical sinusoidal vibration input. fig. 4.3 shows that the overhead location performs worst in the frequency range of $4 - 6Hz$. Notably, both the radio and glove box location seem to be causing a significant performance degradation as well, indicating that the location of the conventional Control Display Unit (CDU) in aircraft cockpits, is a location prone to a high error rate due to atmospheric turbulence when operating a touch based interface [29]. Rider and Martin, [32], have not been the only ones to research the impact of target locations on the usability during turbulence. Dodd et al, [9], researched four specific touchscreen locations throughout a cockpit to determine the impact the location has on the data entry performance in using the touchscreen in a turbulent environment. Also the fatigue experienced by the operator, together with the perceived workload were analysed in an experiment that varied the levels of turbulence, target size and target spacing. The set-up can be seen in fig. 4.4. Dodd et al. [9], found similar results to Rider and Martin, [32], in the sense that the overhead and the outboard panel were most prone to errors, however these could not necessarily be attributed

to BDFT as it could be explained by the handedness of participants [29], [9].

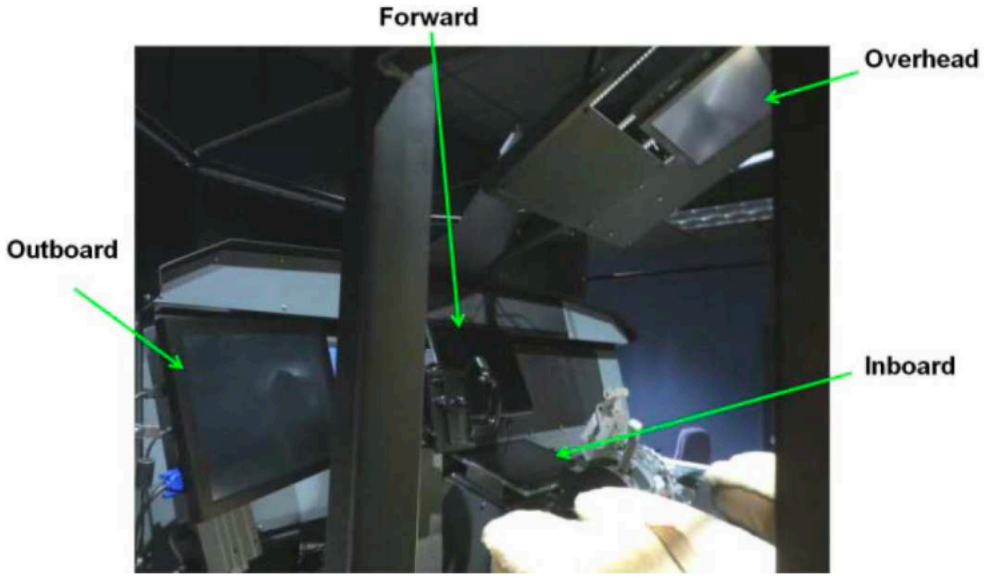


Figure 4.4: Set-up of touchscreen locations evaluated by Dodd et al. [9]

There are, however, more factors that influence the usability of a touch based interface under turbulent environments. One of which is the task that is performed on the touchscreen. For instance, Cockburn et al., [6], found that performing a drag-based task that requires constant touch was inaccurate when compared to single touch inputs, when performed in a simulated turbulent environment. Not only where the touches inaccurate, also the movement times, error rates and the subjective workload were increased as a consequence of the higher level of turbulence. Coutts et al. [7], have also shown the relationship between an increased level of turbulence and a higher movement time to hold. Furthermore, it has been shown that using a fixed touch based interface in a turbulent environment is prone to a reduced performance due to the combination of slow interactions, and a higher error rate [7].

## 4.4. Mitigating adverse effects of turbulence on touchscreen use

There are several ways suggested in research to mitigate the adverse effect atmospheric turbulence and the ensuing BDFT has on the use of a touch based interface. Generally speaking, they can be split up into two main categories, passive mitigation systems and active mitigation systems.

### 4.4.1. Passive mitigation techniques

The most basic of them being to offer a physical, or passive, support to enable a braced touch for pilots operating a touchscreen in a turbulent environment as was shown by Cockburn et al. [5], [6]. Several different braced touches were evaluated, as shown in fig. 4.5, offering support to the operator of the touchscreen, mitigating the effect of BDFT. Participants were instructed to keep several fingers on the bezel, whilst selecting the target with either the index finger or thumb. The research showed that a firm grasp on the bezel improved accuracy, but required awkward hand postures to do so [5].

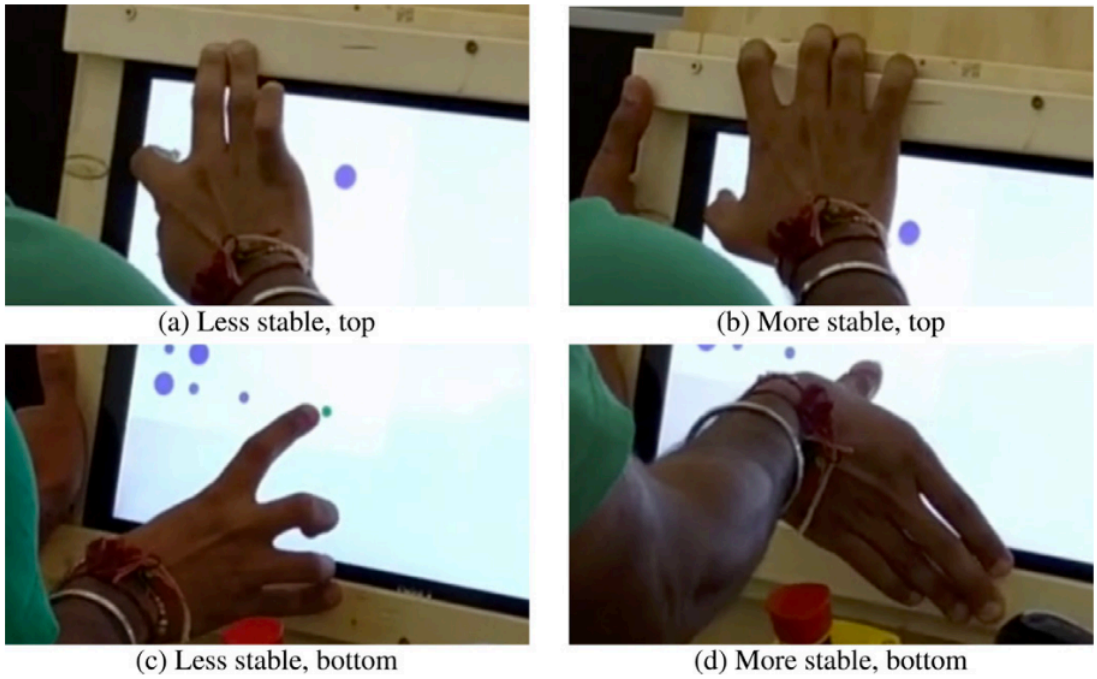


Figure 4.5: Bezel edge bracing at top and bottom of the display. Left shows less stable grasps; right shows more stable grasps, [5]

Next to a braced touch, Cockburn et al. analysed the functionality of an overlay stencil that could be placed on the touchscreen, effectively isolating the target and ensuring an erroneous input would not be registered, as well as offering an edge against which the finger could be stabilised [6]. In an experiment analysing the use of a trackball, a touchscreen and a touchscreen with stencil overlay under three levels of turbulence, the stencil overlay was not shown to be a successful solution to increase usability and decrease errors in a turbulent environment. However, it does have potential to improve touch interaction with small targets under high vibrations [6]. The separate stencil edge profiles can be seen in fig. 4.6.

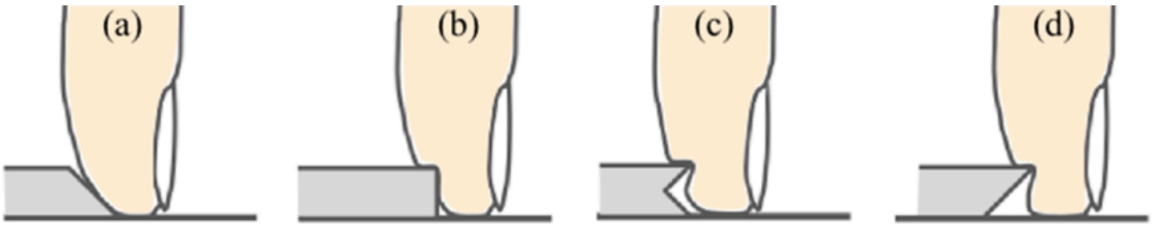


Figure 4.6: Canditate stencil edge profiles, from most (left) to least (right) comfortable (and least to most stable), [6]

These passive support systems have already been introduced into the aviation industry, with industry leaders such as Garmin, [12], Gulfstream [46] and Boeing, [35], all selecting touchscreens that include bezel support.

### 4.4.2. Active mitigation techniques

Apart from passive support systems such as the braced touch, research is focusing on active mitigation techniques to counter the adverse effect of BDFT on the use of touchscreens in turbulent environments [20]. Active mitigation techniques focus on filtering out erroneous inputs. This can be done in various ways, by either approaching the problem from the touchscreen interface or from the motion of the entire aircraft [20]. When approaching the problem from the touchscreen interface, the erroneous touches are mitigated using signal filtering. The fact that deliberate movement on the touchscreen has a different frequency than the erroneous movement caused by the vibration of the cockpit and the ensuing

BDFT, can be used to dissect the two inputs. This method is called the separation assumption [43]. Input filtering on the touchscreen would only work on dragging tasks as pointing tasks do not generate enough data to allow for filtering of the signal [20].
Approaching the problem of mitigation of BDFT from the perspective of dynamics of the aircraft also involves filtering the input signal, it is, however, done differently than when assessing the touchscreen inputs only. As shown by Khoshnewiszadeh, [20], a model that outputs both the intended and unintended inputs on the touchscreen can be cancelled when subtracting the expected BDFT as a consequence of the vehicle acceleration. This is shown schematically in fig. 4.7. The figure shows that the BDFT model has to accurately represent the expected actual BDFT as experienced by the pilot as a consequence from the vehicle acceleration. These two signals are then used to cancel out the influence of the BDFT, thus leaving the input as originally intended by the pilot.

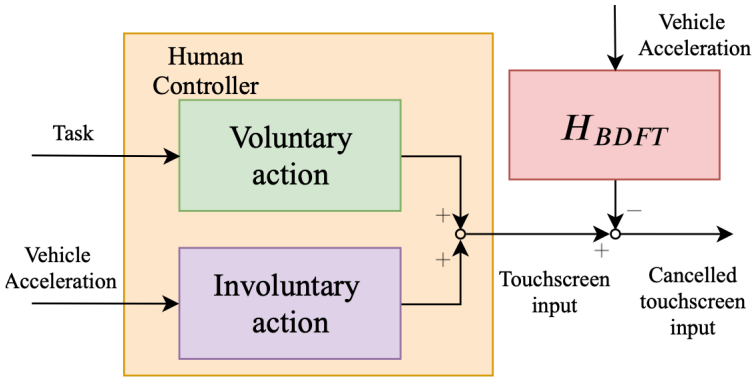


Figure 4.7: Model-based cancellation, based on a BDFT model, [20]

Contrary to the input filtering mitigation of the impact of BDFT, the method shown in fig. 4.7, does not assume a frequency range in which BDFT occurs on the touchscreen as input. Instead, it requires an accurate BDFT model of the pilot's behaviour as a consequence of the measured accelerations of the surroundings of the pilot [20]. The success of this method therefore depends on the accuracy of the model, as there are many separate environmental factors to take into account, creating such an accurate model is a difficult task, [20], [42].
Another active mitigation technique is called gesture interpretation, as researched by Van den Berg et al. [37]. Gesture interpretation was researched by adding two thresholds in amount of movement on a touchscreen a participant must perform before the touches are registered as a deliberate input. The influence of gesture thresholds is evaluated under three levels of motion, representing no, medium and high atmospheric turbulence intensity. It is found that a higher level of atmospheric turbulence causes higher task completion times, [37]. A higher gesture threshold also causes a higher task completion time, [37]. However, only a very low gesture threshold is deemed useful as a high gesture threshold takes too much time to overcome the threshold before the task can be completed, therefore missing the point of the exercise and causing high task completion times by itself, regardless of the turbulence levels [37].

## 4.5. Summary

Therefore, the key takeaways from this chapter are first of all that touchscreen technology is seen as the way forward in the design of next generation flight decks. Not only do they offer an intuitive operation but their information density and resulting improved situational awareness mean touch based interfaces are here to stay. Secondly, touch based interfaces still have significant drawbacks, most notably of which is the issue of usability when flying through atmospheric turbulence. As shown in this chapter, the overview of both passive and active mitigation techniques offer some respite against the influence of BDFT on the use of touch based interfaces, but a certain influence still remains present [5]. Because the turbulence will remain to have a negative effect on the use of touch based interfaces in the cockpit, it is necessary to be able to accurately predict the influence it has on the usability of touchscreens in a turbulent cockpit environment. This is required to support the development of guidelines and recommendations for proper use and integration of novel touch based interfaces in the flight deck [9]. Therefore validating the need for further research into the development of an accurate predictive tool, predicting the data throughput of a specific interface under various levels of atmospheric turbulence as will be shown in part III.

# III

# Preliminary Research

Note: This part has already been evaluated under the course: AE4020 - 'Literature Study'

# 5

# Extending Finger Fitts' law

In this chapter Finger Fitts' law will be extended. In order to incorporate both the influence of atmospheric turbulence as well as offer the detailed prediction of Movement Time for certain interface designs they will be added together in a single Fitts' law expression. Later on, in section 5.2, a preliminary data analysis will be performed to see whether the proposed Finger Fitts' law extension makes sense and holds for larger values of turbulence, before the validation experiment is performed.

## 5.1. Extension of Fitts' law

As has been shown previously in chapter 3, Fitts' law has been extended many times, tailored to different specific use cases. For the research as proposed in this report, Fitts' law will be extended for the specific use of touch based interfaces under turbulent environments.

### 5.1.1. Combining turbulence and Finger Fitts' law

To ensure an accurate prediction can be made for the usability of a touch based interface in a turbulent environment, the Finger Fitts' law as proposed by Bi, [3], will be extended to incorporate the influence of turbulence. The influence of turbulence on the use of a touch based cockpit interface will be done as proposed by Coutts et al. [7]. Both Fitts' laws have been explained in chapter 3, but are repeated below for simplicity. The Finger Fitts' law basis of the extension is as can be seen in eq. (5.1), thus offering an accurate basis for prediction of the useability of a touch based interface in the cockpit.

$$MT = a + b \cdot \log_2\left(\frac{A}{\sqrt{2\pi e(\sigma^2 - \sigma_a^2)}} + 1\right) \tag{5.1}$$

The Finger Fitts' law, as shown in eq. (5.1), however, does not incorporate the effects of turbulence. To incorporate the influence certain levels of atmospheric turbulence have on the movement time, the extension as proposed by Coutts et al. [7], will be used, as repeated below, in eq. (5.2).

$$MT = (-0.56 - 2.5 \cdot V) + (0.29 + 0.88 \cdot V) \cdot \log_2\left(\frac{2A}{W}\right) \tag{5.2}$$

Here, in eq. (5.2), the influence of turbulence on the Movement Time (MT) can clearly be seen, as depicted by the term $V$, which represents the RMS of the atmospheric turbulence accelerations. Also, the Index of Difficulty (ID) is shown, to illustrate the difference in ID, between the Finger Fitts' law, in eq. (5.1) and the original extension by Coutts et al. in eq. (5.2). Combining the two Fitts' laws into a new Fitts' law incorporating both the specific use of touch based interfaces and the influence of atmospheric turbulence yields the following equation, as shown in eq. (5.3).

$$MT = (a + b \cdot V) + (c + d \cdot V) \cdot \log_2\left(\frac{A}{\sqrt{2\pi e(\sigma^2 - \sigma_a^2)}} + 1\right) \tag{5.3}$$

In this novel expansion of Fitts' law, shown in eq. (5.3), the y-intercept coefficients $a, b, c$ and $d$, have intentionally been indicated by a symbol instead of a numerical value, as the exact numerical values

of the y-intercept coefficients are to be determined empirically by means of an experiment and are dependent on the type and location of the touchscreen as well as the task performed [7], [40]. Furthermore, the variance of the touch input error, $\sigma_a^2$, is to be determined in a stationary environment, to determine the accuracy of touch selection per participant. This novel expansion will be validated in an experiment, similar to that of Van Zon et al. [40], to show that it accurately predicts the usability of touch based cockpit interfaces under realistic atmospheric turbulence. The setup of this experiment will be detailed in part IV, in chapter 6. A preliminary data analysis and feasibility study will be done first in section 5.2, based on a sensitivity analysis of the data collected in the experiment by Van Zon et al. in 2017, in [40].

## 5.2. Preliminary data sensitivity analysis

Before the proposed extension of the Finger Fitts' law, as shown in eq. (5.3), will be validated in an experiment, a feasibility study has been performed based on a preliminary data analysis. The feasibility of the extension was checked by evaluating the impact of a fictitious turbulence input to the data found in the Finger Fitts' law experiment, as found in the preliminary thesis experiment by Van Zon et al. [40], and published in [41]. In his experiment Van Zon et al. demonstrates the use of Finger Fitts' law to evaluate the usability of touch based interfaces in a cockpit. It shows the throughput of a touch based interface to be slightly lower than that of the traditional Control Display Unit (CDU), and higher than the Mode Control Panel (MCP), but more importantly it is the same experiment as the one that will be conducted in the proposed future research, as described in chapter 6, to validate the proposed Finger Fitts' law extension, but without taking place in a turbulent motion environment. The data of the experiment as performed by Van Zon et al. [41], is also relevant as it demonstrates the usability of Finger Fitts' law when using fixed touch based interfaces in a cockpit, as opposed to only being applicable to hand held touch based devices. As Van Zon et al. has already demonstrated the use of Finger Fitts' law for the cockpit environment, the influence of atmospheric turbulence disturbances on this environment as modelled by Coutts et al. [7], was checked. To make a sensitivity analysis of the influence of atmospheric turbulence on Finger Fitts' law, first an overview of the atmospheric turbulence intensity levels as used by Coutts et al. [7], was collected, as shown below in table 5.1.

Table 5.1: Turbulence values as used in Fitts' law experiment by Coutts et al. in [7]

| Turbulence level | Filtered at [Hz] | Vertical $[\frac{m}{s^2}]$ | Roll $[\frac{m}{s^2}]$ | Pitch $[\frac{m}{s^2}]$ | Overall $[\frac{m}{s^2}]$ |
|---|---|---|---|---|---|
| No movement | 0 | 0 | 0 | 0 | 0 |
| Light chop | 2-6 | 0.37 | 0 | 0 | 0.37 |
| Light turbulence | 1-6 | 0.25 | 0.03 | 0.02 | 0.26 |
| Moderate turbulence | 1-6 | 0.51 | 0.06 | 0.04 | 0.52 |

From the turbulence magnitudes as shown in table 5.1, the overall values of light and moderate turbulence were used as indication in the sensitivity analysis. In the Coutts et al. expansion of Fitts' law, eq. (5.2), the term $V$ represents the value of total turbulence as shown in the last column of table 5.1, [7]. Only the values for light and moderate turbulence represent real atmospheric turbulence accurately as they include rotational accelerations as well and not just vertical acceleration, [7]. Once an accurate image of the atmospheric turbulence was found, the Finger Fitts' law as found by Van Zon et al. [40], was examined, as shown below in fig. 5.1.

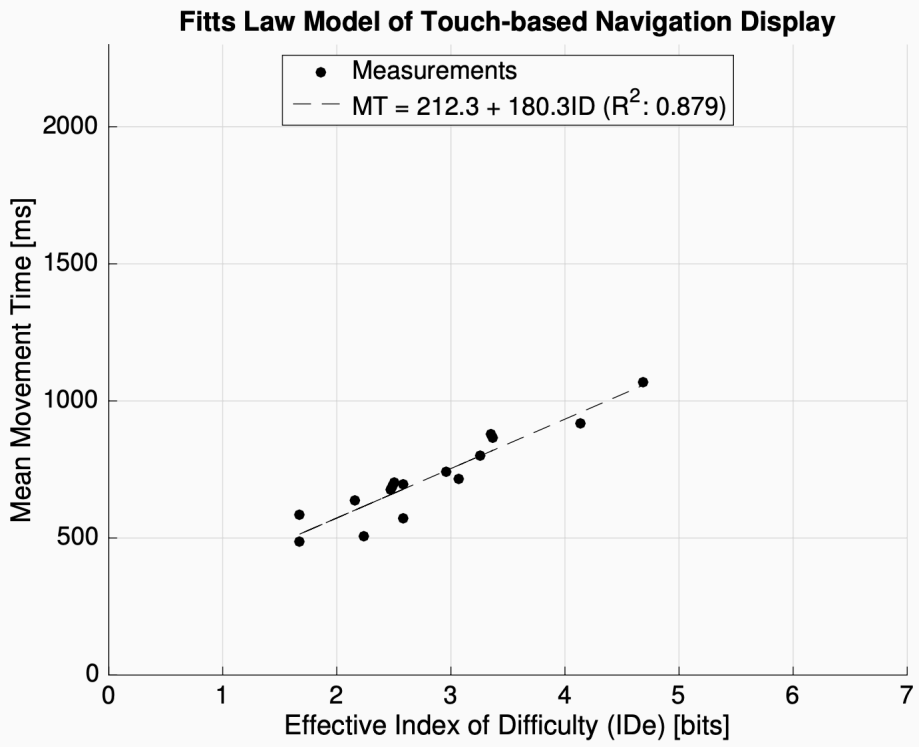


Figure 5.1: Mean movement times against accuracy-adjusted effective index of difficulty, [40]

Once both the Finger Fitts' law and the indication for the turbulence levels were found, they were combined to figure out what the influence would be of adding turbulence to the Finger Fitts' law. First a set of equations were set up, based on an assumption that the MT would increase by $100ms$ for the first step of increased turbulence and by $300ms$ and $500ms$ for the second and third level of turbulence, respectively. The turbulence magnitudes used for the feasibility study were as follows.

- $V_1 = 0.1\frac{m}{s^2}$
- $V_2 = 0.3\frac{m}{s^2}$
- $V_3 = 0.5\frac{m}{s^2}$

The equations used to determine general values for $c$ and $d$, where each turbulence value causes an assumed increase in Movement Time are found below in eq. (5.4), eq. (5.5), eq. (5.6), and eq. (5.7).

$$MT = 213.3 + 180.3 \cdot ID \tag{5.4}$$

$$MT + 100 = (213.3 + c_1 \cdot V_1) + (180.3 + d_1 \cdot V_1) \cdot ID \tag{5.5}$$

$$MT + 300 = (213.3 + c_2 \cdot V_2) + (180.3 + d_2 \cdot V_2) \cdot ID \tag{5.6}$$

$$MT + 500 = (213.3 + c_3 \cdot V_3) + (180.3 + d_3 \cdot V_3) \cdot ID \tag{5.7}$$

In order to find the values for $c_1, c_2$ and $c_3$ and $d_1, d_2$ and $d_3$, two combinations of MT and ID from fig. 5.1 were used per equation. In this way eq. (5.5), eq. (5.6) and eq. (5.7) could be solved to find the corresponding values for $c_1, c_2$ and $c_3$ and $d_1, d_2$ and $d_3$. A least squares fit was then performed on both $c_1, c_2$ and $c_3$ and $d_1, d_2$ and $d_3$, to find the general value for $c$ and $d$, and thus for a new Fitts' law. These values were found to be $c = 657$ and $d = 136$. The resulting extended Finger Fitts' law can be seen below, in eq. (5.8).

$$MT = (213.3 + 657 \cdot V) + (180.3 + 136 \cdot V) \cdot \log_2\left(\frac{A}{\sqrt{2\pi e(\sigma^2 - \sigma_a^2)}} + 1\right) \tag{5.8}$$

The resulting extended Finger Fitts' law, shown in eq. (5.8), returns to the original Finger Fitts' law as found by Van Zon et al. in fig. 5.1, [40], in case there is no atmospheric turbulence and $V = 0\frac{m}{s^2}$. Next, to check whether the Fitts' law held for other values of turbulence, a new combination of MT and ID was used from fig. 5.1. The turbulence magnitudes used for this verification were $V = 0\frac{m}{s^2}$, $V = 0.3\frac{m}{s^2}$, $V = 0.5\frac{m}{s^2}$, and $V = 0.7\frac{m}{s^2}$. The turbulence value of $V = 0.7\frac{m}{s^2}$ was chosen as it was higher than the values used by Coutts et al. in [7], but well within the range of probable turbulence, [49]. Using a value of $ID = 4.7$ in combination with the four values for $V$, yielded the following values, as can be seen below in table 5.2.

| ID | V | MT |
|---|---|---|
| 4.69 | 0 | 1060 |
| 4.69 | 0.3 | 1447 |
| 4.69 | 0.5 | 1706 |
| 4.69 | 0.7 | 1965 |

Table 5.2: Verification results extended Finger Fitts' law

The values for MT as shown in table 5.2 show a reasonable increase in Movement Time, for the increased turbulence magnitude. The increase is, however, less pronounced than with the experiment as performed by Coutts et al. [7]. This can be attributed to several factors, such as the assumed increase in MT to determine the $c$ and $d$ coefficients, as well as the difference in the task performed between Van Zon et al. [41], and Coutts et al. [7].

## 5.3. Summary

In summary, it can be stated that the proposed extension of Finger Fitts' law is expected to offer an accurate prediction of the usability of a touch based interface for various magnitudes of atmospheric turbulence. The proposed extension of Finger Fitts' as shown in eq. (5.8), shows a probable result. Even though there is a notable difference between this extension and that as designed by Coutts et al. [7], namely in the y-intercept coefficient values. In the Coutts et al. equation, shown in eq. (5.2), the y-intercept coefficients contain negative coefficients. The proposed extension of Finger Fitts' law as shown in eq. (5.8), does not. This difference, however, can be attributed to various factors. First, the equation governing the experiment as performed by Coutts et al. contains a task that experiences a larger increase in MT than the one evaluated in eq. (5.8). To cause Fitts' law to increase that much, the y-intercept can turn to a negative value, even though this would indicate a negative reaction time by the operator for a task with zero Index of Difficulty. However, as the ID is never zero in reality, this does not occur and therefore does not pose a problem and merely indicates the steepness of the curve as a consequence of the increase of Movement Time due to the increase in atmospheric turbulence. Second, the Coutts et al. equation, eq. (5.2), does not return to an original Fitts' law, when not in a turbulent environment, the extended Finger Fitts' law, in eq. (5.8), is set up from a Finger Fitts' law, that accurately predicts the use of a touch based interface under stationary conditions, as well as when used in atmospheric turbulence.

# IV

# Future Research

Note: This part has already been evaluated under the course: AE4020 - 'Literature Study'

# 6

# Evaluating the Extended Finger Fitts' Law

In this chapter the proposed experiment that verifies and validates parts of the Finger Fitts' Law extension will be highlighted. First the design and methodology will be explained in section 6.1, detailing the type of task the participants will be performing. Also, the atmospheric turbulence profiles as experienced by the participants will be shown here. The setup and order of the experiment conditions will also be explained, before highlighting the specific hypotheses of the experiment in section 6.2. Finally the verification and validation process will be detailed, as this is a vital part of the whole process in demonstrating the functionality of the extension of Fitts' law.

## 6.1. Proposed verification experiment

The proposed experiment will be performed to act as a verification of the extension of Finger Fitts' Law, as has been shown in chapter 5. The experiment will be based upon an earlier experiment as conducted by Van Zon et al. in 2017, [40], [41]. The experiment conduct a similar tracking task as performed in preliminary research by Van Zon et al. [40], however it will be performed in both a stationary environment and a turbulent environment, in order to demonstrate the functioning of the extension of Finger Fitts' Law, thus properly relating the impact of atmospheric turbulence to the movement time of the participants.

### 6.1.1. Preliminary experiment design and methodology

The experiment will be conducted in the SIMONA Research Simulator (SRS), which is the 6-degree of freedom full motion simulator of the Delft University of Technology (DUT). As mentioned in section 6.1, the experiment will be held in both a stationary and a turbulent environment. Participants will be performing a drag-based selection task on a capacitive touch based interface. Before the experiment is held, a calibration will be performed where participants are asked to select stationary targets, to determine the accuracy of their pointing device, which is in this case their finger, to find the variance of the selection error as explained in section 3.2.2. An illustration of the setup of the experiment is shown below in fig. 6.1.

The dragging task is one where participants are asked to select a white circular object and drag it towards a magenta target circle. The orientation of the magenta target circle with respect to the circular object varies, as well as the size of the target. An illustration is shown in fig. 6.1b. The participant will perform the task from the captain seat, on the left hand side of the cockpit, and will thus use his or her right hand to perform the task, as can be seen in fig. 6.1a. To determine the impact of the turbulence on the performance of the participant the Movement Time will be measured. The measured time will be the time taken from the successful selection of the object, up to the point the participant has successfully dragged the object to the target. To complete the validation of the proposed Fitts' law extension as seen in eq. (5.3), the index of difficulty and the turbulence intensity levels are needed, these are both known inputs. Finally, once all this data is collected the y-intercept coefficients can then be determined using a least-squares regression as explained in chapter 3. Next to the data required to determine the

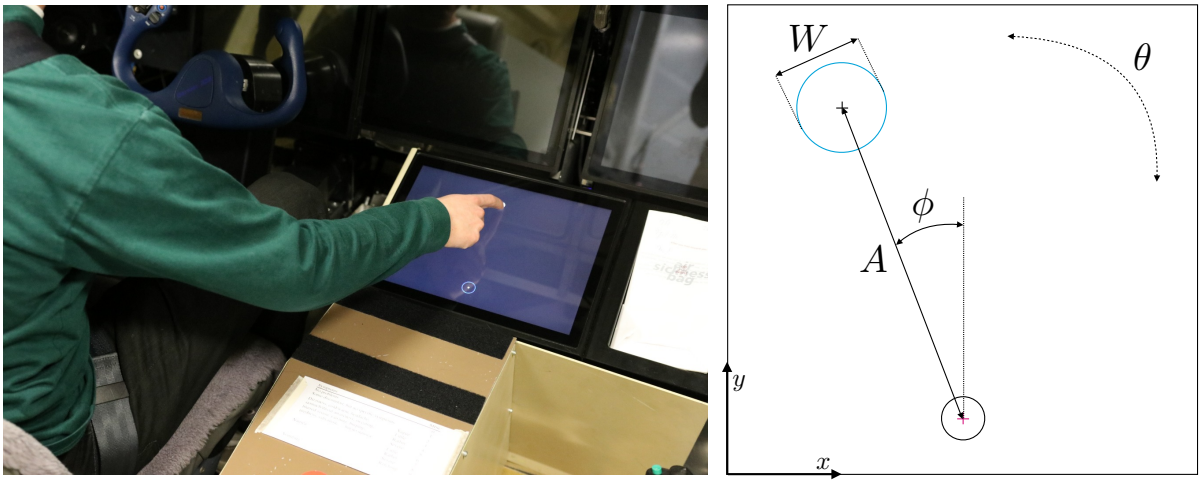


(a) Cabin setup

(b) Touchscreen interface

Figure 6.1: Cabin setup and touchscreen interface Fitts' law experiment

proposed new Fitts' law, also the continuous touch data will be collected. This shows the exact path the participants' finger has taken across the screen and can thus be used to verify as well as further explain the expected increase in movement time due to the presence of atmospheric turbulence.

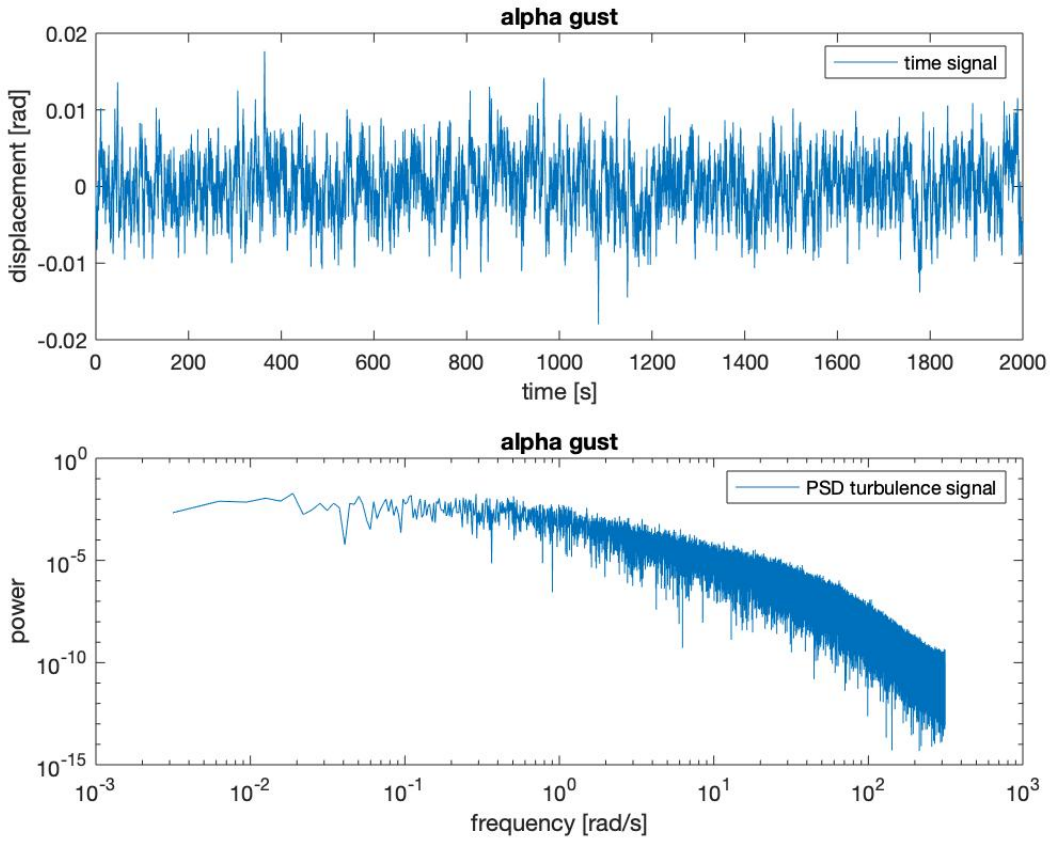


Figure 6.2: Turbulence gust input on angle of attack

Excluding the stationary environment, there will be three intensity levels of Dryden-modelled patchy atmospheric turbulence as described in chapter 2 and based on the turbulence generator as used by

Lam, [21]. The atmospheric turbulence profile has been generated with a Kurtosis value of $K = 3.3$. The value of $K > 3$, indicating the turbulence is not normally distributed [36], indicating the turbulence is patchy turbulence. Having a Kurtosis value close to three means the patchiness is low enough, and therefore the turbulence constant enough, to ensure there are no participants that can fulfil a complete dragging task in between two turbulence inputs, which could have been the case had the patchiness been too great. The turbulence signal itself can be seen in fig. 6.2, both the actual signal and the power spectral density for the turbulence gust input on the angle of attack of the aircraft can be seen. As can be seen in fig. 6.2, the generated turbulence signal is $2000s$ long, this is to ensure a participant always has enough time to finish all the tasks before the original turbulence signal runs out and a loop would be required. Before the participant experiences realistic atmospheric turbulence as is experienced in the cockpit of a Cessna Citation 2, the turbulence is fed through an aircraft model, as described in section 2.2.4. Here, the aircraft accelerations were scaled to match the turbulence profiles as set out by Coutts et al. in [7]. This has resulted in three turbulence profiles, the turbulence intensities used are shown in table 6.1, as found below.

Table 6.1: Turbulence values as used in Fitts' law extension validation experiment

| Turbulence level | Filter [Hz] | $\ddot{x}\ [\frac{m}{s^2}]$ | $\ddot{y}\ [\frac{m}{s^2}]$ | $\ddot{z}\ [\frac{m}{s^2}]$ | $\dot{q}\ [\frac{rad}{s^2}]$ | $\dot{p}\ [\frac{rad}{s^2}]$ | $\dot{r}\ [\frac{rad}{s^2}]$ | Total $[\frac{m}{s^2}]$ |
|---|---|---|---|---|---|---|---|---|
| No movement | - | 0 | 0 | 0 | 0 | 0 | 0 | 0 |
| Low turbulence | 2-10 | 0.038 | 0.082 | 0.243 | 0.050 | 0.021 | 0.010 | 0.26 |
| Medium turbulence | 2-10 | 0.076 | 0.164 | 0.486 | 0.100 | 0.043 | 0.021 | 0.52 |
| High turbulence | 2-10 | 0.113 | 0.246 | 0.729 | 0.150 | 0.064 | 0.031 | 0.78 |

As can be seen in table 6.1, the accelerations caused by the atmospheric turbulence have been split up into both normal and angular acceleration components. Where $\ddot{x}, \ddot{y}$ and $\ddot{z}$ represent the acceleration magnitude in the body-frame $x, y$ and $z$ direction, respectively, and $\dot{q}, \dot{p}$ and $\dot{r}$ represent the pitch, roll and yaw-accelerations of the aircraft, respectively. The magnitude of the atmospheric turbulence intensities have been scaled to match the intensities as used by Coutts et al. [7], in order to properly compare the results of the experiments. An additional level of atmospheric turbulence has been added, compared to the experiment performed by Coutts et al. [7], to be able to check the linearity of the relation between atmospheric turbulence and the increase in Movement Time. Asking participants to perform the experiment in more than 3 active levels of atmospheric turbulence was deemed too intense for participants. The schedule for participants can be seen in fig. 6.3. The total experiment is expected to last around 1 hour, depending on the duration of the break. To ensure the effects of learning will not affect the results of the experiment, both the order of the dragging tasks and the order in which the turbulence levels are experienced, are varied according to a latin-square distribution. The experiment briefing to be shared with the participants before their participation in the experiment can be found in appendix A.

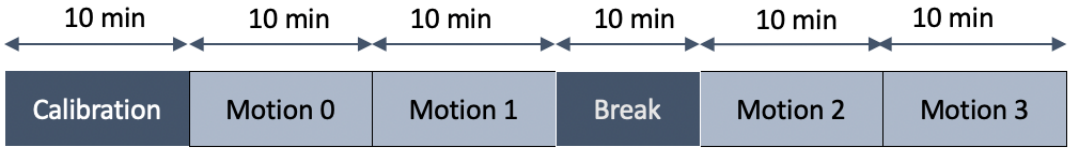


Figure 6.3: Experiment planning

## 6.2. Hypotheses

The experiment has been set up in order to best verify the proposed Fitts' law extension. In order to do so, several hypotheses have been determined.

1. The experiment condition without atmospheric turbulence yields similar results, with respect to the generated Finger Fitts' law, as the experiment by Van Zon et al. performed in [41].

2. The movement time relates to the increase in turbulence level according to the relationship as determined by Coutts et al. in [7], when using similar methodology. This relationship is also

expected to accurately model the influence of atmospheric turbulence for higher values of atmospheric turbulence than tested in the experiment by Coutts et al.

Hypothesis $1$ has been set up to verify that the Finger Fitts' law experiment has been set up properly, and that it yields similar results to the experiment as set up by Van Zon et al. in [40], [41]. This is important as this forms the basis of the experiment verifying the extension of Finger Fitts' law as laid out in this report, and therefore accurately reproducing the experiment results by Van Zon et al. [40], [41], is imperative to demonstrating the functionality of the extended Finger Fitts' law in a stationary condition, before going on to evaluate the influence of atmospheric turbulence. Hypothesis $2$ has been set up to verify the actual extension imposed on the Finger Fitts' law. It is specifically relevant for the case where $V > 0.52\frac{m}{s^2}$, as that is the maximum value of RMS weighted atmospheric turbulence used by Coutts et al. [7]. For the values of $V < 0.52\frac{m}{s^2}$ the extended Finger Fitts' law is expected to behave similarly to the extension of Fitts' law as found by Coutts et al. More specifically, the increase in MT as a consequence of increasing atmospheric turbulence should be modelled closely by the addition of the term $V$ in the Finger Fitts' law.

## 6.3. Verification and Validation

Specific attention has gone towards validating the atmospheric turbulence mimicking motion the participants will be experiencing when performing the dragging task. Performing the experiment in the most realistic turbulence was deemed very important to proving the extension of Finger Fitts' law would accurately predict real-life touchscreen use in an aircraft cockpit. This has also been mentioned as recommendation for future research by Khoshnewiszadeh in [20] and Mobertz in [28] and is lacking in the work performed by Coutts et al. [7]. In order to demonstrate the accuracy of the turbulence disturbance input, the input signal has been compared to previous turbulence signals used by the Delft University of Technology verified to be accurate [21]. The two compared power spectral densities can be seen in fig. 6.4. It can be seen that the two signals have a similar distribution of power over the frequency range between $2 - 10Hz$. The new signal does have a more distinctive low frequency range, but that can be explained by the fact that the new signal has a longer duration and thus it is possible to detect a lower frequency. The previous signal, as used by [21], has been used many times as atmospheric turbulence in the SIMONA Research Simulator when flying demo's. Based on conversations with the test pilots of the Delft University of Technology test aircraft, the Cessna Citation 2, this atmospheric turbulence is accurate in mimicking the turbulence as experienced in the actual aircraft.

## 6.4. Summary

In summary, the experiment set up to validate the extension of the Finger Fitts' law to include the influence of atmospheric turbulence on the movement time has been focused on two main aspects. The first is the Fitts' law part of the validation, where the experiment has been set up to reproduce as accurately as possible the work performed by both Van Zon et al. [40], [41], as well as the work performed by Coutts et al. in [7]. It is important that for the parts of the experiment that overlap with the previous research, similar results are found. That adds a large amount of confidence to the accuracy of the results when extending the experiment conditions to novel situations, such as a turbulence condition that is greater than the ones demonstrated by [7]. Secondly, the experiment set up has focused on mimicking the atmospheric turbulence as experienced by pilots at cruise altitude as accurately as possible. This adds importance to the research as it demonstrates not only the principle of the functionality of the extension of Finger Fitts' law in any turbulent environment, but also the specific case of flying a Cessna Citation 2 at cruise speed and cruise altitude through patchy clear air turbulence.

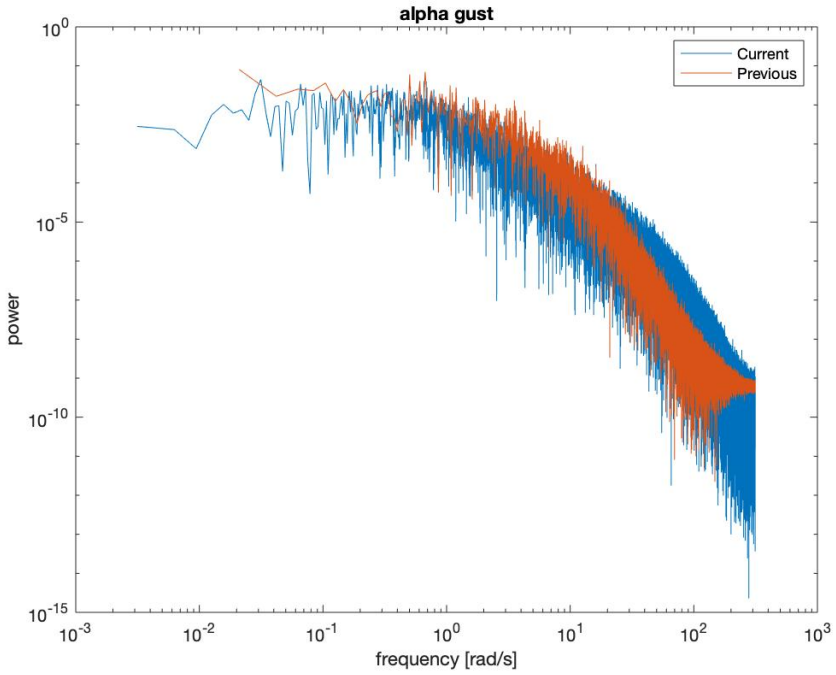


Figure 6.4: Validation PSD of turbulence signal

# Bibliography


[1] Abir Al Hajri, Sidney Fels, Gregor Miller, and Michael Ilich. Moving target selection in 2D graphical user interfaces. In *Lecture Notes in Computer Science (including subseries Lecture Notes in Artificial Intelligence and Lecture Notes in Bioinformatics)*, number PART 2, pages 141–161, 2011. ISBN 9783642237706. doi: 10.1007/978-3-642-23771-3{_}12.

[2] Huseyin Avsar, Joel E. Fischer, and Tom Rodden. Designing touch screen user interfaces for future flight deck operations. In *2016 IEEE/AIAA 35th Digital Avionics Systems Conference (DASC)*, volume 2016-Decem, pages 1–9. IEEE, 9 2016. ISBN 978-1-5090-2523-7. doi: 10.1109/DASC.2016.7777976. URL http://ieeexplore.ieee.org/document/7777976/.

[3] Xiaojun Bi, Yang Li, and Shumin Zhai. *FFitts Law: Modeling Finger Touch with Fitts' Law*. 2013. ISBN 9781450318990.

[4] Juan Sebastián Casallas. Prediction of user action in moving-target selection tasks. Technical report, 2015. URL https://lib.dr.iastate.edu/etd.

[5] A. Cockburn, D. Masson, C. Gutwin, P. Palanque, A. Goguey, M. Yung, C. Gris, and C. Trask. Design and evaluation of braced touch for touchscreen input stabilisation. *International Journal of Human Computer Studies*, 122:21–37, 2 2019. ISSN 10959300. doi: 10.1016/j.ijhcs.2018.08.005.

[6] Andy Cockburn, Carl Gutwin, Philippe Palanque, Yannick Deleris, Catherine Trask, Ashley Coveney, Marcus Yung, and Karon MacLean. Turbulent touch: Touchscreen input for cockpit displays. In *Conference on Human Factors in Computing Systems - Proceedings*, volume 2017-May, pages 6742–6753, New York, New York, USA, 5 2017. Association for Computing Machinery. ISBN 9781450346559. doi: 10.1145/3025453.3025584. URL http://dl.acm.org/citation.cfm?doid=3025453.3025584.

[7] Louise V Coutts, Katherine L Plant, Mark Smith, Luke Bolton, Katie J Parnell, James Arnold, and Neville A Stanton. Future technology on the flight deck: assessing the use of touchscreens in vibration environments. 2018. ISSN 1366-5847. doi: 10.1080/00140139.2018.1552013. URL https://doi.org/10.1080/00140139.2018.1552013.

[8] Asaf Degani, Everett A Palmer, and Kristin G Bauersfeld. "SOFT" CONTROLS FOR HARD DISPLAYS: STILL A CHALLENGE. Technical report, 1992.

[9] Sonia Dodd, Jeff Lancaster, Andrew Miranda, Steve Grothe, Bob De Mers, and Bill Rogers. Touch screens on the flight deck: The impact of touch target size, spacing, touch technology and turbulence on pilot performance. In *Proceedings of the Human Factors and Ergonomics Society*, volume 2014-Janua, pages 6–10. Human Factors an Ergonomics Society Inc., 2014. ISBN 9780945289456. doi: 10.1177/1541931214581002.

[10] Hugh L Dryden. A Review of the statistical theory of turbulence. Technical report, 1942.

[11] Paul M Fitts'. THE INFORMATION CAPACITY OF THE HUMAN MOTOR SYSTEM IN CONTROLLING THE AMPLITUDE OF MOVEMENT 1. Technical Report 6, 1954.

[12] Garmin. Flight Decks and Displays | Garmin, 2020. URL https://buy.garmin.com/en-US/US/in-the-air/avionics-safety/mfd-pfd/cInTheAir-cAvionics-cMFDs-p1.html.

[13] M. J. Griffin. Handbook of Human Vibration - 1st Edition, 1990. URL https://www.elsevier.com/books/handbook-of-human-vibration/griffin/978-0-12-303041-2.

[14] Errol R Hoffmann. Capture of moving targets: a modification of Fitts' Law. *ERGONOMICS*, 34(2): 1–1, 1991. ISSN 1366-5847. doi: 10.1080/00140139108967307. URL https://doi.org/10.1080/00140139108967307.

[15] Errol R Hoffmann. Capture of shrinking targets. *Ergonomics*, 54(6):519–530, 2011. ISSN 1366-5847. doi: 10.1080/00140139.2011.576775. URL https://doi.org/10.1080/00140139.2011.576775.

[16] John C. Houbolt. *Dynamic response of airplanes to atmospheric turbulence including flight data on input and response.* 1964.

[17] Richard Jagacinski. A test of Fitts' law with moving targets, 1980.

[18] E. A. Johnson. Touch display—a novel input/output device for computers. *Electronics Letters*, 1 (8):219–220, 1965. ISSN 00135194. doi: 10.1049/el:19650200.

[19] Sridher Kaminani. Human computer interaction issues with touch screen interfaces in the flight deck. In *AIAA/IEEE Digital Avionics Systems Conference - Proceedings*, 2011. ISBN 9781612847979. doi: 10.1109/DASC.2011.6096098.

[20] Arwin Khoshnewiszadeh. Model-Based Mitigation of Biodynamic Feed through for Touchscreen Dragging Tasks in Turbulence. 2020.

[21] Mung Lam. A Comparative Study between Display Augmentation and Control Augmentation for Tunnel-in-the-Sky Displays Complementary report. 2003.

[22] Sandi Ljubic, Vlado Glavinic, and Mihael Kukec. Finger-based pointing performance on mobile touchscreen devices: Fitts' law fits. In *Lecture Notes in Computer Science (including subseries Lecture Notes in Artificial Intelligence and Lecture Notes in Bioinformatics)*, volume 9175, pages 318–329. Springer Verlag, 2015. ISBN 9783319206776. doi: 10.1007/978-3-319-20678-3{_}31.

[23] I. Scott MacKenzie. A note on the information-theoretic basis for fitts' law. *Journal of Motor Behavior*, 21(3):323–330, 1989. ISSN 19401027. doi: 10.1080/00222895.1989.10735486.

[24] I. Scott MacKenzie. Fitts' Law as a Research and Design Tool in Human-Computer Interaction. *Human–Computer Interaction*, 7(1):91–139, 1992. ISSN 15327051. doi: 10.1207/s15327051hci0701{_}3.

[25] I. Scott MacKenzie and William Buxton. Extending Fitts' law to two-dimensional tasks. In *Conference on Human Factors in Computing Systems - Proceedings*, pages 219–226, New York, New York, USA, 1992. Publ by ACM. doi: 10.1145/142750.142794. URL http://portal.acm.org/citation.cfm?doid=142750.142794.

[26] Pierangelo Masarati, Giuseppe Quaranta, Andrea Bernardini, and Giorgio Guglieri. Voluntary pilot action through biodynamics for helicopter flight dynamics simulation. *Journal of Guidance, Control, and Dynamics*, 38(3):431–441, 3 2015. ISSN 15333884. doi: 10.2514/1.G000837. URL https://arc.aiaa.org/doi/abs/10.2514/1.G000837.

[27] R. W. McLeod and M. J. Griffin. Review of the effects of translational whole-body vibration on continuous manual control performance. *Journal of Sound and Vibration*, 133(1):55–115, 8 1989. ISSN 10958568. doi: 10.1016/0022-460X(89)90985-1.

[28] X. R.I. Mobertz, D. M. Pool, M. M. Van Paassen, and M. Mulder. A cybernetic analysis of biodynamic effects in touchscreen operation in turbulence. In *AIAA Modeling and Simulation Technologies Conference, 2018*, number 209959. American Institute of Aeronautics and Astronautics Inc, AIAA, 2018. ISBN 9781624105289. doi: 10.2514/6.2018-0115.

[29] X. R.I. Mobertz, D. M. Pool, M. M. Van Paassen, and M. Mulder. A cybernetic analysis of biodynamic effects in touchscreen operation in turbulence - MSc Thesis. *AIAA Modeling and Simulation Technologies Conference, 2018*, (209959), 2018. doi: 10.2514/6.2018-0115.

[30] J A Mulder, J C van der Vaart, and M Mulder. Stochastic Aerospace Systems. (November), 2007.

[31] P. M. Reeves, G. S. Campbell, V. M. Ganzer, and R. G. Joppa. Development and application of a non-Gaussian atmospheric turbulence model for use in flight simulators, 1974. URL https://www.researchgate.net/publication/24327524_Development_and_application_of_a_non-Gaussian_atmospheric_turbulence_model_for_use_in_flight_simulators.

[32] Kevin A. Rider and Bernard J. Martin. Effects of Ride Motion on the Speed and Accuracy of In-Vehicle Pointing Tasks. *Proceedings of the Human Factors and Ergonomics Society Annual Meeting*, 49(12):1119–1123, 9 2005. ISSN 2169-5067. doi: 10.1177/154193120504901204. URL http://journals.sagepub.com/doi/10.1177/154193120504901204.

[33] C. Soutis. Carbon fiber reinforced plastics in aircraft construction. *Materials Science and Engineering A*, 412(1-2):171–176, 12 2005. ISSN 09215093. doi: 10.1016/j.msea.2005.08.064.

[34] Martin F. Stoelen and David L. Akin. Assessment of fitts law for quantifying combined rotational and translational movements. *Human Factors*, 52(1):63–77, 2010. ISSN 00187208. doi: 10.1177/0018720810366560.

[35] Stephen Trimble. Boeing selects Rockwell Collins for 777X touchscreens | News | Flight Global, 2020. URL https://www.flightglobal.com/boeing-selects-rockwell-collins-for-777x-touchscreens/121765.article.

[36] G. A. J. Van de Moesdijk. The description of patchy atmospheric turbulence, based on a non-gaussian simulation technique, 1975.

[37] René Van Den Berg. Investigating the Effects of Turbulence and Spatial Gesture Thresholds on Multi-Touch Interaction. 2014.

[38] C. A. A. M. Van Der Linden. DASMAT-Delft University Aircraft Simulation Model and Analysis Tool, A Matlab/Simulink Environment for Flight Dynamics and Control Analysis. Technical report, 1998. URL https://repository.tudelft.nl/islandora/object/uuid%3A25767235-c751-437e-8f57-0433be609cc1.

[39] W.H.J.J. Van Staveren. Analyses of Aircraft Responses to Atmospheric Turbulence. Technical report, 2003.

[40] Nout C. M. van Zon. Evaluation of a touch-based navigation display for lateral weather avoidance. 2017.

[41] Nout C.M. van Zon, Clark Borst, Daan M. Pool, and Marinus M. van Paassen. Touchscreens for Aircraft Navigation Tasks: Comparing Accuracy and Throughput of Three Flight Deck Interfaces Using Fitts' Law. *Human Factors*, 62(6):897–908, 9 2020. ISSN 15478181. doi: 10.1177/0018720819862146.

[42] Joost Venrooij. *Measuring, modeling and mitigating biodynamic feedthrough*. Number 45. 2015. ISBN 978-3-8325-4105-7. URL http://www.logos-verlag.de/cgi-bin/engbuchmid?isbn=4105&lng=eng&id=.

[43] Joost Venrooij, Max Mulder, Marinus M. Van Paassen, Mark Mulder, and David A. Abbink. A review of biodynamic feedthrough mitigation techniques. In *IFAC Proceedings Volumes (IFAC-PapersOnline)*, volume 11, pages 316–321. IFAC Secretariat, 1 2010. ISBN 9783902661944. doi: 10.3182/20100831-4-fr-2021.00056.

[44] Theodore Von Karman. On the statistical theory of isotropic turbulence. *Proceedings of the Royal Society A*, 382:25–42, 1938. ISSN 13645021.

[45] Theodore Von Karman. Progress in the statistical theory of turbulence. Technical report, 1948.

[46] Christopher B. Watkins, Colleen Nilson, Susan Taylor, Kristin B. Medin, Igor Kuljanin, and Huy B. Nguyen. Development of touchscreen displays for the gulfstream G500 and G600 Symmetry™ flight deck. In *AIAA/IEEE Digital Avionics Systems Conference - Proceedings*, volume 2018-Septe. Institute of Electrical and Electronics Engineers Inc., 12 2018. ISBN 9781538641125. doi: 10.1109/DASC.2018.8569532.

[47] A T Welford. Fundamentals of Skill. Technical report, 1968.

[48] R. William Soukoreff and I. Scott Mackenzie. Theoretical upper and lower bounds on typing speed using a stylus and a soft keyboard. *Behaviour and Information Technology*, 14(6):370–379, 1995. ISSN 13623001. doi: 10.1080/01449299508914656.

[49] Paul D. Williams. Increased light, moderate, and severe clear-air turbulence in response to climate change. *Advances in Atmospheric Sciences*, 34(5):576–586, 5 2017. ISSN 02561530. doi: 10.1007/s00376-017-6268-2.

# A

# Experiment Briefing

# Extending Finger Fitts' Law for use in turbulent flight deck environments

By Bart (R.F.) Jacobson,

Control and Operations, Control and Simulation

## 1. Background

The aviation industry has been moving towards more technically advanced flight decks from the outset of aviation. Even though the use of touchscreens is already very common in everyday life, via smartphones and tablets, their use as flight deck interface is relatively new. Touchscreen use offers many advantages over conventional interfaces, but it also has a large downside, namely its use in a turbulent environment. Quite some research has so far been done on the use of touchscreens as flight deck interface in turbulent environments. However, research has so far only focused on evaluating the active use of touchscreens in atmospheric turbulence conditions and trying to mitigate the negative effects. Research has not yet shown a credible way of predicting the usability of touchscreens under various levels of atmospheric turbulence.

Through the experiments you will perform, a proposed predictive model will be validated and verified in a full-motion research simulator, in which participants will perform a touch selection tasks under various levels of turbulence. Thus creating a model designers can use when developing touch-based interfaces to ensure it can be used safely under specified levels of turbulence, further adding to the safety of the aviation industry.

## Research objective

The objective of the research is to develop a predictive model that can be used to assess whether or not a touch-based navigation display is safe to use under various levels of atmospheric turbulence by means of demonstrating the functionality of an extension to Finger Fitts' Law, thus evaluating the speed-accuracy trade-off, in a motion based research simulator capable of accurately mimicking atmospheric turbulence.

'Safe' in this instance indicates an acceptable level of data throughput in order to perform a weather rerouting task successfully. Of course this cannot all be tested at once, so before the final experiment is done in which the overall functionality is demonstrated, the building blocks will be demonstrated. This gives rise to a new set of relevant research objectives that are required to be completed before the final experiment can take place.

## Experimental Set-up

In the experiment participants will be asked to perform a dragging task on a touch-based interface, as can be seen in fig. 1, in both a stationary and a turbulent environment. The experiment will be as performed by van Zon [2017], but extended to include turbulent environments and it will focus only on the use of touchscreens. The test will be performed in a stationary environment as a baseline reference, before repeating the experiment in an environment of several levels of turbulence, to demonstrate the influence the turbulent environment has on the movement time. The research will be conducted in the SIMONA Research Simulator (SRS) at the TU Delft. To accurately verify the model, three levels of

turbulence will be used in the experiment. This is required to show whether the correlation between the turbulence and movement time is indeed linear as well as showing the experiment results hold with Coutts' model of incorporating turbulence in Fitts' law, Coutts et al. [2018].

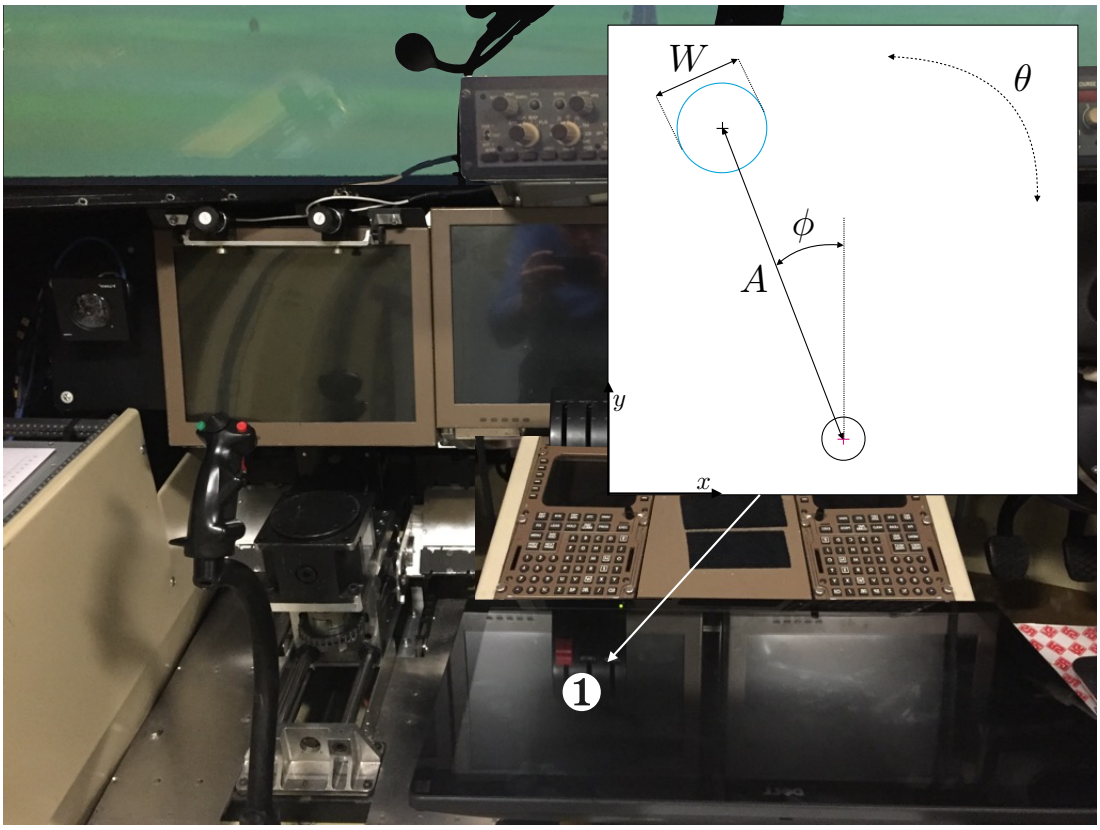


Figure 1: Experiment apparatus

The experiment set-up is as shown in fig. 1, it shows a large touchscreen on which the experiment will be performed. The display shows a white circle with a magenta crosshair, this is the object that is to be moved towards the target, a cyan coloured circle with a white crosshair. The path distance $A$, target size $W$, and directional variables $\phi$ and $\theta$ will be varied throughout the experiment. Your task will be to move the object to the target as fast, smoothly and accurately as possible. Overshooting or undershooting the target is acceptable, however, you are requested to aim for a hit-rate of around 96% so a small margin of error is possible. Before the experiment will be conducted a finger calibration task will be performed, in which you are requested to select targets appearing randomly on the screen. The time schedule of the experiment can be seen below in fig. 2, where the order of the motion levels may change according to the order of participants. The total experiment will take roughly an hour.


Figure 2: Experiment planning

## References

Louise V Coutts, Katherine L Plant, Mark Smith, Luke Bolton, Katie J Parnell, James Arnold, and Neville A Stanton. Future technology on the flight deck: assessing the use of touch-screens in vibration environments. 2018. ISSN 1366-5847. doi: 10.1080/00140139.2018.1552013. URL https://doi.org/10.1080/00140139.2018.1552013.

N. C. M. van Zon. Evaluation of a touch-based navigation display for lateral weather avoidance. 2017.

# B

# Participant accuracy scores

Table B.1: Participant accuracy scores - Fitts' law experiment

| | T0 | T1 | T2 | T3 |
|---|---|---|---|---|
| S1 | 99.0% | 99.5% | 100.0% | 99.5% |
| S2 | 99.0% | 97.4% | 98.5% | 100.0% |
| S3 | 100.0% | 100.0% | 100.0% | 100.0% |
| S4 | 100.0% | 100.0% | 100.0% | 100.0% |
| S5 | 100.0% | 100.0% | 100.0% | 99.5% |
| S6 | 100.0% | 100.0% | 99.5% | 100.0% |
| S7 | 100.0% | 100.0% | 99.5% | 100.0% |
| S8 | 100.0% | 100.0% | 100.0% | 99.5% |
| S9 | 98.4% | 98.4% | 99.0% | 99.0% |
| S10 | 100.0% | 100.0% | 100.0% | 100.0% |
| S11 | 100.0% | 100.0% | 100.0% | 99.5% |
| S12 | 100.0% | 100.0% | 100.0% | 100.0% |
| S13 | 99.5% | 99.5% | 99.5% | 97.4% |
| S14 | 100.0% | 99.5% | 100.0% | 100.0% |
| S15 | 100.0% | 100.0% | 99.0% | 99.5% |
| S16 | 100.0% | 100.0% | 100.0% | 100.0% |

# C

# Generation parameters turbulence profile

```
% This M-file is used to generate the Patchy turbulence velocities
% Based on patchy3, updated for use in Fitts Law Turbulence project
% Updated by Bart Jacobson on 23-08-2020
% For experiment V=165 m/s scale length lg300 and tau column 2 are used
%P, Q, R and K values are tuned according to vd Moesdijk (1975)

c = 2.022; % average chord length Cessna Citation ii (dimensionless
    scaling factor)

%basic gust intensities rms, to be scaled later on by SRS
sigma_ug = 1;
sigma_wg = 1;
sigma_vg = 1;

% scaling parameters for Dryden model
Lug = 300;
Lvg = 300;
Lwg = 300;

Q = 0.5;
R = 0.7;
Vref = 165;

K = (9*Q^4 + 6*Q^2 + 3)/(1 + Q^2)^2;

Ka = 1;
Kb = 1;
Kc = 1;

sigma_u1 = Q*sigma_ug/sqrt(1+Q^2);
sigma_c1 = sigma_ug/sqrt(1+Q^2);

sigma_u2 = Q*sigma_wg/sqrt(1+Q^2);
sigma_c2 = sigma_wg/sqrt(1+Q^2);

sigma_u3 = Q*sigma_vg/sqrt(1+Q^2);
sigma_c3 = sigma_vg/sqrt(1+Q^2);
```

```
37
38 Ts = 0.01; %100 hz
39 w1 = 1; %intensity
40 w2 = 1;
41 w3 = 1;
42 w4 = 1;
43 w5 = 1;
44 w6 = 1;
45 w7 = 1;
46 w8 = 1;
47 w9 = 1;
48 w10 = 1;
49 w11 = 1;
50 w12 = 1;
51 w13 = 1;
52 w14 = 1;
53 w15 = 1;
54
55 % gains
56 gain1 = 1;
57 gain2 = 1.2;
58 gain3 = 2;
59 gain4 = 2;
60 gain5 = 2;
61 gain6 = 2;
62 gain7 = 2;
63 gain8 = 3;
64 gain9 = 3;
65 gain10 = 5;
66
67 Seedw1 = 89;
68 Seedw2 = 34;
69 Seedw3 = 12;
70 Seedw4 = 23;
71 Seedw5 = 78;
72 Seedw6 = 62;
73 Seedw7 = 68;
74 Seedw8 = 20;
75 Seedw9 = 77;
76 Seedw10 = 78;
77 Seedw11 = 14;
78 Seedw12 = 61;
79 Seedw13 = 40;
80 Seedw14 = 33;
81 Seedw15 = 3;
82                  %used for the experiment Lg300 are used now
83 lug_0B =  0.14008324;  % original in this code 0.007918894; % lg100:
       0.0472065;
84 lag_0B =  0.10068652; %originally 0.0054214371; % lg100: 0.0342911;
85
86 tau1 =    0.21287628; %originally 0.059134856; % lg100:0.130196;
87 tau2 =    0.69046268; % originally 0.456390523; %lg100: 0.603906;
88 tau3 =    0.53044024;  % originally 0.338947525; %lg100: 0.455195;
89
90 tau4 =    0.145590608; %originally  0.038532119; %lg100: 0.080022;
91 tau5 =    0.42541976; %originally 0.249998425; %lg100: 0.356320;
```

```
92  tau6 =     0.305779096; %originally 0.207222510; %lg100: 0.241075;
93
94  A1 = Lug/Vref*(R+1)/R*tau2;
95  B1 = sqrt(tau2*(R+1)-tau1*R)*sqrt(1+(tau2^2-tau3^2)*R/(tau2*(tau2+tau1)));
96  C1 = Q/sqrt(1+Q^2)*sqrt(2/pi*lug_0B*((tau2^2-tau3^2)/(tau2*(tau2^2-tau3^2)
        )+(tau1^2-tau3^2)/(tau1*(tau1^2-tau2^2))))*Lug/Vref*tau2*(R+1)/R;
97  D1 = Lug/Vref*(R+1)*tau2;
98  E1 = Lug/Vref*(R+1)*sqrt(tau2*tau3^2-(R*tau2^2*(tau1^2-tau3^2)/(tau2+tau1)
        ));
99  F1 = Q/sqrt(1+Q^2)*sqrt(2/pi*lug_0B*(tau2*tau1*(tau2^2-tau1^2)/(tau1*tau2
        ^2-tau1*tau3^2-tau2*tau1^2+tau2*tau3^2)))*(Lug/Vref*tau2*(R+1)/(tau2*(R
        +1)-tau1*R)^2);
100 G1 = Lug/Vref*(tau2*tau1*(R+1)/(tau2*(R+1)-tau1*R));
101 H1 = 1/(1+Q^2)*lug_0B;
102 L1 = Lug/Vref*tau3;
103 M1 = Lug/Vref*tau1;
104 N1 = Lug/Vref*tau2;
105
106 A2 = Lwg/Vref*(R+1)/R*tau5;
107 B2 = sqrt(tau5*(R+1)-tau4*R)*sqrt(1+(tau5^2-tau6^2)*R/(tau5*(tau5+tau4)));
108 C2 = Q/sqrt(1+Q^2)*sqrt(2/pi*lag_0B*((tau5^2-tau6^2)/(tau5*(tau5^2-tau6^2)
        )+(tau4^2-tau6^2)/(tau4*(tau4^2-tau5^2))))*Lwg/Vref*tau5*(R+1)/R;
109 D2 = Lwg/Vref*(R+1)*tau5;
110 E2 = Lwg/Vref*(R+1)*sqrt(tau5*tau6^2-(R*tau5^2*(tau4^2-tau6^2)/(tau5+tau4)
        ));
111 F2 = Q/sqrt(1+Q^2)*sqrt(2/pi*lag_0B*(tau5*tau4*(tau5^2-tau4^2)/(tau4*tau5
        ^2-tau4*tau6^2-tau5*tau4^2+tau5*tau6^2)))*(Lwg/Vref*tau5*(R+1)/(tau5*(R
        +1)-tau4*R)^2);
112 G2 = Lwg/Vref*(tau5*tau4*(R+1)/(tau5*(R+1)-tau4*R));
113 H2 = 1/(1+Q^2)*lag_0B;
114 L2 = Lwg/Vref*tau6;
115 M2 = Lwg/Vref*tau4;
116 N2 = Lwg/Vref*tau5;
117
118
119 %%filter
120 zeta1 = 1;   % comparison value
121 zeta2 = 1;   % used value
122
123 omega1 = 10*2*pi;  % comparison value
124 omega2 = 10*2*pi;  % used value
125 %
126 % Filter ON
127 filtnum = [0 0 omega2^2];
128 filtden = [1 2*zeta2*omega2 omega2^2];
129 filtnum1 = [0 0 omega2^2 0];
130 filtden1 = [1 2*zeta2*omega2 omega2^2];
131
132 % Filter OFF
133 %  filtnum = [1];
134 %  filtden = [1];
135 %
136 %  filtnum1 = [1 0];
137 %  filtden1 = [0 1];
138
139
```

```
140 %patchymodel: with filter
141 %patchymodel2:without filter
142 %patchymodel3:without filter, switched derivative
143 [T,X,ug,wg,vg,ugasym,agasym,ugdot,wgdot,vgdot] = sim('patchy_model_FLT');
144
145 % convert to knots
146 ugk = ug/0.51444;
147 vgk = vg/0.51444;
148 wgk = wg/0.51444;
149 ugasymk = ugasym/0.51444;
150 agasymk = agasym/0.51444;
151
152 % Making dimensionless
153 ug_v = ug/Vref;
154 ag   = wg/Vref;
155 bg   = vg/Vref;
156 ug_vdot = ugdot/Vref*c/Vref;
157 agdot = wgdot/Vref*c/Vref;
158 bgdot = vgdot/Vref*c/Vref;
159 ugasym_v = ugasym/Vref;
160 agasym_v = agasym/Vref;
161
162 % Gives dimensionless gust velocity vector containing u,alpha,beta gust,
      udot, alphadot
163 %and betadot gust, u and a gust asymetric
164 velocity = [ug_v ag bg ug_vdot agdot bgdot ugasym_v agasym_v];
165
166 save turb_Bart_R07Q05 T ug_v ag bg ug_vdot agdot bgdot ugasym_v agasym_v
167 save turb_Bart_R07Q05.dat velocity -ascii %-double
```

# D

# Filter settings Simona Research Simulator

```
% Classical Washout Filter Values
%
% This file contains required parameters for
% a motion filter.
%
%-----------------------------------------------------------
% (c) Bas Gouverneur, February 2003
%  modified Olaf Stroosma, March 2006
%  modified Bart Jacobson, September 2020
%-----------------------------------------------------------

%-----------------------------------------------------------
% General parameters
%-----------------------------------------------------------
g = 9.80665;
LZDERPUGP = 1.2075;

%-----------------------------------------------------------
% Reference points, relative to UGP.
% Aircraft motion is transformed from aircraft reference point
% to filter reference point before filtering.
% Simulator motion is then transformed from filter reference
% point to the motion base reference point (=UGP).
%
% Use ref_ac = (0,0,-1.2075) and ref_filt = (0,0,0) for
% behaviour of cw08 and earlier.
% Use ref_ac = (0,0,-1.2075) and ref_filt = (0,0,-1.2075) for
% doing everything in DERP.
%-----------------------------------------------------------
xref_ac = 0.0;
yref_ac = 0.0;
zref_ac = -1.2075;

xref_filt = 0.0;
yref_filt = 0.0;
zref_filt = -1.2075;

```

```
38 %------------------------------------------------------------
39 % Feedback parameters for synchronization with motion limiter
40 %------------------------------------------------------------
41
42 Kfeedbackx = 0.5;
43 Kfeedbackxd = 0.1;
44 Kfeedbackeuler = 0.2;
45 Kfeedbackeulerrate = 0.5;
46
47 %------------------------------------------------------------
48 % Controller parameters for achieving tilt coordination
49 % Available methods:
50 % 1) straight differentiation (Bas)
51 % 2) differentiation with rate limit compensation (Herman)
52 % 3) sim state feedback controller (Olaf)
53 %------------------------------------------------------------
54 tiltcoordinationmethod = 2;
55 Ktiltrate = 3.0; % method 2
56 Ktilteuler = 0.2; % method 3
57 Ktilteulerrate = 0.5; % method 3
58
59 %------------------------------------------------------------
60 % Motion Filter channel selection gains (select 0 or 1)
61 %------------------------------------------------------------
62
63 gainfx = 1;
64 gainfy = 1;
65 gainfz = 1;
66
67 gainfxtilt = 1;
68 gainfytilt = 1;
69
70 gainp = 1;
71 gainq = 1;
72 gainr = 1;
73
74 % gainfx = 1;
75 % gainfy = 0;
76 % gainfz = 1;
77 %
78 % gainfxtilt = 1;
79 % gainfytilt = 0;
80 %
81 % gainp = 0;
82 % gainq = 1;
83 % gainr = 0;
84
85 %------------------------------------------------------------
86 % Motion Filter Gains (k)
87 %------------------------------------------------------------
88
89
90 kfx = 1.0;                          %surge gain
91 kfy = 0.5;                          %sway gain
92 kfz = 0.5;                          %heave gain
93
```

```
94  kwp = 0.5;                          %roll gain
95  kwq = 0.5;                          %pitch gain
96  kwr = 0.5;                          %yaw gain
97
98  kf = [kfx 0 0; 0 kfy 0; 0 0 kfz];
99  kw = [kwp 0 0; 0 kwq 0; 0 0 kwr];
100
101 %-------------------------------------------------------
102 % Motion Filter 2nd order Break-Frequencies (omega_n)
103 % (set to zero for 1st order only)
104 %-------------------------------------------------------
105
106
107 HPomeganx      = 1.5;               %high pass surge omega_n
108 HPomegany      = 1.5;               %high pass sway omega_n
109 HPomeganz      = 4.0;               %high pass heave omega_n
110
111 LPomeganx      = 3.0;               %low pass surge omega_n
112 LPomegany      = 3.0;               %low pass sway omega_n
113
114 HPomeganphi    = 1.0;               %high pass phi (roll)
115 HPomegantheta  = 1.0;               %high pass theta (pitch)
116 HPomeganpsi    = 1.0;               %high pass psi (yaw)
117
118 %-------------------------------------------------------
119 % Motion Filter 1st order Break-Frequencies (omega_b)
120 % (set to zero for 2nd order only)
121 %-------------------------------------------------------
122
123 HPomegabx      = 0.0;               %high pass surge omega_b
124 HPomegaby      = 0.0;               %high pass sway omega_b
125 HPomegabz      = 0.3;               %high pass heave omega_b
126
127 HPomegabphi    = 0.0;               %high pass roll omega_b
128 HPomegabtheta  = 0.0;               %high pass pitch omega_b
129 HPomegabpsi    = 0.0;               %high pass yaw omega_b
130
131 %-------------------------------------------------------
132 % Motion Filter Damping Coefficients (zeta)
133 %-------------------------------------------------------
134
135 HPzetax      = 1.0;                 %high pass surge zeta
136 HPzetay      = 1.0;                 %high pass sway zeta
137 HPzetaz      = 1.0;                 %high pass heave zeta
138
139 LPzetax      = 1.0;                 %low pass surge zeta
140 LPzetay      = 1.0;                 %low pass sway zeta
141
142 HPzetaphi    = 1.0;                 %high pass roll zeta
143 HPzetatheta  = 1.0;                 %high pass pitch zeta
144 HPzetapsi    = 1.0;                 %high pass yaw zeta
145
146
147 %-------------------------------------------------------
148 % Tilt coordination angular rate limit (deg/sec)
149 %-------------------------------------------------------
```

```
150
151 Beta_rate = 3*(pi/180);
```

# E

# Continuous touch data results

The continuous touch data results are split up into four parts. This has been done as the experiment conditions were varied through A, W, $\phi$ and $\theta$ and only the variance in A and W have been logged in the experiment results. Therefore it is unfortunately not possible to exactly match the 192 different conditions to each other as the experiment has been performed in four different orders. The average values over the separate intensities of turbulence can still be determined, as well as the average performance per condition as performed by groups of four participants, as shown in the four tables below. The percentage increase in path length travelled across the screen is shown, along with the quantitative non-linearity (QNL) of the dragging input. Negative values of path length increase indicate the participant overlapped the circles just enough to successfully reach the target circle, but remain partly in between the origin and target, thus causing a slight undershoot. The averaged values over all participants is shown in Table E.1.

Table E.1: Overall average values continuous data

| All participants | Path length increase [%] | | | | QNL [mm] | | | |
|---|---|---|---|---|---|---|---|---|
| Turbulence condition | No | Low | Medium | Severe | No | Low | Medium | Severe |
| Averaged | 7.80 | 8.57 | 10.17 | 11.82 | 2.12 | 2.23 | 2.29 | 2.45 |

| Participants 1-4 | | | Path length increase [%] | | | | QNL [mm] | | | |
|---|---|---|---|---|---|---|---|---|---|---|
| condition | A | W | no | low | med | severe | no | low | med | severe |
| 1 | 45 | 5 | 5.81 | 7.43 | 11.47 | 18.17 | 1.86 | 1.57 | 1.92 | 1.35 |
| 2 | 45 | 5 | -0.98 | -2.77 | 1.09 | 2.40 | 1.22 | 1.54 | 2.18 | 3.09 |
| 3 | 150 | 35 | 19.92 | 22.08 | 76.10 | 59.71 | 1.18 | 2.92 | 5.60 | 3.22 |
| 4 | 45 | 5 | -0.05 | 1.50 | 0.31 | 2.23 | 1.23 | 2.05 | 1.48 | 2.28 |
| 5 | 150 | 35 | 15.93 | 10.93 | 14.48 | 21.47 | 1.04 | 1.67 | 2.20 | 2.09 |
| 6 | 45 | 5 | -0.69 | -1.88 | -0.44 | -0.17 | 2.88 | 2.04 | 5.32 | 2.91 |
| 7 | 150 | 35 | 14.66 | 10.07 | 7.09 | 10.31 | 1.65 | 2.60 | 1.00 | 1.76 |
| 8 | 45 | 5 | 2.59 | 2.41 | 2.73 | 1.99 | 2.37 | 3.13 | 2.89 | 3.33 |
| 9 | 150 | 35 | 8.53 | 8.37 | 11.23 | 21.31 | 1.67 | 1.57 | 1.83 | 1.41 |
| 10 | 45 | 5 | 4.44 | 2.97 | 6.88 | 4.97 | 1.79 | 1.76 | 2.44 | 2.22 |
| 11 | 150 | 35 | 14.14 | 18.26 | 28.77 | 26.26 | 0.82 | 1.16 | 1.61 | 1.88 |
| 12 | 45 | 5 | 6.05 | 11.59 | 7.34 | 8.51 | 1.68 | 1.73 | 2.52 | 2.45 |
| 13 | 150 | 35 | 4.41 | 9.76 | 13.34 | 35.42 | 1.01 | 1.42 | 1.08 | 1.39 |
| 14 | 45 | 5 | 9.86 | 11.58 | 12.70 | 11.02 | 2.09 | 1.46 | 4.01 | 1.97 |
| 15 | 150 | 35 | 9.01 | 12.09 | 8.58 | 19.22 | 1.71 | 2.28 | 1.36 | 1.48 |
| 16 | 45 | 5 | 4.94 | 4.83 | 3.98 | 6.95 | 2.03 | 2.00 | 2.51 | 4.14 |
| 17 | 150 | 35 | 11.10 | 4.42 | 19.47 | 122.56 | 1.54 | 0.85 | 2.63 | 8.52 |
| 18 | 45 | 5 | 1.03 | 0.71 | 3.32 | 2.97 | 2.82 | 2.12 | 3.55 | 3.39 |
| 19 | 150 | 35 | 15.03 | 12.10 | 12.22 | 10.62 | 1.30 | 1.26 | 1.36 | 1.85 |

| | | | | | | | | | | |
|---|---|---|---|---|---|---|---|---|---|---|
| 20 | 45 | 5 | 3.66 | 1.42 | 1.81 | 3.97 | 2.84 | 2.58 | 2.82 | 2.13 |
| 21 | 150 | 35 | 16.38 | 32.00 | 22.08 | 30.11 | 1.19 | 1.42 | 1.00 | 1.85 |
| 22 | 45 | 5 | 1.71 | -0.29 | 1.82 | 3.66 | 3.82 | 1.92 | 2.63 | 2.19 |
| 23 | 150 | 35 | 3.21 | 8.12 | 0.51 | 8.83 | 1.36 | 1.42 | 0.90 | 1.65 |
| 24 | 45 | 15 | 1.97 | 3.23 | 5.91 | 5.50 | 2.86 | 1.68 | 2.24 | 3.57 |
| 25 | 150 | 35 | 8.96 | 12.16 | 20.71 | 19.95 | 1.43 | 1.54 | 1.51 | 1.30 |
| 26 | 45 | 15 | 4.80 | -0.17 | 3.74 | 2.36 | 1.58 | 1.86 | 2.26 | 1.15 |
| 27 | 150 | 25 | 4.38 | 12.99 | 12.97 | 17.44 | 1.73 | 1.92 | 1.78 | 1.99 |
| 28 | 45 | 15 | 6.80 | 3.01 | 3.05 | 4.02 | 1.47 | 1.91 | 2.17 | 2.04 |
| 29 | 150 | 25 | 9.36 | 13.73 | 13.11 | 30.02 | 1.04 | 1.69 | 1.77 | 2.02 |
| 30 | 45 | 15 | 2.55 | 1.17 | 6.60 | 6.13 | 2.19 | 1.83 | 5.31 | 3.53 |
| 31 | 150 | 25 | 7.21 | 6.25 | 6.97 | 2.22 | 2.10 | 1.85 | 1.59 | 1.43 |
| 32 | 45 | 15 | 0.93 | 1.49 | 3.24 | 3.91 | 2.44 | 2.36 | 1.89 | 2.44 |
| 33 | 150 | 25 | 11.27 | 9.39 | 10.82 | 37.38 | 1.56 | 1.79 | 1.25 | 1.75 |
| 34 | 45 | 15 | 6.04 | 7.40 | 4.94 | 6.52 | 2.46 | 2.06 | 1.93 | 3.92 |
| 35 | 150 | 25 | 2.20 | 5.79 | 8.13 | 22.62 | 1.01 | 1.56 | 1.76 | 1.66 |
| 36 | 45 | 15 | 2.34 | 4.45 | 7.60 | 3.35 | 1.82 | 2.10 | 3.89 | 3.77 |
| 37 | 150 | 25 | 8.54 | 10.87 | 17.73 | 16.31 | 0.87 | 0.81 | 1.08 | 1.41 |
| 38 | 45 | 15 | 3.47 | 7.44 | 9.80 | 8.57 | 1.19 | 1.42 | 2.53 | 4.49 |
| 39 | 150 | 25 | 4.66 | 7.77 | 9.37 | 2.47 | 1.73 | 1.90 | 2.00 | 1.94 |
| 40 | 45 | 15 | 3.45 | 6.20 | 1.53 | 2.60 | 2.31 | 2.42 | 2.25 | 2.52 |
| 41 | 150 | 25 | 8.57 | 10.35 | 15.58 | 100.54 | 1.06 | 1.12 | 3.03 | 3.67 |
| 42 | 45 | 15 | -0.17 | 0.12 | 4.48 | 2.32 | 2.23 | 1.88 | 2.31 | 3.31 |
| 43 | 150 | 25 | 9.84 | 7.13 | 9.52 | 5.69 | 1.20 | 1.15 | 1.02 | 1.30 |
| 44 | 45 | 15 | 4.15 | 3.59 | 3.29 | 3.69 | 1.50 | 1.83 | 3.71 | 4.02 |
| 45 | 150 | 25 | 12.64 | 4.88 | 23.02 | 26.90 | 1.62 | 1.55 | 2.07 | 1.94 |
| 46 | 45 | 15 | -0.01 | -0.27 | 2.19 | 6.34 | 1.70 | 2.06 | 1.94 | 2.72 |
| 47 | 150 | 25 | -9.72 | -5.82 | -4.48 | -3.24 | 1.21 | 1.60 | 1.24 | 1.64 |
| 48 | 45 | 25 | 2.22 | 3.63 | 3.18 | 4.19 | 2.46 | 3.50 | 2.90 | 2.40 |
| 49 | 150 | 25 | 4.40 | 34.37 | 20.80 | 17.01 | 1.37 | 1.81 | 0.90 | 1.95 |
| 50 | 45 | 25 | 3.72 | 4.37 | 6.32 | 7.05 | 1.98 | 2.20 | 2.20 | 2.39 |
| 51 | 150 | 15 | 14.45 | 24.59 | 23.22 | 9.63 | 1.97 | 2.21 | 0.86 | 1.45 |
| 52 | 45 | 25 | 4.57 | 4.88 | 5.63 | 6.02 | 2.20 | 1.58 | 2.80 | 1.12 |
| 53 | 150 | 15 | 1.36 | 4.99 | 5.06 | 2.98 | 0.69 | 0.89 | 2.03 | 0.97 |
| 54 | 45 | 25 | 4.22 | 4.03 | 3.57 | 5.84 | 2.55 | 2.13 | 3.28 | 2.44 |
| 55 | 150 | 15 | 3.08 | -0.13 | -0.19 | 71.49 | 1.60 | 1.78 | 1.57 | 2.72 |
| 56 | 45 | 25 | 2.71 | 1.98 | 4.60 | 5.00 | 1.93 | 2.22 | 3.36 | 2.02 |
| 57 | 150 | 15 | -0.48 | 6.15 | 23.11 | 19.70 | 0.88 | 1.35 | 1.83 | 1.98 |
| 58 | 45 | 25 | 4.00 | 4.11 | 6.37 | 22.16 | 2.16 | 2.05 | 1.49 | 8.19 |
| 59 | 150 | 15 | 17.08 | 23.87 | 20.10 | 24.58 | 0.61 | 1.51 | 1.38 | 1.37 |
| 60 | 45 | 25 | 3.75 | 3.23 | 5.52 | 1.17 | 1.83 | 2.66 | 2.69 | 2.70 |
| 61 | 150 | 15 | 0.18 | -6.43 | -5.88 | 7.13 | 0.78 | 0.65 | 1.09 | 1.27 |
| 62 | 45 | 25 | 2.88 | 5.77 | 3.59 | 7.01 | 1.74 | 1.67 | 3.07 | 3.85 |
| 63 | 150 | 15 | 0.42 | 3.46 | 6.08 | 5.54 | 1.61 | 1.75 | 2.03 | 1.18 |
| 64 | 45 | 25 | 2.74 | 2.76 | 4.12 | 8.26 | 1.51 | 3.13 | 3.09 | 3.75 |
| 65 | 150 | 15 | 6.87 | 12.10 | 16.78 | 12.96 | 0.47 | 1.04 | 1.73 | 2.08 |
| 66 | 45 | 25 | 2.11 | 1.85 | 4.37 | 5.71 | 1.73 | 2.58 | 3.08 | 2.41 |
| 67 | 150 | 15 | -4.68 | 10.36 | -0.01 | 2.76 | 0.91 | 1.18 | 1.78 | 1.56 |
| 68 | 45 | 25 | 6.53 | 5.98 | 4.55 | 11.13 | 3.77 | 4.38 | 3.87 | 5.44 |
| 69 | 150 | 15 | 15.89 | 22.27 | 24.54 | 23.11 | 0.96 | 1.48 | 0.76 | 1.96 |
| 70 | 45 | 25 | 1.09 | 0.59 | 0.99 | 5.76 | 2.38 | 1.47 | 1.30 | 4.48 |
| 71 | 150 | 15 | -2.97 | 17.24 | 11.40 | 18.83 | 1.47 | 1.92 | 2.12 | 1.60 |
| 72 | 45 | 35 | 0.82 | 2.72 | 1.24 | 3.82 | 2.72 | 2.15 | 3.54 | 2.90 |
| 73 | 150 | 15 | 10.70 | 15.53 | 12.57 | 99.43 | 1.32 | 1.77 | 1.92 | 2.15 |
| 74 | 45 | 35 | 6.11 | 9.06 | 6.01 | 8.17 | 2.32 | 2.27 | 2.46 | 3.23 |
| 75 | 150 | 5 | 7.59 | 5.01 | 8.97 | 20.26 | 1.84 | 1.35 | 2.26 | 1.24 |

| | | | | | | | | | | |
|---|---|---|---|---|---|---|---|---|---|---|
| 76 | 45 | 35 | 4.29 | 2.45 | 7.03 | 4.82 | 2.96 | 1.93 | 2.53 | 2.79 |
| 77 | 150 | 5 | 5.29 | 0.99 | 5.55 | 4.75 | 1.32 | 1.44 | 2.57 | 1.53 |
| 78 | 45 | 35 | 4.15 | 7.22 | 6.69 | 15.81 | 2.77 | 3.47 | 4.72 | 5.90 |
| 79 | 150 | 5 | -3.47 | -14.65 | -9.17 | -2.77 | 2.08 | 1.67 | 1.50 | 1.44 |
| 80 | 45 | 35 | 3.12 | 3.59 | 4.14 | 9.06 | 1.77 | 1.89 | 2.73 | 3.38 |
| 81 | 150 | 5 | 7.49 | 12.08 | 23.26 | 9.92 | 1.63 | 1.35 | 2.25 | 2.16 |
| 82 | 45 | 35 | 7.14 | 8.69 | 3.56 | 6.31 | 2.91 | 1.67 | 2.11 | 2.04 |
| 83 | 150 | 5 | 5.97 | 7.46 | 8.01 | 10.71 | 1.16 | 1.86 | 0.97 | 1.54 |
| 84 | 45 | 35 | 2.32 | 2.75 | 4.54 | 5.12 | 2.34 | 2.19 | 2.69 | 1.88 |
| 85 | 150 | 5 | 5.00 | 5.50 | 20.85 | 11.42 | 1.84 | 1.55 | 1.28 | 2.09 |
| 86 | 45 | 35 | 4.26 | 5.01 | 6.38 | 5.69 | 2.62 | 5.19 | 2.10 | 3.31 |
| 87 | 150 | 5 | 10.95 | 6.71 | 6.17 | 4.22 | 1.86 | 1.72 | 2.13 | 2.18 |
| 88 | 45 | 35 | 4.11 | 4.70 | 3.16 | 6.32 | 2.66 | 2.85 | 2.26 | 2.91 |
| 89 | 150 | 5 | 9.63 | -4.87 | -11.24 | -5.77 | 1.62 | 1.69 | 1.96 | 1.57 |
| 90 | 45 | 35 | 2.73 | 1.99 | 2.73 | 11.10 | 2.49 | 2.19 | 1.88 | 3.14 |
| 91 | 150 | 5 | 2.88 | -0.74 | 14.32 | 8.08 | 1.18 | 1.51 | 1.27 | 1.27 |
| 92 | 45 | 35 | 8.42 | 8.77 | 6.97 | 13.44 | 2.32 | 3.78 | 3.83 | 5.92 |
| 93 | 150 | 5 | -2.64 | 6.20 | 3.53 | 6.21 | 0.84 | 1.90 | 1.92 | 1.82 |
| 94 | 45 | 35 | 4.51 | 2.53 | 3.94 | 7.39 | 3.18 | 2.71 | 2.37 | 2.28 |
| 95 | 150 | 5 | 3.01 | 7.78 | 5.59 | 11.60 | 2.19 | 2.65 | 2.47 | 1.73 |
| 96 | 80 | 5 | 2.55 | 2.62 | 3.62 | 3.27 | 3.10 | 3.02 | 2.67 | 3.95 |
| 97 | 150 | 5 | 5.34 | 7.57 | 6.66 | 11.52 | 1.92 | 0.74 | 2.86 | 1.59 |
| 98 | 80 | 5 | 9.51 | 13.89 | 21.76 | 11.40 | 1.58 | 1.68 | 1.68 | 2.55 |
| 99 | 115 | 35 | 6.68 | 10.70 | 19.26 | 18.36 | 1.46 | 1.94 | 2.09 | 2.86 |
| 100 | 80 | 5 | 4.37 | 3.17 | 5.56 | 11.71 | 1.74 | 1.50 | 1.86 | 1.57 |
| 101 | 115 | 35 | 8.21 | 6.40 | 6.93 | 12.23 | 1.39 | 2.40 | 1.32 | 2.85 |
| 102 | 80 | 5 | 4.03 | 2.12 | 7.82 | 2.11 | 2.33 | 2.97 | 3.19 | 3.67 |
| 103 | 115 | 35 | 5.87 | 3.34 | 5.67 | 13.61 | 2.25 | 1.21 | 2.10 | 2.39 |
| 104 | 80 | 5 | 6.81 | 6.57 | 10.79 | 9.12 | 1.98 | 2.48 | 1.54 | 2.44 |
| 105 | 115 | 35 | 2.48 | 6.19 | 14.15 | 9.08 | 1.59 | 1.32 | 1.61 | 2.56 |
| 106 | 80 | 5 | 2.95 | 3.03 | 7.55 | 4.11 | 1.16 | 1.77 | 2.88 | 1.58 |
| 107 | 115 | 35 | 3.08 | 7.83 | 3.98 | 11.75 | 0.89 | 1.67 | 2.06 | 1.47 |
| 108 | 80 | 5 | 4.06 | 4.51 | 7.66 | 6.82 | 2.40 | 1.96 | 1.93 | 1.69 |
| 109 | 115 | 35 | 7.56 | 14.09 | 27.80 | 11.19 | 1.71 | 1.49 | 1.95 | 1.83 |
| 110 | 80 | 5 | -0.19 | 0.33 | 2.73 | -0.89 | 1.61 | 1.77 | 2.89 | 2.39 |
| 111 | 115 | 35 | 5.64 | 6.58 | 11.28 | 11.37 | 1.45 | 1.76 | 2.16 | 1.63 |
| 112 | 80 | 5 | 0.28 | 1.40 | 13.36 | -0.50 | 1.41 | 1.58 | 1.74 | 2.41 |
| 113 | 115 | 35 | 5.06 | 9.38 | 10.23 | 11.06 | 1.69 | 2.94 | 3.27 | 1.92 |
| 114 | 80 | 5 | -0.66 | 1.14 | -0.08 | -0.12 | 2.20 | 1.86 | 2.74 | 2.58 |
| 115 | 115 | 35 | 6.85 | 6.49 | 7.65 | 9.88 | 1.51 | 1.10 | 2.06 | 1.73 |
| 116 | 80 | 5 | 4.16 | 3.65 | 12.07 | 8.72 | 2.49 | 2.02 | 3.07 | 2.92 |
| 117 | 115 | 35 | 11.37 | 16.78 | 20.41 | 15.79 | 2.01 | 1.57 | 2.29 | 1.40 |
| 118 | 80 | 5 | 1.80 | 4.44 | 2.30 | 2.95 | 2.18 | 2.18 | 3.05 | 2.07 |
| 119 | 115 | 35 | 2.22 | 6.77 | 8.27 | 6.80 | 1.47 | 2.66 | 1.46 | 2.20 |
| 120 | 80 | 15 | -2.08 | 2.22 | 2.56 | 1.65 | 2.52 | 2.91 | 2.64 | 1.95 |
| 121 | 115 | 35 | 6.34 | 10.17 | 11.21 | 24.54 | 1.08 | 2.27 | 1.85 | 1.68 |
| 122 | 80 | 15 | 4.71 | 10.80 | 14.76 | 9.95 | 1.22 | 1.94 | 2.69 | 2.36 |
| 123 | 115 | 25 | 10.84 | 10.68 | 8.23 | 14.95 | 1.63 | 1.99 | 1.92 | 3.37 |
| 124 | 80 | 15 | 4.62 | 5.04 | 8.40 | 4.46 | 1.57 | 1.45 | 2.09 | 1.86 |
| 125 | 115 | 25 | 4.69 | 11.53 | 3.71 | 7.86 | 1.72 | 1.97 | 2.12 | 1.73 |
| 126 | 80 | 15 | 1.22 | 5.16 | 0.98 | -1.33 | 2.47 | 2.48 | 4.12 | 1.86 |
| 127 | 115 | 25 | 4.90 | 3.63 | 4.93 | 1.77 | 1.99 | 1.55 | 2.28 | 1.98 |
| 128 | 80 | 15 | 1.57 | 14.58 | 1.52 | 2.33 | 2.39 | 5.41 | 1.57 | 3.24 |
| 129 | 115 | 25 | 8.18 | 12.24 | 11.23 | 9.61 | 1.35 | 2.46 | 2.16 | 1.48 |
| 130 | 80 | 15 | 6.04 | 7.26 | 9.01 | 6.41 | 2.26 | 1.50 | 1.99 | 2.12 |
| 131 | 115 | 25 | 5.34 | 10.43 | 5.70 | 10.85 | 1.09 | 1.60 | 1.79 | 1.95 |

| | | | | | | | | | | |
|---|---|---|---|---|---|---|---|---|---|---|
| 132 | 80 | 15 | 4.50 | 7.50 | 7.26 | 6.36 | 1.17 | 1.43 | 1.52 | 1.69 |
| 133 | 115 | 25 | 10.24 | 11.21 | 15.30 | 16.14 | 1.50 | 1.27 | 1.45 | 1.72 |
| 134 | 80 | 15 | 5.85 | 6.60 | 8.64 | 11.34 | 1.38 | 1.60 | 1.97 | 2.93 |
| 135 | 115 | 25 | 4.39 | 0.59 | 2.34 | 2.82 | 2.50 | 1.65 | 2.37 | 1.98 |
| 136 | 80 | 15 | -0.06 | 0.80 | 0.21 | 1.24 | 2.81 | 2.52 | 2.44 | 2.31 |
| 137 | 115 | 25 | 9.66 | 8.58 | 10.35 | 16.08 | 1.67 | 1.13 | 2.40 | 3.62 |
| 138 | 80 | 15 | -4.03 | 3.12 | -3.68 | 4.28 | 1.35 | 2.73 | 1.47 | 2.92 |
| 139 | 115 | 25 | 6.89 | 3.36 | 4.68 | 10.55 | 1.87 | 1.62 | 1.85 | 1.36 |
| 140 | 80 | 15 | 4.64 | 6.18 | 9.28 | 5.66 | 2.36 | 1.77 | 3.30 | 2.12 |
| 141 | 115 | 25 | 10.19 | 8.23 | 12.05 | 8.62 | 1.36 | 1.20 | 0.88 | 1.57 |
| 142 | 80 | 15 | -0.91 | 3.92 | 5.81 | 7.25 | 2.46 | 2.68 | 1.99 | 1.99 |
| 143 | 115 | 25 | 0.46 | -2.31 | -2.92 | -4.06 | 1.63 | 1.93 | 2.45 | 2.54 |
| 144 | 80 | 25 | 3.19 | 5.54 | 6.62 | 19.22 | 2.91 | 3.66 | 2.26 | 4.56 |
| 145 | 115 | 25 | -0.57 | 2.25 | 0.75 | 1.32 | 1.31 | 1.88 | 2.05 | 1.95 |
| 146 | 80 | 25 | 8.25 | 7.90 | 5.57 | 9.55 | 1.83 | 1.87 | 1.65 | 1.89 |
| 147 | 115 | 15 | 2.02 | 2.12 | -0.35 | 2.66 | 1.07 | 1.86 | 1.78 | 1.95 |
| 148 | 80 | 25 | 2.13 | 4.39 | 5.35 | 5.22 | 1.56 | 1.38 | 2.53 | 1.73 |
| 149 | 115 | 15 | 0.52 | 3.67 | -2.26 | 1.10 | 1.63 | 1.63 | 1.90 | 1.03 |
| 150 | 80 | 25 | 6.10 | 10.92 | 8.89 | 7.53 | 1.73 | 4.05 | 1.51 | 1.93 |
| 151 | 115 | 15 | 5.70 | 11.31 | 6.97 | 8.88 | 2.18 | 2.16 | 1.93 | 2.84 |
| 152 | 80 | 25 | 2.17 | 0.51 | 2.32 | 1.60 | 0.94 | 2.06 | 2.16 | 2.59 |
| 153 | 115 | 15 | 0.16 | 0.24 | 2.65 | 5.50 | 1.30 | 1.60 | 2.50 | 2.38 |
| 154 | 80 | 25 | 3.53 | 5.72 | 6.52 | 8.89 | 1.91 | 2.05 | 2.10 | 2.01 |
| 155 | 115 | 15 | 11.79 | 9.19 | 8.59 | 12.22 | 1.04 | 1.65 | 1.56 | 2.33 |
| 156 | 80 | 25 | 4.23 | 6.47 | 3.99 | 4.64 | 1.73 | 1.61 | 2.38 | 1.79 |
| 157 | 115 | 15 | 12.00 | 8.45 | 8.63 | 8.59 | 1.26 | 1.12 | 2.18 | 1.48 |
| 158 | 80 | 25 | 3.81 | 9.06 | 8.70 | 11.41 | 1.77 | 2.14 | 3.44 | 3.88 |
| 159 | 115 | 15 | 0.63 | 1.83 | -1.25 | 4.25 | 1.57 | 1.76 | 1.60 | 2.22 |
| 160 | 80 | 25 | 1.56 | 1.96 | 2.84 | 3.13 | 2.22 | 2.88 | 2.90 | 3.18 |
| 161 | 115 | 15 | -1.31 | 4.95 | 7.31 | 11.83 | 1.52 | 3.24 | 2.71 | 3.29 |
| 162 | 80 | 25 | 2.61 | 0.06 | 2.77 | 4.40 | 2.53 | 1.30 | 2.62 | 2.33 |
| 163 | 115 | 15 | 3.56 | 4.83 | 3.46 | 7.63 | 1.74 | 2.57 | 2.41 | 2.68 |
| 164 | 80 | 25 | 7.28 | 2.28 | 5.13 | 8.30 | 1.99 | 1.72 | 2.87 | 5.02 |
| 165 | 115 | 15 | 5.96 | 8.84 | 2.94 | -0.87 | 1.89 | 1.46 | 1.80 | 2.05 |
| 166 | 80 | 25 | 7.57 | 3.49 | 4.90 | 4.83 | 2.54 | 2.82 | 1.98 | 2.53 |
| 167 | 115 | 15 | 0.13 | 0.19 | -0.19 | 5.38 | 0.96 | 2.70 | 2.56 | 2.52 |
| 168 | 80 | 35 | 2.21 | 1.80 | 5.02 | 2.55 | 1.52 | 3.13 | 2.24 | 2.73 |
| 169 | 115 | 15 | 8.25 | 2.35 | 6.44 | 13.55 | 2.47 | 1.23 | 2.33 | 2.19 |
| 170 | 80 | 35 | 5.96 | 3.44 | 2.82 | 6.17 | 2.08 | 1.48 | 1.93 | 1.82 |
| 171 | 115 | 5 | 3.48 | 4.54 | 8.41 | 2.98 | 2.31 | 2.14 | 1.77 | 3.43 |
| 172 | 80 | 35 | 6.68 | 7.05 | 10.35 | 11.25 | 1.56 | 1.99 | 1.71 | 2.77 |
| 173 | 115 | 5 | 2.25 | 0.82 | 0.13 | 2.91 | 2.03 | 1.90 | 1.78 | 2.96 |
| 174 | 80 | 35 | 7.82 | 6.98 | 10.60 | 13.74 | 3.18 | 2.70 | 1.73 | 4.97 |
| 175 | 115 | 5 | -2.95 | 3.81 | -1.77 | 1.60 | 1.53 | 1.84 | 2.46 | 2.65 |
| 176 | 80 | 35 | 3.68 | 1.39 | 3.32 | 6.49 | 1.42 | 1.59 | 2.49 | 3.43 |
| 177 | 115 | 5 | 4.79 | 1.34 | 3.08 | 13.42 | 1.41 | 0.82 | 1.10 | 2.91 |
| 178 | 80 | 35 | 6.08 | 4.65 | 7.41 | 9.67 | 2.14 | 2.00 | 2.12 | 3.44 |
| 179 | 115 | 5 | 2.26 | 9.74 | 8.64 | 8.07 | 1.30 | 1.31 | 2.46 | 1.17 |
| 180 | 80 | 35 | 4.69 | 4.25 | 5.69 | 3.97 | 1.50 | 1.55 | 2.14 | 1.85 |
| 181 | 115 | 5 | 0.14 | 4.08 | 6.14 | 3.20 | 2.33 | 1.60 | 2.44 | 1.22 |
| 182 | 80 | 35 | 2.01 | 3.38 | 7.88 | 6.88 | 1.91 | 2.02 | 1.97 | 3.63 |
| 183 | 115 | 5 | 6.69 | -1.52 | -2.92 | 2.46 | 1.33 | 1.80 | 1.99 | 2.54 |
| 184 | 80 | 35 | 2.27 | 7.78 | 3.90 | 6.18 | 2.22 | 2.66 | 3.08 | 3.26 |
| 185 | 115 | 5 | -3.24 | -2.46 | 5.99 | 5.01 | 1.27 | 2.35 | 1.74 | 4.30 |
| 186 | 80 | 35 | 3.18 | 3.66 | 71.70 | 5.65 | 1.52 | 1.63 | 9.56 | 1.69 |
| 187 | 115 | 5 | 13.96 | 9.65 | 8.63 | 13.19 | 1.55 | 1.51 | 1.94 | 1.95 |

| | | | | | | | | | | |
|---|---|---|---|---|---|---|---|---|---|---|
| 188 | 80 | 35 | 5.39 | 11.76 | 7.57 | 4.04 | 2.66 | 2.37 | 3.05 | 2.03 |
| 189 | 115 | 5 | 1.93 | 3.31 | 3.43 | 3.07 | 1.51 | 1.41 | 1.79 | 1.38 |
| 190 | 80 | 35 | 1.70 | 3.89 | 4.63 | 6.42 | 1.45 | 3.40 | 2.07 | 2.34 |
| 191 | 115 | 5 | 4.67 | 4.87 | 3.90 | 7.22 | 3.44 | 4.06 | 2.63 | 3.20 |
| mean value | 97.41 | 20.08 | 4.71 | 6.02 | 7.80 | 10.70 | 1.80 | 1.98 | 2.26 | 2.46 |

| Participants 5-8 | | | Path length increase [%] | | | | QNL [mm] | | | |
|---|---|---|---|---|---|---|---|---|---|---|
| condition | A | W | no | low | med | severe | no | low | med | severe |
| 1 | 45 | 5 | 10.98 | 19.18 | 10.88 | 8.21 | 1.77 | 2.35 | 2.05 | 1.77 |
| 2 | 45 | 5 | 12.38 | 10.29 | 12.06 | 12.68 | 1.34 | 1.45 | 1.40 | 2.05 |
| 3 | 45 | 5 | 24.75 | 30.69 | 74.00 | 184.22 | 1.26 | 1.19 | 3.91 | 4.39 |
| 4 | 45 | 5 | 9.65 | 9.34 | 10.65 | 17.01 | 2.02 | 2.30 | 2.15 | 1.58 |
| 5 | 150 | 35 | 6.92 | 13.26 | 21.64 | 8.04 | 1.68 | 1.62 | 1.99 | 1.68 |
| 6 | 45 | 5 | 1.58 | 2.51 | 4.04 | 3.84 | 1.37 | 2.81 | 1.57 | 1.29 |
| 7 | 150 | 35 | 3.88 | 14.09 | 15.26 | 10.48 | 1.49 | 2.04 | 1.75 | 2.41 |
| 8 | 45 | 5 | 15.06 | 16.13 | 21.35 | 20.73 | 2.45 | 2.66 | 3.07 | 2.85 |
| 9 | 150 | 35 | 5.70 | 6.10 | 8.27 | 12.32 | 1.49 | 1.39 | 1.58 | 1.29 |
| 10 | 45 | 5 | 3.33 | 0.81 | 6.35 | 6.17 | 2.35 | 2.49 | 3.09 | 2.69 |
| 11 | 150 | 35 | 13.19 | 18.14 | 15.24 | 24.93 | 1.77 | 1.05 | 1.25 | 0.91 |
| 12 | 45 | 5 | 3.44 | 3.15 | 6.32 | 4.44 | 1.90 | 1.86 | 2.51 | 1.92 |
| 13 | 150 | 35 | 10.63 | 14.16 | 19.31 | 9.52 | 1.66 | 1.43 | 2.28 | 1.99 |
| 14 | 45 | 5 | 4.43 | 4.56 | 9.62 | 4.12 | 1.75 | 2.12 | 2.39 | 2.16 |
| 15 | 150 | 35 | 12.50 | 14.20 | 21.64 | 186.61 | 1.01 | 1.53 | 1.13 | 13.21 |
| 16 | 45 | 5 | 1.99 | 1.27 | 2.13 | 1.28 | 1.39 | 1.96 | 1.96 | 2.92 |
| 17 | 150 | 35 | 25.36 | 20.62 | 20.18 | 27.05 | 1.12 | 1.41 | 1.82 | 1.19 |
| 18 | 45 | 5 | 1.95 | 1.43 | 1.72 | 1.93 | 1.79 | 2.65 | 1.88 | 2.22 |
| 19 | 150 | 35 | 12.92 | 10.48 | 34.31 | 21.00 | 1.33 | 1.57 | 1.43 | 1.94 |
| 20 | 45 | 5 | 2.23 | 2.67 | 5.48 | 4.76 | 2.25 | 1.51 | 2.14 | 2.60 |
| 21 | 150 | 35 | 10.09 | 10.14 | 10.93 | 6.08 | 1.46 | 1.52 | 1.64 | 1.07 |
| 22 | 45 | 15 | 4.15 | 3.52 | 7.28 | 5.81 | 3.21 | 3.72 | 3.63 | 2.89 |
| 23 | 150 | 35 | 23.09 | 14.79 | 18.25 | 20.07 | 1.47 | 1.51 | 2.05 | 1.36 |
| 24 | 45 | 15 | 0.18 | -0.23 | 3.58 | 2.23 | 2.98 | 1.88 | 2.53 | 1.99 |
| 25 | 150 | 35 | 7.32 | 11.59 | 6.39 | 8.46 | 1.31 | 1.11 | 1.52 | 1.35 |
| 26 | 45 | 15 | -0.17 | -0.69 | 2.11 | 0.05 | 1.92 | 2.49 | 3.90 | 2.65 |
| 27 | 150 | 35 | 15.31 | 19.27 | 30.90 | 21.00 | 1.52 | 1.59 | 1.61 | 1.45 |
| 28 | 45 | 15 | 3.18 | 2.36 | 5.41 | 1.89 | 2.63 | 2.56 | 2.53 | 1.73 |
| 29 | 150 | 25 | 3.35 | 8.49 | 7.40 | 10.60 | 1.51 | 2.29 | 1.70 | 2.23 |
| 30 | 45 | 15 | 1.78 | 3.25 | 6.07 | 5.13 | 1.34 | 1.05 | 1.68 | 1.06 |
| 31 | 150 | 25 | 0.93 | 3.49 | 7.73 | 2.95 | 1.04 | 1.58 | 1.96 | 1.50 |
| 32 | 45 | 15 | 2.57 | 2.82 | 15.80 | 2.19 | 1.66 | 0.85 | 13.62 | 1.65 |
| 33 | 150 | 25 | 12.49 | 21.95 | 22.77 | 16.47 | 1.41 | 1.66 | 2.10 | 1.97 |
| 34 | 45 | 15 | 1.94 | 1.39 | 3.10 | 1.66 | 3.36 | 3.01 | 2.75 | 3.21 |
| 35 | 150 | 25 | 16.09 | 16.70 | 31.64 | 22.45 | 0.66 | 1.28 | 1.14 | 1.25 |
| 36 | 45 | 15 | 1.83 | 1.02 | 3.27 | 4.31 | 2.22 | 1.61 | 1.15 | 1.94 |
| 37 | 150 | 25 | 10.36 | 7.05 | 17.38 | 11.57 | 2.22 | 1.88 | 2.55 | 2.56 |
| 38 | 45 | 15 | 7.15 | 1.72 | 5.86 | 2.56 | 2.33 | 1.27 | 1.83 | 1.92 |
| 39 | 150 | 25 | 8.11 | 14.24 | 18.33 | 11.41 | 1.43 | 1.46 | 1.48 | 1.03 |
| 40 | 45 | 15 | 4.22 | -0.39 | 6.51 | 7.27 | 1.34 | 2.10 | 2.26 | 3.13 |
| 41 | 150 | 25 | 10.61 | 23.58 | 15.62 | 31.90 | 1.40 | 0.88 | 1.26 | 1.41 |
| 42 | 45 | 15 | 1.03 | 0.43 | 4.04 | 2.03 | 2.18 | 1.97 | 2.86 | 2.26 |
| 43 | 150 | 25 | 10.75 | 14.50 | 15.85 | 31.45 | 1.41 | 1.83 | 1.51 | 2.41 |
| 44 | 45 | 15 | 2.29 | 4.99 | 15.73 | 7.54 | 2.33 | 2.11 | 3.54 | 2.67 |
| 45 | 150 | 25 | 4.96 | 0.61 | 11.23 | 8.42 | 1.14 | 1.54 | 2.11 | 1.02 |
| 46 | 45 | 25 | 9.85 | 11.52 | 10.76 | 9.20 | 3.57 | 3.73 | 4.01 | 3.44 |
| 47 | 150 | 25 | 8.16 | 9.92 | 15.47 | 12.16 | 1.89 | 0.96 | 2.14 | 1.21 |

| | | | | | | | | | | |
|---|---|---|---|---|---|---|---|---|---|---|
| 48 | 45 | 25 | 3.49 | 4.00 | 4.56 | 6.64 | 1.98 | 2.91 | 2.34 | 2.94 |
| 49 | 150 | 25 | 16.91 | 14.12 | 12.14 | 13.05 | 1.54 | 1.51 | 1.35 | 0.90 |
| 50 | 45 | 25 | 4.00 | 5.67 | 7.47 | 4.38 | 2.89 | 2.58 | 2.71 | 3.52 |
| 51 | 150 | 25 | 13.08 | 8.43 | 17.68 | 7.86 | 1.75 | 1.17 | 1.66 | 1.84 |
| 52 | 45 | 25 | 6.28 | 5.34 | 7.15 | 6.68 | 2.25 | 2.60 | 1.98 | 2.64 |
| 53 | 150 | 15 | 4.36 | 4.20 | 6.97 | 13.83 | 1.67 | 1.80 | 1.89 | 2.15 |
| 54 | 45 | 25 | 1.86 | 1.74 | 2.38 | 1.42 | 1.61 | 1.75 | 2.57 | 1.63 |
| 55 | 150 | 15 | 11.61 | -1.74 | 38.39 | 8.52 | 1.77 | 1.04 | 2.06 | 1.73 |
| 56 | 45 | 25 | 3.72 | 11.95 | 6.00 | 5.73 | 1.57 | 2.10 | 2.02 | 2.01 |
| 57 | 150 | 15 | 33.22 | 9.21 | 13.53 | 11.11 | 2.44 | 1.13 | 1.05 | 0.61 |
| 58 | 45 | 25 | 3.02 | 1.90 | 3.94 | 2.62 | 2.84 | 2.74 | 2.96 | 2.81 |
| 59 | 150 | 15 | 13.60 | 14.84 | 19.24 | 26.54 | 1.32 | 1.23 | 1.49 | 1.63 |
| 60 | 45 | 25 | 7.61 | 2.70 | 9.03 | 6.12 | 2.52 | 2.28 | 2.66 | 2.00 |
| 61 | 150 | 15 | 6.89 | 2.01 | 5.99 | 7.13 | 1.67 | 2.07 | 1.83 | 1.97 |
| 62 | 45 | 25 | 4.62 | 2.86 | 6.90 | 6.15 | 1.78 | 2.44 | 3.35 | 2.19 |
| 63 | 150 | 15 | 15.43 | 27.40 | 91.73 | 29.03 | 1.51 | 1.75 | 10.86 | 0.94 |
| 64 | 45 | 25 | 0.56 | 1.06 | 3.36 | 0.82 | 1.93 | 2.04 | 2.24 | 2.49 |
| 65 | 150 | 15 | 14.94 | 13.54 | 10.33 | 14.51 | 0.83 | 1.33 | 1.19 | 1.24 |
| 66 | 45 | 25 | 4.78 | 3.72 | 3.91 | 5.65 | 2.99 | 3.41 | 2.91 | 3.80 |
| 67 | 150 | 15 | 14.92 | 23.10 | 24.67 | 17.48 | 1.54 | 1.92 | 1.65 | 1.33 |
| 68 | 45 | 25 | 4.22 | 4.69 | 5.96 | 4.62 | 2.37 | 2.65 | 2.81 | 2.13 |
| 69 | 150 | 15 | -7.30 | -3.68 | 0.16 | 2.21 | 1.18 | 1.07 | 1.30 | 1.09 |
| 70 | 45 | 35 | 10.36 | 11.95 | 7.50 | 10.81 | 4.40 | 2.26 | 2.45 | 5.76 |
| 71 | 150 | 15 | 7.74 | 7.85 | 9.43 | 15.31 | 1.23 | 0.98 | 1.00 | 0.79 |
| 72 | 45 | 35 | 1.11 | 3.67 | 0.30 | 1.47 | 1.89 | 2.01 | 1.75 | 2.27 |
| 73 | 150 | 15 | 0.50 | 12.10 | 21.02 | 23.33 | 0.99 | 0.68 | 1.31 | 1.48 |
| 74 | 45 | 35 | 2.86 | 2.41 | 3.26 | 2.84 | 3.51 | 2.83 | 3.52 | 2.49 |
| 75 | 150 | 15 | -0.09 | 9.14 | 12.42 | 0.29 | 1.37 | 1.29 | 1.15 | 0.54 |
| 76 | 45 | 35 | 6.23 | 5.77 | 7.09 | 6.43 | 2.30 | 2.71 | 2.36 | 2.59 |
| 77 | 150 | 5 | 9.09 | 13.11 | 8.13 | 5.07 | 2.28 | 2.35 | 1.89 | 2.05 |
| 78 | 45 | 35 | 8.99 | 3.94 | 6.11 | 4.25 | 1.61 | 1.08 | 1.37 | 1.76 |
| 79 | 150 | 5 | 1.23 | 2.15 | 3.20 | -1.65 | 1.66 | 1.29 | 1.07 | 0.84 |
| 80 | 45 | 35 | 6.60 | 4.26 | 8.31 | 4.51 | 2.88 | 2.56 | 1.99 | 1.92 |
| 81 | 150 | 5 | 11.21 | 15.07 | 11.37 | 11.62 | 1.52 | 0.92 | 1.84 | 1.41 |
| 82 | 45 | 35 | 7.18 | 5.06 | 5.53 | 6.01 | 2.39 | 2.91 | 2.74 | 4.07 |
| 83 | 150 | 5 | 15.37 | 13.94 | 18.33 | 14.97 | 1.27 | 0.97 | 1.34 | 0.98 |
| 84 | 45 | 35 | 5.78 | 7.64 | 6.19 | 5.70 | 2.23 | 2.29 | 2.01 | 2.19 |
| 85 | 150 | 5 | 3.78 | 4.95 | 3.74 | 1.70 | 2.24 | 1.91 | 2.33 | 2.43 |
| 86 | 45 | 35 | 6.63 | 7.89 | 7.15 | 8.11 | 1.61 | 2.93 | 2.23 | 3.33 |
| 87 | 150 | 5 | 7.03 | 18.90 | 93.92 | 21.15 | 1.45 | 1.50 | 12.58 | 1.79 |
| 88 | 45 | 35 | 3.55 | 9.21 | 7.18 | 4.88 | 1.57 | 1.73 | 1.45 | 1.25 |
| 89 | 150 | 5 | 9.18 | 3.55 | 13.07 | 10.15 | 1.74 | 1.05 | 1.56 | 1.74 |
| 90 | 45 | 35 | 1.61 | 2.37 | 4.85 | 6.53 | 2.25 | 2.92 | 2.55 | 2.20 |
| 91 | 150 | 5 | 13.52 | 23.41 | 16.85 | 8.34 | 1.50 | 0.74 | 0.92 | 0.77 |
| 92 | 45 | 35 | 7.25 | 8.51 | 10.73 | 9.56 | 2.53 | 2.21 | 3.59 | 1.98 |
| 93 | 150 | 5 | 6.22 | 8.30 | 2.83 | 6.42 | 1.32 | 1.63 | 1.76 | 2.28 |
| 94 | 80 | 5 | 7.79 | 5.10 | 7.33 | 5.31 | 2.41 | 2.22 | 3.64 | 3.69 |
| 95 | 150 | 5 | 7.15 | 7.72 | 7.61 | 7.46 | 2.10 | 1.57 | 2.47 | 2.11 |
| 96 | 80 | 5 | 8.48 | 9.23 | 8.15 | 7.07 | 2.02 | 1.70 | 2.49 | 2.46 |
| 97 | 150 | 5 | 9.25 | 9.82 | 10.54 | 6.11 | 2.51 | 2.97 | 1.66 | 2.05 |
| 98 | 80 | 5 | 4.35 | 4.21 | 3.92 | 4.92 | 1.68 | 2.51 | 2.41 | 3.97 |
| 99 | 150 | 5 | 7.40 | 10.05 | 11.71 | 9.86 | 1.92 | 1.86 | 1.65 | 2.14 |
| 100 | 80 | 5 | 1.34 | 8.13 | 10.82 | 5.52 | 1.37 | 1.55 | 2.58 | 1.97 |
| 101 | 115 | 35 | 6.10 | 8.35 | 6.01 | 9.63 | 1.72 | 2.59 | 2.20 | 2.22 |
| 102 | 80 | 5 | 6.93 | 4.78 | 6.02 | 4.50 | 1.93 | 1.68 | 1.61 | 1.67 |
| 103 | 115 | 35 | 2.99 | 3.42 | 8.15 | 13.80 | 1.66 | 1.51 | 1.63 | 1.46 |

| | | | | | | | | | | |
|---|---|---|---|---|---|---|---|---|---|---|
| 104 | 80 | 5 | 1.57 | 5.65 | 6.88 | 6.14 | 1.64 | 2.38 | 2.15 | 1.86 |
| 105 | 115 | 35 | 11.14 | 8.75 | 10.80 | 12.81 | 1.18 | 2.10 | 2.42 | 1.90 |
| 106 | 80 | 5 | 3.95 | 6.58 | 4.09 | 3.37 | 2.00 | 2.10 | 2.15 | 3.19 |
| 107 | 115 | 35 | 12.63 | 11.34 | 13.34 | 13.93 | 1.85 | 1.86 | 1.27 | 1.56 |
| 108 | 80 | 5 | 6.25 | 1.85 | 2.05 | 6.01 | 1.97 | 2.04 | 3.08 | 3.58 |
| 109 | 115 | 35 | 8.36 | 9.78 | 10.88 | 10.74 | 2.08 | 2.38 | 2.74 | 2.64 |
| 110 | 80 | 5 | -4.21 | -3.43 | -1.45 | -7.82 | 1.58 | 1.81 | 1.74 | 2.03 |
| 111 | 115 | 35 | 5.01 | 6.40 | 7.58 | 13.30 | 1.28 | 1.80 | 1.70 | 1.40 |
| 112 | 80 | 5 | 5.24 | 10.07 | 11.99 | 10.16 | 1.36 | 1.91 | 1.35 | 1.85 |
| 113 | 115 | 35 | 14.14 | 10.54 | 16.52 | 23.80 | 1.37 | 1.12 | 1.57 | 1.97 |
| 114 | 80 | 5 | -1.07 | -1.11 | -0.02 | 2.47 | 1.35 | 1.54 | 2.28 | 1.96 |
| 115 | 115 | 35 | 20.88 | 13.81 | 14.77 | 9.26 | 1.48 | 1.23 | 1.23 | 1.87 |
| 116 | 80 | 5 | 3.24 | 5.93 | 2.69 | 6.49 | 1.96 | 1.52 | 1.36 | 2.25 |
| 117 | 115 | 35 | 3.79 | 2.26 | 1.99 | 1.92 | 2.01 | 1.41 | 1.73 | 1.88 |
| 118 | 80 | 15 | 6.90 | 5.34 | 13.50 | 1.14 | 1.93 | 2.25 | 2.50 | 1.68 |
| 119 | 115 | 35 | 8.28 | 9.79 | 9.92 | 14.84 | 1.90 | 1.74 | 1.91 | 1.77 |
| 120 | 80 | 15 | 6.83 | 5.95 | 9.68 | 12.22 | 1.87 | 2.11 | 2.92 | 3.22 |
| 121 | 115 | 35 | 9.18 | 5.68 | 12.26 | 11.43 | 1.76 | 2.19 | 2.94 | 2.76 |
| 122 | 80 | 15 | 2.45 | 1.07 | 2.07 | 3.69 | 1.85 | 2.48 | 2.41 | 2.55 |
| 123 | 115 | 35 | 11.27 | 11.37 | 15.87 | 14.55 | 1.82 | 1.33 | 1.67 | 1.78 |
| 124 | 80 | 15 | 8.01 | 9.80 | 11.01 | 19.10 | 1.48 | 1.92 | 1.78 | 1.62 |
| 125 | 115 | 25 | 4.45 | 6.32 | 4.28 | 2.19 | 1.84 | 2.71 | 2.24 | 2.12 |
| 126 | 80 | 15 | 5.89 | 8.40 | 9.17 | 10.26 | 1.65 | 1.66 | 1.60 | 2.18 |
| 127 | 115 | 25 | 0.03 | -1.07 | 0.15 | 8.12 | 1.46 | 1.19 | 1.07 | 2.02 |
| 128 | 80 | 15 | 2.33 | 4.57 | 3.94 | 4.88 | 2.01 | 2.63 | 2.01 | 2.89 |
| 129 | 115 | 25 | 3.43 | 8.13 | 7.29 | 12.99 | 1.62 | 2.14 | 1.46 | 2.62 |
| 130 | 80 | 15 | 5.32 | 21.90 | 6.52 | 4.16 | 2.60 | 3.76 | 2.83 | 3.42 |
| 131 | 115 | 25 | 11.42 | 10.52 | 7.53 | 8.34 | 1.89 | 1.80 | 1.25 | 2.29 |
| 132 | 80 | 15 | 7.30 | 7.22 | 7.43 | 10.35 | 1.64 | 2.02 | 1.97 | 1.48 |
| 133 | 115 | 25 | 5.98 | 4.17 | 9.40 | 7.54 | 2.20 | 1.46 | 2.36 | 2.84 |
| 134 | 80 | 15 | 8.62 | 4.80 | 5.09 | 6.42 | 2.22 | 1.30 | 1.68 | 2.19 |
| 135 | 115 | 25 | 14.04 | 16.39 | 10.64 | 12.27 | 2.46 | 1.70 | 1.60 | 2.32 |
| 136 | 80 | 15 | 5.53 | 2.82 | 11.68 | 7.18 | 2.24 | 1.22 | 3.31 | 1.61 |
| 137 | 115 | 25 | 6.69 | 14.02 | 18.58 | 12.56 | 0.83 | 1.10 | 1.17 | 0.96 |
| 138 | 80 | 15 | 1.38 | 2.44 | 5.38 | 6.59 | 2.16 | 2.63 | 1.74 | 3.55 |
| 139 | 115 | 25 | 12.74 | 6.12 | 15.07 | 6.83 | 1.54 | 1.26 | 2.23 | 1.73 |
| 140 | 80 | 15 | 6.77 | 8.00 | 8.69 | 9.11 | 2.69 | 2.66 | 2.41 | 3.21 |
| 141 | 115 | 25 | 7.52 | 3.71 | 13.25 | 8.64 | 1.23 | 1.11 | 2.35 | 2.08 |
| 142 | 80 | 25 | 3.15 | 5.02 | 11.89 | 6.83 | 2.33 | 1.79 | 2.49 | 2.14 |
| 143 | 115 | 25 | 4.96 | 10.54 | 11.42 | 10.02 | 0.82 | 1.49 | 1.97 | 0.99 |
| 144 | 80 | 25 | 3.24 | 11.72 | 5.82 | 6.85 | 2.30 | 2.68 | 1.62 | 2.01 |
| 145 | 115 | 25 | 2.01 | 3.69 | 5.92 | 4.98 | 1.85 | 1.57 | 2.56 | 2.61 |
| 146 | 80 | 25 | 1.83 | 2.40 | 4.21 | 4.00 | 1.58 | 1.84 | 1.77 | 1.61 |
| 147 | 115 | 25 | 11.81 | 11.50 | 13.21 | 15.21 | 1.92 | 1.70 | 1.53 | 2.69 |
| 148 | 80 | 25 | 5.34 | 7.02 | 6.84 | 7.00 | 1.69 | 2.07 | 1.32 | 2.63 |
| 149 | 115 | 15 | 4.27 | 6.43 | 7.33 | 9.64 | 1.80 | 1.59 | 2.41 | 1.99 |
| 150 | 80 | 25 | 2.02 | 5.58 | 6.99 | 5.85 | 1.88 | 1.93 | 2.03 | 2.20 |
| 151 | 115 | 15 | 7.73 | 6.85 | 12.12 | 16.18 | 1.21 | 1.82 | 1.97 | 2.26 |
| 152 | 80 | 25 | 5.47 | 5.58 | 11.78 | 11.84 | 2.43 | 2.33 | 3.28 | 3.24 |
| 153 | 115 | 15 | 4.50 | 15.62 | 6.36 | 7.06 | 1.67 | 1.62 | 2.08 | 1.37 |
| 154 | 80 | 25 | 4.58 | 1.51 | 2.36 | 3.13 | 2.44 | 2.03 | 2.19 | 2.98 |
| 155 | 115 | 15 | 8.65 | 9.93 | 6.92 | 12.54 | 1.50 | 1.58 | 1.12 | 1.11 |
| 156 | 80 | 25 | 7.29 | 10.87 | 7.95 | 10.86 | 1.31 | 1.90 | 2.64 | 1.45 |
| 157 | 115 | 15 | 7.42 | 14.21 | 10.77 | 6.69 | 2.20 | 2.13 | 2.50 | 1.97 |
| 158 | 80 | 25 | 5.46 | 4.97 | 8.26 | 5.08 | 2.11 | 1.56 | 2.00 | 1.94 |
| 159 | 115 | 15 | 4.51 | 2.83 | 11.54 | 6.39 | 2.54 | 2.69 | 2.53 | 2.52 |

| | | | | | | | | | | |
|---|---|---|---|---|---|---|---|---|---|---|
| 160 | 80 | 25 | 3.94 | 4.58 | 6.08 | 5.99 | 0.99 | 1.55 | 1.47 | 1.38 |
| 161 | 115 | 15 | 8.19 | 3.43 | 8.84 | 11.05 | 1.69 | 1.98 | 1.86 | 2.37 |
| 162 | 80 | 25 | 2.17 | 1.78 | 1.84 | 2.53 | 2.38 | 2.55 | 2.58 | 1.37 |
| 163 | 115 | 15 | 8.70 | 10.02 | 11.86 | 14.40 | 2.01 | 2.02 | 2.24 | 2.21 |
| 164 | 80 | 25 | 2.83 | 8.69 | 1.91 | 6.17 | 1.72 | 2.05 | 2.10 | 2.44 |
| 165 | 115 | 15 | 1.95 | 5.07 | 4.74 | 4.22 | 1.77 | 2.01 | 2.34 | 2.71 |
| 166 | 80 | 35 | 11.01 | 11.78 | 12.72 | 10.99 | 2.35 | 2.18 | 1.51 | 3.01 |
| 167 | 115 | 15 | 5.04 | 2.52 | 11.30 | 8.08 | 2.33 | 1.18 | 1.94 | 2.22 |
| 168 | 80 | 35 | 4.47 | 2.05 | 6.87 | 5.58 | 1.74 | 1.90 | 2.63 | 2.17 |
| 169 | 115 | 15 | 11.14 | 6.79 | 6.01 | 13.55 | 1.95 | 1.23 | 1.82 | 2.07 |
| 170 | 80 | 35 | 2.77 | 3.45 | 1.90 | 5.00 | 1.63 | 2.98 | 2.46 | 3.66 |
| 171 | 115 | 15 | 0.30 | 5.11 | 8.03 | 1.90 | 1.97 | 2.48 | 1.44 | 1.92 |
| 172 | 80 | 35 | 8.28 | 12.93 | 11.64 | 13.35 | 2.74 | 2.41 | 2.11 | 3.75 |
| 173 | 115 | 5 | 4.08 | 4.82 | 5.91 | 6.49 | 2.71 | 2.37 | 2.92 | 2.60 |
| 174 | 80 | 35 | 5.17 | 8.25 | 8.08 | 6.07 | 1.21 | 1.72 | 1.31 | 1.24 |
| 175 | 115 | 5 | 7.63 | 12.94 | 5.90 | 16.29 | 1.08 | 1.51 | 1.28 | 2.02 |
| 176 | 80 | 35 | 4.11 | 4.47 | 27.75 | 7.28 | 1.57 | 1.82 | 3.06 | 2.92 |
| 177 | 115 | 5 | 4.63 | 4.44 | 6.36 | 7.46 | 1.51 | 1.40 | 2.26 | 1.11 |
| 178 | 80 | 35 | 5.79 | 6.54 | 33.45 | 10.29 | 2.09 | 2.48 | 2.12 | 1.87 |
| 179 | 115 | 5 | 6.93 | 7.60 | 14.45 | 12.30 | 1.74 | 1.16 | 1.72 | 1.16 |
| 180 | 80 | 35 | 7.36 | 8.34 | 8.23 | 9.29 | 1.68 | 2.03 | 2.40 | 1.81 |
| 181 | 115 | 5 | 6.30 | 7.70 | 13.13 | 6.81 | 2.12 | 1.75 | 2.21 | 2.34 |
| 182 | 80 | 35 | 7.02 | 8.70 | 6.68 | 5.02 | 1.64 | 2.02 | 2.72 | 3.25 |
| 183 | 115 | 5 | 6.70 | 8.82 | 6.58 | 9.10 | 1.81 | 1.33 | 1.27 | 2.07 |
| 184 | 80 | 35 | 4.66 | 9.55 | 8.48 | 9.22 | 2.53 | 1.93 | 2.44 | 2.30 |
| 185 | 115 | 5 | 5.28 | 3.25 | 7.11 | 5.18 | 0.91 | 1.08 | 1.04 | 1.24 |
| 186 | 80 | 35 | 43.80 | 46.50 | 46.45 | 57.62 | 11.86 | 12.93 | 12.48 | 16.17 |
| 187 | 115 | 5 | 4.63 | 7.98 | 4.29 | 13.24 | 1.82 | 1.54 | 1.35 | 2.76 |
| 188 | 80 | 35 | 10.55 | 9.01 | 8.85 | 9.71 | 1.93 | 2.18 | 1.76 | 2.01 |
| 189 | 115 | 5 | 1.35 | 4.52 | 1.12 | 3.37 | 2.87 | 2.53 | 2.39 | 3.58 |
| 190 | 115 | 5 | 7.92 | 3.60 | 7.91 | 13.22 | 2.92 | 1.64 | 2.49 | 2.02 |
| 191 | 115 | 5 | 3.09 | 15.67 | 6.63 | 5.03 | 1.15 | 15.71 | 2.16 | 1.41 |
| mean value | 97.41 | 20.08 | 6.94 | 7.94 | 11.01 | 10.96 | 1.91 | 2.02 | 2.29 | 2.25 |

| Participants 9-12 | | | Path length increase [%] | | | | QNL [mm] | | | |
|---|---|---|---|---|---|---|---|---|---|---|
| condition | A | W | no | low | med | severe | no | low | med | severe |
| 1 | 45 | 5 | 13.76 | 10.61 | 17.77 | 22.92 | 1.67 | 1.52 | 2.20 | 2.33 |
| 2 | 45 | 5 | 16.80 | 7.71 | 9.82 | 15.41 | 1.92 | 1.47 | 0.96 | 1.55 |
| 3 | 45 | 5 | 10.05 | 5.03 | 17.49 | 13.72 | 2.29 | 1.84 | 3.25 | 1.80 |
| 4 | 45 | 5 | 8.24 | 15.74 | 5.42 | 25.51 | 1.90 | 1.88 | 1.70 | 1.37 |
| 5 | 45 | 5 | 4.63 | 18.44 | 11.51 | 89.01 | 1.18 | 1.36 | 1.28 | 8.89 |
| 6 | 45 | 5 | 7.47 | 5.37 | 4.60 | 7.55 | 3.44 | 2.77 | 2.07 | 2.22 |
| 7 | 150 | 35 | 20.44 | 18.77 | 24.12 | 14.15 | 1.90 | 1.95 | 2.15 | 1.62 |
| 8 | 45 | 5 | 1.16 | 2.57 | 3.33 | 3.15 | 2.06 | 1.88 | 2.67 | 2.12 |
| 9 | 150 | 35 | 9.60 | 12.31 | 17.05 | 20.59 | 1.16 | 1.23 | 1.32 | 1.86 |
| 10 | 45 | 5 | -0.69 | 7.10 | 6.71 | 12.71 | 1.86 | 1.95 | 2.52 | 3.39 |
| 11 | 150 | 35 | 10.77 | 14.13 | 13.03 | 14.33 | 1.67 | 2.00 | 1.89 | 2.53 |
| 12 | 45 | 5 | 1.35 | 0.52 | 1.66 | 0.33 | 2.86 | 2.80 | 1.56 | 2.22 |
| 13 | 150 | 35 | 10.20 | 30.79 | 15.63 | 27.94 | 1.21 | 1.41 | 1.16 | 1.79 |
| 14 | 45 | 5 | 2.00 | 7.26 | 6.81 | 28.98 | 3.59 | 1.72 | 2.24 | 3.78 |
| 15 | 150 | 35 | 18.32 | 23.55 | 12.75 | 23.00 | 1.57 | 1.21 | 0.98 | 2.22 |
| 16 | 45 | 5 | 4.14 | 9.23 | 4.18 | 2.19 | 3.52 | 2.65 | 2.06 | 1.73 |
| 17 | 150 | 35 | 11.72 | 23.82 | 22.27 | 40.16 | 1.35 | 1.58 | 1.61 | 1.74 |
| 18 | 45 | 5 | 4.39 | 3.61 | 4.73 | 5.77 | 2.44 | 1.73 | 2.19 | 2.85 |
| 19 | 150 | 35 | 7.45 | 6.31 | 23.17 | 12.70 | 0.80 | 1.25 | 2.63 | 1.62 |

| | | | | | | | | | | |
|---|---|---|---|---|---|---|---|---|---|---|
| 20 | 45 | 15 | -1.13 | 3.39 | -1.79 | 6.42 | 2.15 | 5.31 | 2.94 | 3.59 |
| 21 | 150 | 35 | 20.28 | 10.25 | 16.08 | 31.25 | 1.96 | 1.85 | 1.58 | 2.38 |
| 22 | 45 | 15 | 3.80 | 0.58 | -1.09 | 2.00 | 5.70 | 1.85 | 2.15 | 2.80 |
| 23 | 150 | 35 | 20.47 | 26.46 | 23.75 | 26.34 | 2.09 | 1.13 | 1.91 | 2.26 |
| 24 | 45 | 15 | 11.64 | 9.46 | 6.56 | 8.59 | 5.18 | 4.59 | 3.76 | 2.96 |
| 25 | 150 | 35 | 30.09 | 22.47 | 23.12 | 28.31 | 1.44 | 1.80 | 1.12 | 1.31 |
| 26 | 45 | 15 | 3.62 | 5.51 | 2.87 | 8.40 | 2.78 | 4.40 | 1.75 | 2.42 |
| 27 | 150 | 35 | 17.91 | 10.54 | 19.06 | 21.64 | 1.73 | 1.65 | 1.75 | 1.94 |
| 28 | 45 | 15 | 3.45 | 2.99 | 1.91 | 2.02 | 3.94 | 2.18 | 2.97 | 3.66 |
| 29 | 150 | 35 | 10.28 | 32.48 | 9.41 | 18.26 | 1.39 | 2.46 | 1.45 | 2.60 |
| 30 | 45 | 15 | 3.62 | 2.82 | 3.24 | 7.50 | 1.83 | 1.15 | 1.22 | 2.50 |
| 31 | 150 | 25 | 21.54 | 18.87 | 98.66 | 14.55 | 2.13 | 1.67 | 3.32 | 1.88 |
| 32 | 45 | 15 | 7.39 | 4.92 | 5.15 | 27.44 | 2.37 | 1.67 | 1.62 | 2.93 |
| 33 | 150 | 25 | 18.06 | 14.08 | 34.03 | 20.38 | 1.21 | 1.47 | 3.73 | 1.46 |
| 34 | 45 | 15 | 1.22 | 2.58 | 2.99 | 1.04 | 4.63 | 5.24 | 2.73 | 2.22 |
| 35 | 150 | 25 | 15.83 | 20.82 | 32.36 | 15.20 | 1.84 | 2.05 | 1.95 | 1.63 |
| 36 | 45 | 15 | 3.54 | 1.00 | 2.02 | 2.48 | 3.30 | 1.92 | 1.90 | 2.86 |
| 37 | 150 | 25 | 10.95 | 39.35 | 21.87 | 10.02 | 2.25 | 8.95 | 1.16 | 1.21 |
| 38 | 45 | 15 | 7.34 | 7.32 | 10.11 | 8.52 | 2.14 | 3.01 | 3.46 | 2.13 |
| 39 | 150 | 25 | 16.96 | 17.64 | 11.48 | 21.64 | 1.36 | 1.85 | 1.15 | 1.22 |
| 40 | 45 | 15 | 5.77 | 8.44 | 4.40 | 2.84 | 4.44 | 4.65 | 2.73 | 2.29 |
| 41 | 150 | 25 | 14.48 | 13.74 | 19.12 | 23.18 | 1.33 | 1.51 | 1.26 | 1.04 |
| 42 | 45 | 15 | 4.12 | 6.82 | 7.57 | 4.48 | 2.92 | 3.70 | 2.85 | 3.02 |
| 43 | 150 | 25 | 8.67 | 13.34 | 9.30 | 8.68 | 2.02 | 1.91 | 1.79 | 1.13 |
| 44 | 45 | 25 | 2.21 | 1.06 | 2.82 | 2.41 | 4.38 | 2.91 | 2.66 | 2.18 |
| 45 | 150 | 25 | 19.70 | 17.92 | 19.17 | 28.72 | 1.73 | 1.65 | 1.68 | 1.75 |
| 46 | 45 | 25 | 2.48 | 1.19 | 2.60 | 2.90 | 3.84 | 3.66 | 4.08 | 2.73 |
| 47 | 150 | 25 | 19.32 | 24.82 | 12.53 | 23.09 | 1.68 | 2.03 | 1.23 | 1.54 |
| 48 | 45 | 25 | 8.60 | 6.01 | 3.07 | 4.64 | 5.94 | 2.69 | 3.11 | 2.96 |
| 49 | 150 | 25 | 11.99 | 13.57 | 9.30 | 31.31 | 1.95 | 1.58 | 2.07 | 2.53 |
| 50 | 45 | 25 | 4.88 | 6.15 | 3.39 | 2.82 | 3.64 | 2.68 | 1.65 | 3.12 |
| 51 | 150 | 25 | 4.57 | 11.69 | 7.57 | 17.63 | 1.41 | 1.61 | 0.97 | 2.09 |
| 52 | 45 | 25 | 1.54 | 3.62 | 2.65 | 1.68 | 3.35 | 4.12 | 2.59 | 2.29 |
| 53 | 150 | 25 | 17.91 | 7.19 | 13.38 | 11.18 | 1.65 | 1.16 | 0.96 | 2.10 |
| 54 | 45 | 25 | 9.80 | 6.87 | 9.02 | 11.69 | 4.48 | 2.99 | 3.01 | 3.34 |
| 55 | 150 | 15 | 21.91 | 26.66 | 20.16 | 20.10 | 2.17 | 1.52 | 1.00 | 1.49 |
| 56 | 45 | 25 | 5.17 | 2.76 | 0.58 | 7.27 | 4.00 | 2.98 | 1.54 | 3.28 |
| 57 | 150 | 15 | 18.51 | 18.96 | 16.36 | 18.26 | 2.10 | 1.49 | 1.31 | 1.50 |
| 58 | 45 | 25 | 5.66 | 5.43 | 6.11 | 3.64 | 3.78 | 5.61 | 2.17 | 3.37 |
| 59 | 150 | 15 | 13.22 | 13.30 | 4.29 | 7.97 | 2.31 | 3.10 | 1.86 | 1.61 |
| 60 | 45 | 25 | 13.54 | 2.40 | 4.88 | 1.65 | 4.97 | 2.02 | 2.79 | 2.62 |
| 61 | 150 | 15 | 6.82 | 5.60 | 17.29 | 19.11 | 1.17 | 1.66 | 1.21 | 1.80 |
| 62 | 45 | 25 | 3.07 | 9.17 | 2.23 | 5.39 | 3.87 | 6.69 | 2.32 | 2.00 |
| 63 | 150 | 15 | 7.80 | 13.65 | 31.99 | 8.30 | 1.81 | 1.28 | 1.25 | 0.99 |
| 64 | 45 | 25 | 6.34 | 3.29 | 9.52 | 3.28 | 5.53 | 2.32 | 2.70 | 3.44 |
| 65 | 150 | 15 | 115.97 | 23.96 | 27.13 | 26.61 | 3.53 | 1.19 | 1.71 | 1.34 |
| 66 | 45 | 25 | 3.74 | 4.46 | 4.92 | 6.91 | 3.46 | 3.36 | 1.69 | 2.73 |
| 67 | 150 | 15 | 12.42 | 21.61 | 5.27 | 5.26 | 1.10 | 2.88 | 1.67 | 1.30 |
| 68 | 45 | 35 | 3.85 | 4.91 | 0.02 | 2.41 | 3.45 | 2.50 | 2.16 | 4.33 |
| 69 | 150 | 15 | 21.53 | 12.91 | 10.76 | 39.20 | 1.64 | 1.18 | 1.74 | 4.14 |
| 70 | 45 | 35 | 5.04 | 2.25 | 3.34 | 4.45 | 4.81 | 3.77 | 3.06 | 3.32 |
| 71 | 150 | 15 | 15.94 | 8.18 | 14.14 | 38.81 | 1.76 | 1.54 | 1.95 | 3.50 |
| 72 | 45 | 35 | 5.92 | 5.54 | 8.27 | 8.51 | 5.48 | 1.81 | 4.00 | 4.53 |
| 73 | 150 | 15 | 1.67 | 16.53 | 8.65 | 7.98 | 2.19 | 1.95 | 1.68 | 1.28 |
| 74 | 45 | 35 | 4.39 | 3.26 | 4.52 | 6.10 | 3.14 | 2.90 | 1.98 | 4.12 |
| 75 | 150 | 15 | 27.62 | 30.51 | 28.36 | 28.32 | 1.91 | 1.90 | 2.06 | 1.85 |

| | | | | | | | | | | |
|---|---|---|---|---|---|---|---|---|---|---|
| 76 | 45 | 35 | 3.17 | 8.56 | 4.26 | 6.31 | 3.94 | 6.47 | 2.70 | 2.83 |
| 77 | 150 | 15 | 9.17 | 11.56 | 20.63 | 14.26 | 1.42 | 1.40 | 1.70 | 1.49 |
| 78 | 45 | 35 | 6.47 | 8.90 | 7.26 | 6.10 | 4.36 | 3.46 | 2.80 | 1.81 |
| 79 | 150 | 5 | 10.50 | 2.22 | 15.68 | 22.45 | 1.33 | 1.14 | 1.30 | 2.03 |
| 80 | 45 | 35 | 5.67 | 7.09 | 6.14 | 5.07 | 2.77 | 2.94 | 2.83 | 2.40 |
| 81 | 150 | 5 | 15.38 | 15.79 | 6.31 | 35.56 | 1.35 | 1.24 | 1.98 | 1.35 |
| 82 | 45 | 35 | 5.28 | 8.55 | 8.10 | 9.23 | 2.29 | 4.52 | 2.01 | 4.36 |
| 83 | 150 | 5 | 13.99 | 10.52 | 10.57 | 14.00 | 1.26 | 1.82 | 1.38 | 1.90 |
| 84 | 45 | 35 | 6.29 | 3.23 | 4.20 | 15.55 | 2.20 | 2.58 | 2.47 | 2.60 |
| 85 | 150 | 5 | 6.99 | 18.26 | -2.59 | 9.72 | 1.02 | 2.38 | 2.75 | 2.60 |
| 86 | 45 | 35 | 5.74 | 8.76 | 10.74 | 5.06 | 2.04 | 4.41 | 2.16 | 2.26 |
| 87 | 150 | 5 | 18.37 | 24.27 | 23.82 | 19.84 | 1.32 | 1.49 | 0.73 | 1.32 |
| 88 | 45 | 35 | 8.65 | 6.16 | 5.81 | 9.32 | 3.28 | 2.38 | 2.32 | 2.25 |
| 89 | 150 | 5 | 25.86 | 15.13 | 10.12 | 27.99 | 1.64 | 1.04 | 1.40 | 1.80 |
| 90 | 45 | 35 | 4.54 | 12.11 | 4.95 | 6.99 | 3.12 | 3.81 | 2.76 | 3.08 |
| 91 | 150 | 5 | 3.45 | 9.56 | 7.17 | 4.67 | 1.92 | 3.16 | 2.49 | 2.77 |
| 92 | 80 | 5 | 4.31 | 5.44 | 3.86 | 3.33 | 3.09 | 4.46 | 2.35 | 2.65 |
| 93 | 150 | 5 | 5.62 | 5.84 | 4.16 | 9.84 | 1.14 | 1.51 | 1.82 | 2.34 |
| 94 | 80 | 5 | 6.38 | 7.36 | 8.69 | 6.39 | 3.48 | 3.53 | 4.72 | 4.80 |
| 95 | 150 | 5 | 6.98 | 11.53 | 14.60 | 17.79 | 3.32 | 2.79 | 1.72 | 3.25 |
| 96 | 80 | 5 | 7.42 | 7.72 | 4.14 | 6.67 | 5.31 | 4.17 | 3.55 | 4.99 |
| 97 | 150 | 5 | 12.87 | 13.44 | 14.50 | 17.39 | 2.77 | 2.87 | 2.31 | 2.78 |
| 98 | 80 | 5 | 3.27 | 8.77 | 5.48 | 5.91 | 3.01 | 2.37 | 2.23 | 2.32 |
| 99 | 150 | 5 | 8.55 | 20.06 | 12.51 | 11.87 | 1.73 | 2.59 | 2.04 | 1.79 |
| 100 | 80 | 5 | 3.88 | 5.71 | 3.95 | 14.19 | 2.06 | 6.61 | 2.92 | 3.06 |
| 101 | 150 | 5 | 5.37 | 9.11 | 13.08 | 6.75 | 2.34 | 2.26 | 1.61 | 2.29 |
| 102 | 80 | 5 | 15.54 | 7.25 | 23.06 | 9.16 | 13.57 | 1.83 | 1.55 | 1.31 |
| 103 | 115 | 35 | 6.81 | 13.32 | 12.43 | 14.27 | 2.00 | 1.13 | 1.71 | 1.74 |
| 104 | 80 | 5 | 3.27 | 3.70 | 8.28 | 3.97 | 2.85 | 1.76 | 1.59 | 1.91 |
| 105 | 115 | 35 | 37.70 | 8.40 | 9.04 | 9.88 | 15.20 | 2.40 | 1.42 | 1.01 |
| 106 | 80 | 5 | 10.54 | 15.09 | 12.34 | 15.40 | 1.03 | 3.99 | 1.61 | 3.21 |
| 107 | 115 | 35 | 13.79 | 18.74 | 7.55 | 8.02 | 2.90 | 4.63 | 2.51 | 2.19 |
| 108 | 80 | 5 | 4.82 | 7.52 | 7.21 | 12.89 | 2.41 | 1.55 | 1.58 | 3.46 |
| 109 | 115 | 35 | 3.71 | 9.17 | 5.83 | 11.11 | 1.52 | 2.61 | 1.48 | 2.71 |
| 110 | 80 | 5 | 5.80 | 11.52 | 12.11 | 14.61 | 2.12 | 1.40 | 2.42 | 2.12 |
| 111 | 115 | 35 | 8.06 | 5.53 | 5.82 | 12.74 | 1.97 | 1.71 | 1.39 | 1.70 |
| 112 | 80 | 5 | 8.60 | 10.38 | 10.20 | 12.53 | 1.49 | 2.38 | 1.46 | 1.70 |
| 113 | 115 | 35 | 13.41 | 9.26 | 12.14 | 8.14 | 1.42 | 1.70 | 1.75 | 1.75 |
| 114 | 80 | 5 | 1.01 | 2.32 | 9.72 | 3.01 | 2.14 | 2.31 | 3.43 | 3.24 |
| 115 | 115 | 35 | 0.33 | 4.23 | 3.99 | 9.18 | 1.73 | 2.63 | 1.77 | 3.48 |
| 116 | 80 | 15 | 2.42 | 8.80 | 8.40 | 11.51 | 1.26 | 2.54 | 3.03 | 2.19 |
| 117 | 115 | 35 | 9.71 | 10.56 | 13.18 | 15.05 | 2.12 | 2.15 | 2.53 | 2.57 |
| 118 | 80 | 15 | 4.70 | 7.19 | 8.55 | 6.95 | 1.54 | 4.30 | 1.34 | 1.42 |
| 119 | 115 | 35 | 10.95 | 12.25 | 6.00 | 7.39 | 1.98 | 3.13 | 2.24 | 2.94 |
| 120 | 80 | 15 | 7.53 | 13.84 | 8.63 | 14.42 | 1.87 | 2.98 | 2.35 | 3.38 |
| 121 | 115 | 35 | 5.60 | 5.55 | 4.43 | 11.37 | 1.39 | 2.56 | 2.31 | 1.49 |
| 122 | 80 | 15 | 11.85 | 10.87 | 10.75 | 14.93 | 2.62 | 2.11 | 2.47 | 1.94 |
| 123 | 115 | 35 | 3.18 | 5.91 | 9.99 | 6.69 | 1.44 | 1.64 | 2.70 | 2.55 |
| 124 | 80 | 15 | 2.57 | 4.27 | 0.39 | 8.87 | 1.83 | 2.18 | 2.20 | 3.41 |
| 125 | 115 | 35 | 8.46 | 8.95 | 11.96 | 8.02 | 1.68 | 2.59 | 1.66 | 1.22 |
| 126 | 80 | 15 | 12.17 | 15.29 | 18.06 | 13.05 | 1.32 | 2.96 | 2.38 | 1.59 |
| 127 | 115 | 25 | 7.34 | 8.10 | 11.78 | 7.26 | 2.37 | 3.23 | 1.18 | 1.82 |
| 128 | 80 | 15 | 11.81 | 9.84 | 8.28 | 9.28 | 1.66 | 2.26 | 1.89 | 1.45 |
| 129 | 115 | 25 | 6.04 | 6.38 | 9.42 | 11.99 | 1.52 | 1.06 | 2.03 | 2.63 |
| 130 | 80 | 15 | -1.23 | -1.34 | 1.49 | -0.73 | 1.35 | 5.21 | 2.67 | 2.02 |
| 131 | 115 | 25 | 7.61 | 9.15 | 7.66 | 9.32 | 2.14 | 3.07 | 1.38 | 2.10 |

| | | | | | | | | | | |
|---|---|---|---|---|---|---|---|---|---|---|
| 132 | 80 | 15 | 3.81 | 5.93 | 6.18 | 3.66 | 2.12 | 2.75 | 2.34 | 1.90 |
| 133 | 115 | 25 | 4.10 | 4.77 | 0.48 | 14.57 | 1.84 | 1.41 | 1.89 | 2.46 |
| 134 | 80 | 15 | 9.33 | 17.11 | 17.04 | 12.19 | 2.04 | 5.38 | 2.47 | 2.01 |
| 135 | 115 | 25 | 3.93 | 13.69 | 3.50 | 12.63 | 1.26 | 2.04 | 1.42 | 1.50 |
| 136 | 80 | 15 | 3.67 | 2.76 | 4.68 | 7.43 | 2.01 | 3.16 | 2.43 | 2.77 |
| 137 | 115 | 25 | 13.78 | 18.65 | 19.35 | 29.21 | 1.75 | 2.62 | 3.06 | 3.99 |
| 138 | 80 | 15 | 7.02 | 12.69 | 12.81 | 10.55 | 1.30 | 3.12 | 2.71 | 3.22 |
| 139 | 115 | 25 | 8.78 | 12.72 | 15.31 | 10.26 | 1.35 | 3.39 | 2.78 | 1.70 |
| 140 | 80 | 25 | 2.87 | 5.39 | 5.11 | 6.87 | 1.71 | 3.52 | 2.83 | 2.85 |
| 141 | 115 | 25 | 11.51 | 6.43 | 9.52 | 8.28 | 2.42 | 3.06 | 1.69 | 1.56 |
| 142 | 80 | 25 | 9.85 | 10.97 | 10.70 | 9.50 | 2.80 | 4.76 | 2.00 | 2.17 |
| 143 | 115 | 25 | 1.08 | 3.44 | 3.66 | 10.99 | 2.19 | 2.15 | 1.36 | 1.78 |
| 144 | 80 | 25 | 2.26 | 3.71 | 2.59 | 7.03 | 1.92 | 3.88 | 2.38 | 3.59 |
| 145 | 115 | 25 | 1.65 | 4.41 | 7.97 | 0.89 | 2.09 | 4.59 | 2.54 | 1.36 |
| 146 | 80 | 25 | 5.48 | 5.64 | 6.57 | 12.26 | 2.31 | 2.16 | 1.93 | 2.65 |
| 147 | 115 | 25 | 3.43 | 7.13 | 1.61 | 4.92 | 1.32 | 2.22 | 2.00 | 2.56 |
| 148 | 80 | 25 | 2.32 | 0.67 | 5.65 | 3.75 | 1.63 | 1.75 | 2.96 | 3.85 |
| 149 | 115 | 25 | 10.46 | 15.24 | 14.51 | 17.90 | 2.08 | 2.28 | 1.98 | 2.95 |
| 150 | 80 | 25 | 13.34 | 10.14 | 8.41 | 11.55 | 1.46 | 1.65 | 1.20 | 1.90 |
| 151 | 115 | 15 | 4.86 | 1.35 | 4.28 | 5.63 | 1.64 | 2.45 | 2.27 | 1.35 |
| 152 | 80 | 25 | 6.72 | 7.99 | 9.20 | 7.67 | 1.82 | 2.76 | 1.97 | 1.43 |
| 153 | 115 | 15 | 3.89 | 12.76 | 7.80 | 11.69 | 1.42 | 2.32 | 2.05 | 1.81 |
| 154 | 80 | 25 | 1.39 | 9.79 | 4.33 | 2.30 | 2.16 | 2.51 | 3.40 | 2.39 |
| 155 | 115 | 15 | 2.98 | 4.00 | -3.05 | 1.26 | 3.24 | 3.25 | 2.47 | 2.10 |
| 156 | 80 | 25 | 5.17 | 19.61 | 2.12 | 5.70 | 2.35 | 3.53 | 2.22 | 2.24 |
| 157 | 115 | 15 | -1.50 | -3.07 | -3.73 | -8.68 | 1.72 | 1.87 | 2.07 | 1.71 |
| 158 | 80 | 25 | 19.29 | 11.45 | 14.37 | 11.66 | 8.75 | 3.47 | 2.30 | 1.54 |
| 159 | 115 | 15 | 16.01 | 15.28 | 23.26 | 21.27 | 1.98 | 2.28 | 2.28 | 2.15 |
| 160 | 80 | 25 | 5.75 | 7.99 | 8.13 | 12.31 | 2.65 | 2.63 | 2.30 | 2.46 |
| 161 | 115 | 15 | 13.55 | 14.79 | 10.95 | 14.06 | 2.64 | 1.84 | 1.18 | 2.62 |
| 162 | 80 | 25 | 6.67 | 7.46 | 10.63 | 13.99 | 2.33 | 3.68 | 1.93 | 4.03 |
| 163 | 115 | 15 | 1.78 | 0.85 | -2.72 | 2.95 | 1.81 | 2.31 | 1.83 | 1.85 |
| 164 | 80 | 35 | 3.30 | 5.15 | 4.30 | 6.92 | 2.69 | 1.83 | 2.73 | 2.64 |
| 165 | 115 | 15 | 10.40 | 22.10 | 13.62 | 10.08 | 1.34 | 3.30 | 2.00 | 1.42 |
| 166 | 80 | 35 | 3.34 | 6.25 | 8.00 | 5.90 | 1.71 | 3.30 | 3.46 | 2.65 |
| 167 | 115 | 15 | 16.38 | 15.71 | 18.62 | 19.12 | 1.77 | 2.83 | 1.49 | 2.04 |
| 168 | 80 | 35 | 8.95 | 7.77 | 6.29 | 6.25 | 1.61 | 4.29 | 2.71 | 2.17 |
| 169 | 115 | 15 | -0.69 | 8.58 | 2.18 | 4.31 | 1.10 | 2.77 | 1.27 | 1.46 |
| 170 | 80 | 35 | 6.46 | 6.51 | 6.98 | 8.08 | 2.06 | 2.36 | 3.41 | 2.28 |
| 171 | 115 | 15 | 13.00 | 15.09 | 14.60 | 13.31 | 2.35 | 2.23 | 2.28 | 1.61 |
| 172 | 80 | 35 | 4.18 | 5.10 | 3.57 | 4.02 | 1.24 | 4.07 | 2.50 | 3.76 |
| 173 | 115 | 15 | 10.91 | 9.49 | 17.89 | 19.85 | 1.09 | 1.98 | 2.25 | 3.19 |
| 174 | 80 | 35 | 20.72 | 9.68 | 11.78 | 12.14 | 7.72 | 2.55 | 2.65 | 2.78 |
| 175 | 115 | 5 | 6.84 | 8.47 | 11.11 | 14.69 | 1.31 | 2.10 | 2.02 | 2.49 |
| 176 | 80 | 35 | 7.97 | 8.82 | 9.44 | 9.15 | 2.78 | 2.51 | 2.03 | 2.00 |
| 177 | 115 | 5 | 17.30 | 20.60 | 20.35 | 18.20 | 2.53 | 3.37 | 1.40 | 2.04 |
| 178 | 80 | 35 | 4.23 | 5.67 | 11.50 | 6.71 | 2.63 | 2.93 | 2.91 | 2.75 |
| 179 | 115 | 5 | 7.06 | 8.78 | 5.60 | 1.87 | 2.65 | 2.45 | 1.98 | 1.99 |
| 180 | 80 | 35 | 5.91 | 28.65 | 3.90 | 3.84 | 2.60 | 2.90 | 1.52 | 2.14 |
| 181 | 115 | 5 | 10.79 | 13.09 | 15.36 | 11.68 | 1.26 | 2.59 | 1.97 | 1.46 |
| 182 | 80 | 35 | 6.18 | 7.79 | 6.70 | 13.87 | 2.91 | 3.03 | 1.84 | 2.53 |
| 183 | 115 | 5 | 15.12 | 13.50 | 17.67 | 14.02 | 2.32 | 2.81 | 1.61 | 1.71 |
| 184 | 80 | 35 | 7.35 | 6.75 | 7.07 | 4.20 | 4.13 | 2.76 | 1.57 | 2.17 |
| 185 | 115 | 5 | 20.12 | 25.12 | 18.94 | 23.23 | 2.19 | 1.99 | 1.46 | 1.89 |
| 186 | 80 | 35 | 7.06 | 9.37 | 9.80 | 8.62 | 2.05 | 2.33 | 2.33 | 2.90 |
| 187 | 115 | 5 | 3.79 | 5.44 | 5.44 | 9.71 | 3.30 | 3.06 | 2.59 | 2.10 |

| | | | | | | | | | | |
|---|---|---|---|---|---|---|---|---|---|---|
| 188 | 115 | 5 | 4.14 | 4.91 | 4.31 | 4.46 | 2.56 | 2.79 | 2.36 | 2.92 |
| 189 | 115 | 5 | 7.12 | 3.56 | 7.05 | 9.04 | 2.95 | 2.67 | 1.77 | 1.84 |
| 190 | 115 | 5 | 6.17 | 6.76 | 4.86 | 9.15 | 3.82 | 4.02 | 2.09 | 3.59 |
| 191 | 115 | 5 | 10.44 | 5.24 | 8.27 | 11.23 | 3.99 | 3.16 | 3.25 | 3.11 |
| mean value | 97.41 | 20.08 | 9.18 | 10.20 | 10.06 | 12.05 | 2.53 | 2.65 | 2.12 | 2.39 |

| Participants 13-16 | | | Path length increase [%] | | | | QNL [mm] | | | |
|---|---|---|---|---|---|---|---|---|---|---|
| condition | A | W | no | low | med | severe | no | low | med | severe |
| 1 | 45 | 5 | 16.68 | 16.66 | 15.47 | 13.47 | 1.91 | 1.17 | 2.60 | 2.29 |
| 2 | 45 | 5 | 18.67 | 15.60 | 16.07 | 95.79 | 1.38 | 1.09 | 1.86 | 11.75 |
| 3 | 45 | 5 | 3.18 | 2.19 | 16.49 | 20.39 | 1.34 | 1.22 | 1.70 | 1.51 |
| 4 | 45 | 5 | 10.58 | 16.53 | 10.47 | 11.53 | 0.87 | 1.21 | 1.65 | 1.87 |
| 5 | 45 | 5 | 7.86 | 4.55 | 23.73 | 21.61 | 1.12 | 1.01 | 1.32 | 0.75 |
| 6 | 45 | 5 | 9.68 | 7.67 | 18.06 | 12.21 | 1.63 | 1.50 | 2.39 | 1.44 |
| 7 | 45 | 5 | -33.85 | -46.96 | 17.03 | -50.08 | 6.27 | 1.44 | 6.79 | 1.49 |
| 8 | 45 | 5 | 1.77 | 3.04 | 3.56 | 1.98 | 1.70 | 2.11 | 3.12 | 2.86 |
| 9 | 150 | 35 | 18.61 | 16.46 | 21.65 | 14.30 | 2.00 | 1.77 | 2.36 | 2.21 |
| 10 | 45 | 5 | 1.13 | 1.70 | 1.75 | 18.83 | 2.19 | 1.43 | 2.37 | 1.76 |
| 11 | 150 | 35 | 120.43 | 104.80 | 14.81 | 14.43 | 3.46 | 10.75 | 1.67 | 1.67 |
| 12 | 45 | 5 | 8.89 | 2.52 | -0.12 | 3.75 | 2.62 | 2.94 | 2.72 | 2.06 |
| 13 | 150 | 35 | 20.24 | 19.24 | 34.78 | 82.25 | 1.37 | 1.70 | 1.22 | 8.25 |
| 14 | 45 | 5 | 1.77 | 2.82 | 5.35 | 0.77 | 1.79 | 2.21 | 2.14 | 2.06 |
| 15 | 150 | 35 | 22.80 | 38.44 | 27.27 | 18.69 | 1.10 | 1.13 | 1.63 | 1.54 |
| 16 | 45 | 5 | 2.95 | 1.38 | 1.31 | 3.82 | 3.18 | 2.56 | 2.50 | 2.53 |
| 17 | 150 | 35 | 5.23 | 14.98 | 12.96 | 32.77 | 1.58 | 1.22 | 2.49 | 1.76 |
| 18 | 45 | 15 | 3.34 | 0.45 | 2.40 | -0.52 | 1.80 | 1.85 | 1.90 | 1.55 |
| 19 | 150 | 35 | 15.90 | 5.40 | 5.01 | 7.66 | 2.07 | 1.12 | 1.45 | 1.32 |
| 20 | 45 | 15 | 5.57 | 5.61 | 5.17 | 9.49 | 2.45 | 3.08 | 2.16 | 4.58 |
| 21 | 150 | 35 | 19.88 | 25.54 | 36.57 | 60.13 | 1.06 | 1.17 | 1.56 | 1.71 |
| 22 | 45 | 15 | 6.07 | -1.42 | 8.60 | 11.16 | 4.45 | 2.75 | 2.06 | 2.54 |
| 23 | 150 | 35 | 16.89 | 33.54 | 31.58 | 35.12 | 1.54 | 2.91 | 2.03 | 1.93 |
| 24 | 45 | 15 | 10.69 | 4.65 | 8.69 | 9.48 | 3.25 | 1.95 | 4.06 | 1.90 |
| 25 | 150 | 35 | 10.74 | 17.31 | 6.55 | 7.49 | 1.78 | 2.11 | 2.19 | 1.81 |
| 26 | 45 | 15 | 8.26 | 2.42 | 2.47 | 4.79 | 2.99 | 2.33 | 2.32 | 5.41 |
| 27 | 150 | 35 | 6.73 | 2.53 | 12.55 | 31.29 | 1.41 | 1.65 | 1.78 | 2.70 |
| 28 | 45 | 15 | 0.13 | 3.70 | 0.95 | 2.67 | 2.16 | 3.87 | 3.18 | 2.72 |
| 29 | 150 | 35 | 28.87 | 21.13 | 22.78 | 23.37 | 1.17 | 1.82 | 1.45 | 1.76 |
| 30 | 45 | 15 | 1.32 | 0.02 | 10.23 | 1.58 | 2.92 | 3.00 | 4.03 | 4.43 |
| 31 | 150 | 35 | 16.78 | 6.15 | 17.77 | 16.11 | 1.26 | 1.35 | 1.21 | 1.64 |
| 32 | 45 | 15 | 4.00 | 3.12 | 4.58 | 3.52 | 1.73 | 2.02 | 1.98 | 2.72 |
| 33 | 150 | 25 | 71.35 | 15.78 | 17.19 | 26.50 | 1.59 | 2.20 | 1.66 | 2.47 |
| 34 | 45 | 15 | 3.75 | 6.93 | 3.54 | 4.98 | 3.29 | 1.73 | 2.26 | 1.57 |
| 35 | 150 | 25 | 33.69 | 53.15 | 56.95 | 50.13 | 0.97 | 2.36 | 1.49 | 2.26 |
| 36 | 45 | 15 | 2.25 | 5.34 | 20.22 | 14.32 | 1.36 | 2.67 | 14.57 | 9.35 |
| 37 | 150 | 25 | 17.81 | 8.84 | 67.39 | 19.59 | 1.37 | 1.21 | 2.05 | 1.74 |
| 38 | 45 | 15 | 2.01 | 6.41 | 3.96 | 4.52 | 1.98 | 3.69 | 2.16 | 3.47 |
| 39 | 150 | 25 | 14.67 | 24.85 | 17.68 | 6.17 | 1.66 | 2.72 | 1.62 | 1.80 |
| 40 | 45 | 15 | 4.89 | 7.33 | 8.17 | 4.44 | 2.83 | 2.51 | 2.66 | 2.20 |
| 41 | 150 | 25 | 6.15 | 1.54 | 3.43 | -1.88 | 1.51 | 1.33 | 1.74 | 1.78 |
| 42 | 45 | 25 | 4.84 | 2.79 | 2.60 | 5.89 | 3.04 | 2.01 | 2.44 | 3.23 |
| 43 | 150 | 25 | 13.95 | 9.00 | -0.75 | 13.28 | 2.10 | 1.42 | 4.18 | 1.75 |
| 44 | 45 | 25 | -0.44 | -2.24 | 4.47 | 4.30 | 2.15 | 2.36 | 3.30 | 5.69 |
| 45 | 150 | 25 | 10.29 | 7.81 | 15.63 | 15.91 | 0.84 | 1.31 | 1.45 | 2.09 |
| 46 | 45 | 25 | 1.10 | 4.86 | 3.23 | 3.99 | 2.35 | 3.68 | 2.89 | 2.62 |
| 47 | 150 | 25 | 84.39 | 49.31 | 18.59 | 15.01 | 8.98 | 10.12 | 1.26 | 1.38 |

| | | | | | | | | | | |
|---|---|---|---|---|---|---|---|---|---|---|
| 48 | 45 | 25 | 2.96 | 3.51 | 3.21 | 5.02 | 2.25 | 1.57 | 2.42 | 3.11 |
| 49 | 150 | 25 | 8.19 | 9.69 | 11.84 | 12.52 | 2.04 | 1.41 | 1.89 | 2.45 |
| 50 | 45 | 25 | 6.76 | 6.88 | 3.68 | 8.51 | 1.79 | 1.73 | 2.44 | 2.11 |
| 51 | 150 | 25 | 2.80 | 11.09 | 7.69 | 17.79 | 1.63 | 1.17 | 0.89 | 1.93 |
| 52 | 45 | 25 | 5.81 | 3.94 | 3.79 | 10.10 | 3.51 | 3.38 | 4.16 | 5.86 |
| 53 | 150 | 25 | 3.25 | 13.85 | 11.82 | 20.74 | 1.23 | 1.13 | 1.22 | 0.86 |
| 54 | 45 | 25 | 1.31 | 0.93 | 4.48 | 4.99 | 1.99 | 2.27 | 5.15 | 4.29 |
| 55 | 150 | 25 | 16.13 | 16.82 | 38.94 | 26.25 | 1.40 | 1.37 | 2.42 | 0.73 |
| 56 | 45 | 25 | 20.35 | 7.25 | 9.72 | 7.06 | 16.88 | 3.23 | 2.27 | 2.41 |
| 57 | 150 | 15 | 6.26 | 5.25 | 6.04 | 2.09 | 1.83 | 1.51 | 2.73 | 1.90 |
| 58 | 45 | 25 | 6.27 | 6.33 | 2.24 | 4.29 | 1.98 | 2.37 | 1.67 | 2.07 |
| 59 | 150 | 15 | 4.86 | 23.96 | 16.97 | 26.14 | 0.92 | 1.57 | 1.58 | 1.48 |
| 60 | 45 | 25 | 3.43 | 4.70 | 33.85 | 11.72 | 1.39 | 2.32 | 7.22 | 2.56 |
| 61 | 150 | 15 | 20.31 | 21.51 | 26.45 | 26.47 | 1.12 | 0.99 | 1.48 | 1.60 |
| 62 | 45 | 25 | 4.11 | 3.11 | 3.66 | 21.36 | 2.30 | 3.02 | 3.20 | 3.29 |
| 63 | 150 | 15 | 41.52 | 4.53 | 0.81 | 6.37 | 2.36 | 0.87 | 1.26 | 2.20 |
| 64 | 45 | 25 | 7.60 | 9.44 | 6.77 | 11.41 | 4.36 | 3.44 | 2.08 | 2.61 |
| 65 | 150 | 15 | 10.87 | 18.04 | 17.56 | 30.94 | 1.91 | 1.79 | 1.42 | 1.38 |
| 66 | 45 | 35 | 3.54 | 9.91 | 6.96 | 3.64 | 2.89 | 1.80 | 3.20 | 1.30 |
| 67 | 150 | 15 | 12.16 | 7.30 | -5.25 | 8.45 | 1.46 | 1.55 | 0.83 | 1.05 |
| 68 | 45 | 35 | 2.84 | 5.64 | 0.52 | -1.12 | 2.89 | 2.48 | 2.25 | 3.18 |
| 69 | 150 | 15 | 20.26 | 16.03 | 24.55 | 38.50 | 1.46 | 0.79 | 1.65 | 2.26 |
| 70 | 45 | 35 | 5.29 | 8.50 | 7.61 | 3.43 | 4.39 | 4.49 | 3.51 | 2.81 |
| 71 | 150 | 15 | 19.52 | 25.00 | 31.41 | 23.89 | 2.72 | 0.95 | 1.36 | 1.69 |
| 72 | 45 | 35 | 7.60 | 5.79 | 8.49 | 4.89 | 3.78 | 2.05 | 3.72 | 4.31 |
| 73 | 150 | 15 | 7.03 | 11.51 | 8.80 | 19.94 | 2.57 | 2.14 | 1.64 | 2.02 |
| 74 | 45 | 35 | 4.80 | 5.58 | 10.13 | 7.73 | 1.97 | 3.21 | 1.57 | 4.56 |
| 75 | 150 | 15 | 9.74 | 2.53 | 10.57 | 27.31 | 1.46 | 1.41 | 0.88 | 1.93 |
| 76 | 45 | 35 | 4.75 | 2.63 | 2.79 | 5.38 | 3.83 | 2.98 | 3.56 | 3.11 |
| 77 | 150 | 15 | 16.53 | 18.98 | 20.63 | 20.48 | 1.21 | 1.40 | 1.27 | 0.96 |
| 78 | 45 | 35 | 4.48 | 4.42 | 6.30 | 7.47 | 1.69 | 2.51 | 3.33 | 4.00 |
| 79 | 150 | 15 | 0.81 | 2.56 | 2.60 | 41.04 | 1.74 | 1.34 | 0.71 | 3.46 |
| 80 | 45 | 35 | 3.12 | 10.91 | 7.47 | 12.20 | 1.58 | 2.37 | 1.97 | 1.77 |
| 81 | 150 | 5 | 54.68 | 10.12 | 10.46 | 12.67 | 2.73 | 2.07 | 2.18 | 1.95 |
| 82 | 45 | 35 | 5.73 | 7.62 | 8.80 | 5.02 | 2.13 | 1.20 | 2.50 | 1.93 |
| 83 | 150 | 5 | 24.12 | 14.35 | 39.14 | 35.04 | 1.09 | 1.96 | 0.94 | 2.23 |
| 84 | 45 | 35 | 2.72 | 4.79 | 9.11 | 3.45 | 1.63 | 1.75 | 2.81 | 2.83 |
| 85 | 150 | 5 | 26.07 | 25.65 | 37.56 | 39.59 | 1.36 | 1.78 | 1.65 | 1.25 |
| 86 | 45 | 35 | 6.77 | 4.31 | 5.12 | 15.39 | 2.44 | 1.99 | 2.78 | 3.67 |
| 87 | 150 | 5 | 21.99 | 21.00 | 17.77 | 28.14 | 1.73 | 1.13 | 1.34 | 1.11 |
| 88 | 45 | 35 | 7.42 | 7.62 | 6.03 | 21.18 | 2.82 | 3.05 | 1.82 | 2.82 |
| 89 | 150 | 5 | 9.05 | 5.88 | 27.88 | 10.48 | 2.12 | 1.54 | 5.61 | 1.32 |
| 90 | 80 | 5 | 7.38 | 5.54 | 4.47 | 5.63 | 2.48 | 2.66 | 3.41 | 2.62 |
| 91 | 150 | 5 | 18.98 | 7.11 | 12.83 | 16.00 | 1.28 | 2.01 | 2.07 | 2.67 |
| 92 | 80 | 5 | 3.87 | 7.47 | 8.78 | 14.72 | 2.77 | 5.61 | 2.08 | 3.12 |
| 93 | 150 | 5 | 7.88 | 6.47 | 9.70 | 6.71 | 1.74 | 1.83 | 1.83 | 1.80 |
| 94 | 80 | 5 | 4.25 | 6.13 | 4.98 | 12.17 | 2.19 | 2.26 | 1.78 | 2.18 |
| 95 | 150 | 5 | 18.59 | 8.98 | 12.43 | 9.19 | 6.87 | 1.99 | 1.94 | 1.85 |
| 96 | 80 | 5 | 8.33 | 5.55 | 4.79 | 7.49 | 4.90 | 2.94 | 1.69 | 3.02 |
| 97 | 150 | 5 | 9.99 | 10.01 | 13.85 | 9.96 | 2.81 | 1.61 | 1.83 | 2.31 |
| 98 | 80 | 5 | 9.98 | 8.39 | 6.49 | 7.29 | 3.05 | 4.84 | 2.45 | 3.74 |
| 99 | 150 | 5 | 3.87 | 12.42 | 8.24 | 10.98 | 1.75 | 2.04 | 1.61 | 1.79 |
| 100 | 80 | 5 | 4.41 | 4.51 | 3.94 | 3.82 | 3.49 | 3.56 | 2.45 | 2.36 |
| 101 | 150 | 5 | 7.42 | 13.23 | 11.82 | 11.89 | 1.40 | 1.08 | 1.91 | 1.82 |
| 102 | 80 | 5 | 8.70 | 6.68 | 24.15 | 8.32 | 1.94 | 5.25 | 3.91 | 4.47 |
| 103 | 150 | 5 | 11.03 | 8.50 | 10.14 | 7.29 | 3.44 | 2.24 | 1.72 | 2.16 |

| | | | | | | | | | | |
|---|---|---|---|---|---|---|---|---|---|---|
| 104 | 80 | 5 | 8.50 | 6.67 | 10.31 | 12.25 | 2.17 | 1.25 | 1.43 | 2.55 |
| 105 | 115 | 35 | 8.29 | 11.96 | 7.89 | 11.54 | 2.15 | 1.46 | 2.53 | 2.22 |
| 106 | 80 | 5 | 5.37 | 5.86 | 10.51 | 9.77 | 1.62 | 2.28 | 2.03 | 1.87 |
| 107 | 115 | 35 | 12.25 | 19.02 | 22.85 | 31.27 | 2.27 | 2.27 | 6.90 | 5.08 |
| 108 | 80 | 5 | 8.21 | 13.45 | 13.89 | 13.27 | 2.83 | 2.64 | 2.98 | 2.95 |
| 109 | 115 | 35 | 10.43 | 13.43 | 15.55 | 13.99 | 1.57 | 1.93 | 2.38 | 1.08 |
| 110 | 80 | 5 | 13.16 | 7.60 | 6.21 | 9.18 | 2.15 | 1.31 | 2.25 | 3.52 |
| 111 | 115 | 35 | 14.44 | 9.61 | 15.48 | 16.47 | 1.00 | 1.99 | 1.52 | 1.96 |
| 112 | 80 | 5 | 11.14 | 10.54 | 21.33 | 8.50 | 2.89 | 1.57 | 5.34 | 1.95 |
| 113 | 115 | 35 | 8.39 | 9.22 | 38.96 | 6.93 | 2.91 | 1.95 | 2.40 | 2.57 |
| 114 | 80 | 15 | 7.77 | 7.33 | 10.01 | 9.83 | 1.38 | 1.69 | 1.73 | 2.53 |
| 115 | 115 | 35 | 10.56 | 1.66 | 3.20 | 3.22 | 2.12 | 3.15 | 2.80 | 2.45 |
| 116 | 80 | 15 | 9.25 | 8.21 | 10.06 | 15.16 | 1.76 | 1.93 | 1.60 | 1.83 |
| 117 | 115 | 35 | 11.11 | 12.00 | 18.43 | 21.01 | 2.03 | 2.43 | 1.59 | 2.81 |
| 118 | 80 | 15 | 5.11 | 5.95 | 4.54 | 7.45 | 1.77 | 2.13 | 2.03 | 2.06 |
| 119 | 115 | 35 | 10.97 | 11.35 | 28.21 | 16.55 | 1.57 | 1.43 | 3.61 | 2.30 |
| 120 | 80 | 15 | 9.36 | 17.30 | 12.01 | 21.65 | 2.09 | 3.23 | 2.81 | 10.44 |
| 121 | 115 | 35 | 7.25 | 3.75 | 6.39 | 4.43 | 2.60 | 1.99 | 2.08 | 2.06 |
| 122 | 80 | 15 | 13.49 | 13.65 | 10.64 | 16.82 | 2.00 | 1.29 | 1.84 | 2.36 |
| 123 | 115 | 35 | 15.45 | 20.00 | 8.24 | 34.20 | 1.34 | 2.06 | 1.82 | 5.38 |
| 124 | 80 | 15 | 3.65 | 4.49 | 2.07 | 3.41 | 1.95 | 2.26 | 2.25 | 1.69 |
| 125 | 115 | 35 | 5.08 | 6.91 | 14.27 | 5.82 | 1.30 | 0.97 | 2.28 | 2.35 |
| 126 | 80 | 15 | 3.01 | 9.01 | 15.58 | 11.93 | 1.57 | 4.05 | 2.52 | 2.41 |
| 127 | 115 | 35 | 2.94 | 3.23 | 1.66 | 21.42 | 2.28 | 2.68 | 1.41 | 2.40 |
| 128 | 80 | 15 | 9.76 | 7.08 | 6.02 | 11.04 | 2.36 | 2.30 | 2.07 | 1.44 |
| 129 | 115 | 25 | 15.58 | 18.49 | 13.39 | 16.98 | 2.35 | 1.42 | 2.41 | 2.56 |
| 130 | 80 | 15 | 32.16 | 33.78 | 5.70 | 13.52 | 2.20 | 3.11 | 1.77 | 1.96 |
| 131 | 115 | 25 | 8.61 | 8.21 | 10.68 | 27.27 | 1.71 | 1.25 | 2.64 | 5.03 |
| 132 | 80 | 15 | 21.52 | 11.48 | 26.47 | 8.40 | 3.92 | 4.08 | 5.07 | 2.54 |
| 133 | 115 | 25 | 6.27 | 10.08 | 7.30 | 16.43 | 1.43 | 2.11 | 1.04 | 1.33 |
| 134 | 80 | 15 | 10.92 | 9.71 | 10.16 | 8.70 | 3.56 | 2.48 | 2.22 | 2.73 |
| 135 | 115 | 25 | 14.25 | 15.27 | 16.73 | 22.25 | 2.14 | 1.68 | 1.80 | 1.77 |
| 136 | 80 | 15 | 6.70 | 17.38 | 12.20 | 16.37 | 2.15 | 1.71 | 2.63 | 2.51 |
| 137 | 115 | 25 | 9.09 | 19.17 | 7.46 | 15.34 | 1.65 | 2.44 | 1.80 | 1.52 |
| 138 | 80 | 25 | 11.36 | 6.64 | 8.19 | 7.48 | 2.03 | 2.28 | 2.69 | 2.54 |
| 139 | 115 | 25 | 15.94 | 15.41 | 18.56 | 20.36 | 2.36 | 1.99 | 2.52 | 3.23 |
| 140 | 80 | 25 | 2.68 | 0.53 | 12.30 | 1.02 | 1.47 | 2.33 | 8.35 | 2.42 |
| 141 | 115 | 25 | 9.61 | 8.65 | 7.92 | 14.74 | 1.64 | 1.67 | 2.07 | 3.00 |
| 142 | 80 | 25 | 2.83 | 1.73 | 6.91 | 6.07 | 2.51 | 1.32 | 3.37 | 2.82 |
| 143 | 115 | 25 | 11.37 | 12.76 | 14.74 | 32.36 | 1.76 | 1.71 | 2.04 | 11.36 |
| 144 | 80 | 25 | 9.71 | 6.59 | 6.95 | 5.87 | 2.54 | 2.20 | 1.66 | 2.18 |
| 145 | 115 | 25 | 5.02 | 9.01 | 4.83 | 6.83 | 3.08 | 2.95 | 2.31 | 2.48 |
| 146 | 80 | 25 | 9.06 | 8.10 | 16.23 | 18.03 | 1.41 | 1.59 | 2.33 | 3.96 |
| 147 | 115 | 25 | 4.83 | 6.19 | 12.68 | 12.99 | 1.17 | 1.98 | 1.89 | 1.78 |
| 148 | 80 | 25 | 11.10 | 3.27 | 4.20 | 6.39 | 2.59 | 3.07 | 2.99 | 2.65 |
| 149 | 115 | 25 | -0.64 | 2.38 | 2.99 | 5.21 | 1.77 | 1.15 | 1.64 | 1.46 |
| 150 | 80 | 25 | 2.54 | 4.69 | 6.67 | 6.99 | 2.12 | 1.96 | 3.30 | 2.69 |
| 151 | 115 | 25 | 3.02 | 5.15 | 5.81 | 3.80 | 1.30 | 1.24 | 2.38 | 2.40 |
| 152 | 80 | 25 | 11.73 | 11.97 | 8.97 | 13.08 | 2.42 | 3.11 | 1.70 | 1.33 |
| 153 | 115 | 15 | 2.56 | 2.19 | 1.85 | 4.82 | 2.40 | 4.15 | 1.72 | 2.12 |
| 154 | 80 | 25 | 5.91 | 9.11 | 6.55 | 7.40 | 1.40 | 1.37 | 1.44 | 1.36 |
| 155 | 115 | 15 | 3.04 | 2.10 | 31.98 | 25.81 | 1.71 | 2.16 | 11.97 | 5.29 |
| 156 | 80 | 25 | 8.87 | 4.60 | 29.34 | 10.14 | 1.40 | 1.51 | 11.14 | 2.13 |
| 157 | 115 | 15 | 5.98 | 9.14 | 4.97 | 10.80 | 1.16 | 2.00 | 1.65 | 1.66 |
| 158 | 80 | 25 | 7.70 | 6.48 | 7.70 | 7.60 | 2.11 | 1.80 | 3.01 | 2.51 |
| 159 | 115 | 15 | 9.59 | 13.45 | 7.20 | 18.15 | 1.21 | 1.79 | 2.06 | 2.24 |

| | | | | | | | | | | |
|---|---|---|---|---|---|---|---|---|---|---|
| 160 | 80 | 25 | 3.45 | 5.84 | 3.34 | 3.39 | 1.96 | 2.46 | 1.40 | 2.33 |
| 161 | 115 | 15 | 2.43 | 3.79 | 5.32 | 5.79 | 1.90 | 1.82 | 1.38 | 2.52 |
| 162 | 80 | 35 | 1.01 | 4.58 | 4.37 | 7.04 | 1.59 | 2.65 | 2.04 | 2.97 |
| 163 | 115 | 15 | 12.15 | 9.96 | 18.23 | 14.46 | 1.69 | 2.43 | 2.61 | 2.03 |
| 164 | 80 | 35 | 1.07 | 7.16 | 4.50 | 6.25 | 1.57 | 3.00 | 2.05 | 2.19 |
| 165 | 115 | 15 | 10.80 | 12.96 | 9.68 | 50.44 | 1.15 | 2.00 | 2.07 | 9.88 |
| 166 | 80 | 35 | 5.79 | 0.65 | 4.06 | 5.33 | 2.44 | 2.17 | 3.15 | 2.17 |
| 167 | 115 | 15 | 12.62 | 12.44 | 18.27 | 11.26 | 2.66 | 1.97 | 1.61 | 3.09 |
| 168 | 80 | 35 | 6.09 | 7.92 | 10.42 | 7.88 | 3.23 | 2.51 | 2.63 | 1.74 |
| 169 | 115 | 15 | 14.70 | 16.09 | 12.56 | 19.64 | 1.51 | 2.08 | 1.94 | 4.31 |
| 170 | 80 | 35 | 9.36 | 10.57 | 11.10 | 7.11 | 3.69 | 2.14 | 1.71 | 1.95 |
| 171 | 115 | 15 | 2.51 | 37.53 | 7.76 | 14.16 | 1.63 | 4.81 | 1.49 | 2.16 |
| 172 | 80 | 35 | 4.18 | 18.91 | 5.85 | 7.58 | 1.77 | 5.00 | 2.65 | 3.12 |
| 173 | 115 | 15 | 5.92 | 10.31 | 11.64 | 4.73 | 1.13 | 1.69 | 1.45 | 1.73 |
| 174 | 80 | 35 | 16.74 | 6.78 | 6.20 | 5.37 | 2.30 | 2.25 | 2.02 | 2.83 |
| 175 | 115 | 15 | 9.13 | 12.70 | 14.74 | 6.40 | 1.21 | 1.45 | 1.84 | 1.72 |
| 176 | 80 | 35 | 9.01 | 8.41 | 14.25 | 8.37 | 1.45 | 1.83 | 2.07 | 2.80 |
| 177 | 115 | 5 | 11.40 | 6.08 | 17.96 | 9.09 | 1.93 | 2.60 | 2.67 | 2.76 |
| 178 | 80 | 35 | 6.84 | 6.61 | 12.71 | 11.54 | 1.61 | 1.32 | 3.19 | 2.68 |
| 179 | 115 | 5 | 0.44 | 6.34 | 4.19 | 36.18 | 1.99 | 2.09 | 2.23 | 2.30 |
| 180 | 80 | 35 | 3.80 | 10.08 | 11.38 | 11.18 | 1.88 | 1.56 | 2.20 | 5.27 |
| 181 | 115 | 5 | 2.17 | -1.00 | -0.25 | -5.33 | 1.62 | 1.56 | 1.50 | 1.87 |
| 182 | 80 | 35 | 8.24 | 4.78 | 5.14 | 7.83 | 2.17 | 2.55 | 2.91 | 3.01 |
| 183 | 115 | 5 | 23.54 | 15.23 | 11.73 | 20.77 | 1.24 | 1.43 | 2.02 | 1.25 |
| 184 | 80 | 35 | 5.60 | 10.07 | 7.55 | 6.48 | 2.22 | 1.99 | 2.70 | 3.14 |
| 185 | 115 | 5 | 9.03 | 5.12 | 7.84 | 15.30 | 3.48 | 2.42 | 1.57 | 4.17 |
| 186 | 115 | 5 | 5.69 | 9.36 | 7.78 | 8.82 | 2.03 | 1.97 | 2.92 | 1.94 |
| 187 | 115 | 5 | 9.50 | 7.76 | 6.70 | 5.37 | 5.70 | 2.24 | 3.11 | 2.43 |
| 188 | 115 | 5 | 2.53 | 2.61 | 10.98 | 7.93 | 2.14 | 1.45 | 1.42 | 3.09 |
| 189 | 115 | 5 | 8.29 | 9.31 | 13.31 | 15.33 | 2.00 | 2.02 | 3.32 | 2.58 |
| 190 | 115 | 5 | 8.18 | 8.99 | 6.18 | 14.75 | 1.53 | 2.41 | 2.76 | 2.55 |
| 191 | 115 | 5 | 4.71 | 33.77 | 6.58 | 8.05 | 1.87 | 9.21 | 1.86 | 2.23 |
| mean value | 97.41 | 20.08 | 10.38 | 10.10 | 11.80 | 13.58 | 2.23 | 2.26 | 2.50 | 2.69 |